Visual analysis of the lysate of single eukaryotic cells by combining μ-fluidics with electron microscopy

Inauguraldissertation

zur
Erlangung der Würde eines Doktors der Philosophie
vorgelegt der
Philosophisch-Naturwissenschaftlichen Fakultät
der Universität Basel

von

S I M O N K E M M E R L I N G

aus Deutschland

Basel, Schweiz 2013

Genehmigt von der Philosophisch-Naturwissenschaftlichen Fakultät

auf Antrag von:

Prof. Dr. Henning Stahlberg, Fakultätsverantwortlicher

Prof. Dr. Roderick Lim, Koreferent

Basel, den 18.6.2013

Prof. Dr. Jörg Schibler (Dekan)

II

I dedicate this thesis to
my beloved grandmother
who passed away during
the course of my doctoral studies

Summary

Systems biology aims to understand the emergence of biological functions from underlying interaction networks. The behavior of these networks is stochastic, making the investigation of cell-to-cell variability an important aspect of systems biology. The proteome defines the functional capacity of a cell at a certain point in time. Thus, tools and assays that investigate the concentrations, locations, functions and interactions of proteins at the single cell level will provide new insights in fundamental biology and biomedicine. However, due to the huge diversity of protein species, the dynamic range of protein expression levels, the minute sample volumes, and the lack of amplification techniques, single-cell proteomic studies remain a challenging task, that requires novel and correlative approaches. This is especially true for the analysis of eukaryotic cells, which still challenges existing techniques.

This thesis is part of a project that aims to establish a new approach to proteomic studies on single eukaryotic cells. The project is based on the idea to physically lyse single cells and spread their components onto sample carriers for visual and mass analysis by electron microscopy (EM) and mass spectrometry (MS). The work presented in this thesis focuses on the implementation of some of the basic microfluidic modules that will be part of the envisaged sample preparation pipeline.

The microfluidic pipeline must both prepare the lysate of single cells and deposit it on the sample carriers in an efficient and unbiased manner. A prototype consisting of a versatile conditioning module for in-line sample conditioning and a hand-over module for lossless sample deposition and micro-patterning of EM grids was built [1]. The implemented semiautomatic procedure is capable of processing minute sample volumes and the transferred test samples are suitable for structural analysis by negative stain transmission electron microscopy (TEM). Further results showed that this method can be used to process the total content of cell lysates; lysate components, such as soluble proteins, filaments and membranes were efficiently stained and clearly resolved on the TEM images; stain quality was excellent and highly reproducible. In addition initial tests demonstrated that the modules could be used to prepare sample grids that are suitable for mass determination by scanning TEM (STEM). Further development of the hand-over module focused on its adaption to MS sample carriers [2]. With this modification, the setup was successfully applied to spot sample-matrix mixtures onto MS plates, resulting in homogenous sample spots for matrix-assisted laser desorption/ionization (MALDI) MS analysis.

The next aim was to collect single cell samples. A module allowing single-cell lysis and rapid uptake of the cell lysate was developed to achieve this [3]. Using a freely positionable microcapillary electrode this module is capable of targeting individual adherent cells in situ under light microscopy (LM) observation. It allows fast electrical lysis of single cells followed by rapid aspiration of the cellular components into the microcapillary. The combination with LM enables live cell monitoring and thus facilitates the evaluation of the lysis and aspiration procedure as well as the correlation of LM information with subsequently derived data. The investigation of single cell lysate samples by classical negative stain TEM revealed the presence of several cellular components, such as membrane patches, filaments and other prominent structures with distinctive shapes. This preliminary data indicates that the whole lysate of individual cells can be prepared for a visual investigation by negative stain TEM.

The modules developed during this thesis provide novel and promising methods for the analysis of the protein content of single eukaryotic cells and their combination will result in a versatile sample preparation pipeline that can be applied to biological questions on the single cell level.

List of peer-reviewed manuscripts included in this thesis

[1]   Kemmerling, S., Ziegler, J., Schweighauser, G., Arnold, S. A., Giss, D., Müller, S. A., Ringler, P., Goldie, K. N., Goedecke, N., Hierlemann, A., Stahlberg, H., Engel, A. & Braun, T. **Connecting μ-fluidics to electron microscopy**. *Journal of Structural Biology* 177, 128-134, (2012).

[2]   Weidmann, S., Kemmerling, S., Mädler, S., Stahlberg, H., Braun, T. & Zenobi, R. **Ionic liquids as matrices in microfluidic sample deposition for high-mass matrix-assisted laser desorption/ionization mass spectrometry.** *European Journal of Mass Spectrometry* 18, 279-286, (2012).

[3]   Kemmerling, S., Arnold, S. A., Bircher, B. A., Sauter, N., Escobedo, C., Dernick, G., Hierlemann, A., Stahlberg, H. & Braun, T. **Single-cell lysis for visual analysis by electron microscopy**. *Journal of Structural Biology*, (2013), http://dx.doi.org/10.1016/j.jsb.2013.06.012

Table of Contents

1 General Introduction

1.1 The stochastic nature of biological systems

The basic processes underlying all biological functions are subject to stochastic fluctuations. Consequently uncertainty and randomness are inherent properties of biological systems, with profound consequences. Stochasticity is especially pronounced at the molecular level and, thus, plays an important role in the biochemical processes that control cellular properties and behavior. In a single cell, the basic unit of life, stochastic fluctuations can lead to variations in the concentrations, positions and activities of the molecular components that control cellular functions. As it is important to overcome the undesirable effects of this intrinsic noise to achieve robust function [1] various mechanisms have evolved to control or tolerate it [2-4]. The costs to precisely control molecular noise seem to be very high [5] and, therefore, such mechanisms are only applied to essential functions [1]. In other cases noise seems to be tolerated or even utilized, and can be observed in both prokaryotes [6] and eukaryotes [7].

Biochemical processes that involve molecules in low copy numbers are strongly affected by stochastic fluctuations. The best-studied example is noise in gene expression, which involves only one or a few DNA molecules per cell. Random fluctuations in gene expression can result in cellular heterogeneity and phenotypic variability in a population of genetically identical cells under the same environmental conditions [6]. Noisy gene expression can in some contexts be beneficial [2] and even have a functional role [8]. A stochastic gene expression, for example, allows the probabilistic differentiation of isogenic cells without the need of genetic modification. This random state switching establishes a non-genetic dynamic heterogeneity in populations, that has been linked to various phenomena, e.g., the development of persistence phenotypes that allow microbial populations to survive antibiotic stress [9], and the ability of certain cancer cells of a population to withstand drug treatment [10] because they have switched into a drug-tolerant state. Generally, the ability to spontaneously and reversibly switch between different states can be an advantageous adaption and stress response strategy in an unpredictable environment [11]. Stochastic cell fate decisions also seem to play a role in cellular differentiation and the development of higher organisms [11]. Some findings suggest a heterogeneous and dynamic state of stem cell populations, facilitating stochasticity for fate decisions of subpopulations [12,13]. Moreover, stochastic gene expression has been linked to processes in evolution [14], aging [15] and disease [16].

Although the exact mechanisms that enable biological systems to control, tolerate and exploit stochastic fluctuations are not fully understood, noise is increasingly appreciated as an important force in biology. Therefore, knowledge about the sources and consequences of biological noise can lead to important implications extending from fundamental biology to medicine.

1.2 Single cell analysis

The properties and behavior of individual cells in a population can have important biological consequences, making methods with single cell resolution essential to gain new insights into certain biological and medical questions. Revealing and understanding the cell-to-cell variability within a population is an important aspect of systems biology, stem cell and cancer research as well as biotechnology and diagnostics.

Individual cells of a population can show differences in the amount and type of the biomolecules they contain, as well as in their responses to physical and chemical stimuli and time dynamics. These variations are not always due to genetic differences. Genetically identical cells can exhibit heterogeneity because they are at a different stage of the cell cycle, in a different epigenetic state or under the influence of different environmental conditions. Moreover, even if all of these parameters are identical for all the cells within a population, a phenotypic variation can still be present owing to the stochastic nature of intracellular processes discussed above. In the presence of cell-to-cell variation, data from tools and assays that measure the average responses or contents of an ensemble of cells can be difficult to interpret or even misleading. Bulk measurements are not able to resolve the properties and responses of single cells as they result in a mean value, which masks variations of individual cells and subpopulations, i.e., bulk measurements are not well suited to investigate the heterogeneity of populations and the differences between single cells within them. Single cell analysis (SCA) not only reduces biological noise but also allows more meaningful data analysis and experimental design. The need for single cell resolution is a major driving force for the emergence of new methods and tools to handle, manipulate and investigate single cells.

Classical approaches for the investigation of individual cells are based on microscopy techniques. Since its invention, light microscopy (LM) offers the possibility to study biological samples down to a resolution of about 200 nm. Nowadays LM has overcome the diffraction limit and can be used to resolve sub-cellular structures down to 10-20 nm [17]. Various labeling techniques allow the spatial distribution and dynamics of subcellular structures and molecular components to be studied in chemically fixed or living samples.

Electron microscopy (EM) provides a higher resolution and is employed to study cellular components, in isolation or in the context of fixed cells and tissue, on the nanometer scale [18,19]. Furthermore, correlative light and electron microscopy (CLEM) approaches now combine the advantages of these two classical imaging techniques [20,21]. Moreover techniques such as X-ray diffraction microscopy [22] and atomic force microscopy [23] allow the investigation of whole individual cells.

The need to investigate individual cells is automatically accompanied by the need for tools and methods to handle, manipulate and control single cells. A number of tools to analyze and sort heterogeneous cell populations exist today and are based on flow cytometry. These techniques are capable of sorting complex samples based on properties of each individual cell and are routinely used to identify and purify subpopulations in a high throughput fashion. Some of these assays, e.g., fluorescence activated cell sorting (FACS) and magnetic activated cell sorting (MACS), are based on labeling techniques, while others, e.g., iso-dielectric separation (IDS) or Raman tweezers, are label-free an based on intrinsic biomarkers and properties of the cells. Laser capture microdissection (LCM) is another important single cell manipulation technique. It allows the separation of a specific cell of interest from a tissue and other samples for further analysis.

Many of the other new tools rely on miniaturized systems to provide an interface to classical analysis techniques (e.g., capillary electrophoresis coupled to mass spectrometry [24]) and access to a new experimental space that approaches the dimensions of single cells. Micro- and nanofabrication allows methods and principles from the macroscale to be applied in miniaturized systems and physical phenomena that are only practically accessible at the microscale to be exploited. For example, microfluidic systems utilize various physical and chemical principles to sort, trap, manipulate and lyse individual cells in combination with the possibility to precisely handle and process small sample volumes [25,26]. The confinement of single cells in finite volume elements or their trapping in a microfluidic stream also enables a better control of cellular microenvironments and allows the incorporation of cell-culturing techniques [27]. In general these new tools not only facilitate the downscaling of classical assays and enhancement of their analytical performance [28], but also make new kinds of single cell experiments and sample preparation methods possible. They also offer the potential to increase throughput via parallelization and automation.

One research field that greatly benefits from the advances in single cell analysis is systems biology [29-31]. Systems Biology aims to understand the emergence of biological functions from underlying interaction networks [32].

The basic unit of this systemic approach is the single cell and knowledge about how single cells accomplish their biological function is fundamental. This requires experimental information about the spatial and temporal arrangements of the network components as well as their structure on the single cell level. The development of comprehensive models requires experimental information about the individual components of the system, i.e., the genome, the transcriptome, the proteome, the metabolome and the interactome. Therefore, systems biology combines bioinformatics with the data from all the omic disciplines.

1.2.1 Single cell Omics

The field of single cell analysis is rapidly evolving, making it almost impossible to give a comprehensive overview here. A variety of recent reviews provide a deeper insight into various aspects of this exciting field [25,30,33-37]. An overview of the most important technologies for the analysis of single cells on all the omic levels is given in table 1-1. The different methods can be separated into invasive, non-invasive and non-invasive time-resolved. The development of all the analytical technologies towards single cell resolution is mainly based on the improvement of single cell manipulation, sample preparation and detection sensitivity.

The field of non-invasive single cell analysis is dominated by opto-based methods that mainly facilitate fluorescent labels on all of the omic levels. Fluorescence spectroscopy and microscopy are used to study intact cells and are essential to time resolved studies in living cells. Aptamer-based technologies, FRET and LIF are the most prominent approaches for metabolite analysis on the single cell level, and immunoassay microarrays can be used to detect and quantify secreted proteins [38]. Methods based on flow cytometry (e.g., FACS) cannot provide spatiotemporal resolution but are frequently used for high throughput non-invasive studies. However, despite constant progress [39] all of the flourecence-based methods are still quite limited in terms of simultaneous detection and correlated measurements within a single cell. Cryo-electron tomography (cryo-ET) is an example of a technique that is not based on fluorescence and offers the possibility to study intact cells. This technique is applied for visual proteomics and will be discussed in more detail in the next section.

Omics Level	Major SCA technologies	Classificatio	Reference
Genomics	MDA; ploning	invasive	[40-43]
	Immunofluoresence	non-invasive	[44]
	Fusion protein	non-invasive time-resolved	[44]
Transcriptomics	mRNA-Seq; (q)RT-PCR	invasive	[45,46]
	FISH	non-invasive	[47]
	FISH and chips	non-invasive time-resolved	[48]
Proteomics	LC-MS(nano-ESI); MALDI-TOF; Cryo-ET (sections)	invasive	[49-54]
	Immunoflurecence; Cryo-ET (intact cells)	non-invasive	[55-57]
	FRET	non-invasive time-resolved	[58]
Metabolomics	LC-MS; CE-ESI-MS; MALDI-TOF	invasive	[33,59-61]
	Aptamer technology; FRET; LIF	non-invasive	[62-65]
	Aptamer technology; FRET; LIF	non-invasive time-resolved	[62-65]

Table 1-1*: Overview of the most important technologies for single-cell analysis on all the omic levels adapted from [25]; Abbreviations: CE, capillary electrophoresis; ESI, electrospray ionization; FISH, fluorescence in situ hybridization; FRET, fluorescence resonance energy transfer; LC, liquid chromatography; LIF, laser-induced fluorescence; MALDI-TOF matrix-assisted laser desorption ionization time of flight; MDA, multiple displacement amplification; MS, mass spectrometry; qRT-PCR, quantitative reverse transcription polymerase chain reaction; Seq, Sequencing.*

Among the invasive approaches, the analysis of the nucleic acids from single cells mainly relies on amplification techniques to produce sufficient material for sequencing. In single cell genomics, approaches such as multiple displacement amplification (MDA) have revolutionized the field of whole genome amplification (WGA) techniques. MDA enables the amplification of all template material without *a priory* sequence knowledge by using short random primers. Since its introduction MDA has continuously improved in terms of sequence coverage and sensitivity [43], and new WGA methods have been introduced to overcome amplification bias [66]. Single cell expression profiling is based on amplification and analysis of complementary DNA (cDNA) produced by reverse transcription polymerase chain reaction (RT-

PCR). Detection and quantification is achieved using quantitative PCR (qPCR) or next-generation sequencing technologies [67] such as mRNA sequencing (mRNA-Seq).

On the proteome and metabolome level the invasive studies are dominated by mass spectrometry (MS), which will be discussed in more detail in the next section. Besides MS, affinity based methods such as microarray technologies are also frequently applied as analytical tools. Separation procedures such as liquid chromatography (LC) or electrophoresis have been miniaturized (e.g., capillary electrophoresis; CE) and coupled with classical analytical methods, e.g., MS or laser-induced fluorescence (LIF). The precise handing and the required lysis of individual cells is mainly realized with microfuidic platforms. These devices either directly integrate or are coupled to sample preparation and/or analytical techniques.

1.2.2 The challenging proteome

Proteins are essential to virtually all cellular functions and, hence, the proteome defines the functional capacity of a cell at a certain point in time. Although genomic and transcriptomic studies can provide qualitative information they cannot supply detailed information about the quantity and activity of proteins. Therefore, tools and assays to directly investigate the concentrations, locations, modifications, interactions and functions of proteins are necessary. However, due to the huge protein diversity (1×10^9 proteins of $1\text{-}3\times10^4$ different protein species), the broad range of protein abundances (50 copies per cell for low abundance proteins to up to 1×10^5 copies per cell for high abundance proteins) and the minute sample volumes [25,35], proteomic studies of single eukaryotic cells remain a challenging task. Low abundance proteins and the lack of amplification techniques are the main hurdles to be overcome by approaches geared to study the proteome of a single cell, putting demanding requirements on the applied methods in terms of sensitivity and dynamic range.

MS is one of the most powerful techniques in proteomic research and became routinely available for biological studies when new soft ionization techniques such as matrix-assisted laser desorption ionization (MALDI) and electrospray ionization (ESI) were developed [68]. These approaches are capable of ionizing and vaporizing large biomolecules, i.e., proteins and peptides up to a mass of 2-3 MDa [69,70]. Nowadays a variety of different instrument configurations are available, and enable discovery-driven as well as hypothesis-driven proteomic measurements [71]. MS not only allows proteins to be identified and characterized, but also to be detected in a

quantitative manner [72]. Approaches such as peptide mass fingerprinting (PMF) or tandem MS (MS/MS) are routinely performed to identify isolated or purified proteins. Most approaches in proteomics are based on proteolytic and/or otherwise induced fragmentation (e.g., collision induced dissociation CID) of proteins or peptides into peptide fragments with subsequent matching of the derived fragment masses to experimental databases or to theoretical masses resulting from *in silico* digests and proteolysis. With increasing sample complexity it becomes more difficult to detect and identify all of the proteins in a single sample simultaneously with high confidence [73]. In these cases, intensive sample fractionation by separation techniques (e.g., LC and gel or capillary electrophoresis) and extended data analysis techniques have to be applied [74]. Despite constant progress, the comprehensive analysis of complex protein mixtures in minute volumes, as required for single cell proteome profiling, is still a major challenge. Sample preparation as well as the complexity and high dynamic range of cellular proteomes, lead to a biased identification of high abundance proteins and often preclude the detection of low abundance species [72,75]. This results in incomplete proteome coverage especially for higher organisms, i.e., mammalian cells [76]. Global quantification of relative or absolute protein abundance is even more challenging and requires substantial effort to be invested in instrument calibration, sample fractionation, labeling and MS analysis. Targeted MS approaches such as single reaction monitoring (SRM) are applied to increase sensitivity and reproducibility [77]. Targeted MS allows the selective detection and quantification of predetermined peptide ions, but is currently limited to the analysis of a few hundred peptides in a single experiment [72]. Despite these limitations MS is an essential technique for proteomic research, however other powerful techniques such as EM are required for structural investigations extending beyond the primary sequence.

EM allows the detection and structural investigation of proteins and protein-complexes at the single molecule level down to subnanometer resolution. In the approach termed visual proteomics, cryo-ET is applied to obtain nanometer resolution 3D-snapshots of a complete and unperturbed cell in a close-to-native state [55,56,78,79]. Rapid cooling (vitrification) of the sample embeds it in a crystal-free state of solid water, called vitreous water or amorphous ice [80]; macromolecules inside the cell maintain their native conformation and spatial relationship. Subsequent tomographic imaging by cryo-EM reveals the spatial organization of the proteome of the cell and allows the structural investigation of its components [81,82]. Proteins are commonly identified by comparison with a library of structural templates from known proteins that have the mass densities found in the tomogram [83]. This template matching relies on the quality of the tomograms, as well

as on the size and quality of the template library [79,84]. In practice a robust and reliable identification of macromolecules in the cellular context is hampered by the low signal-to-noise ratio (SNR) and the limited resolution of the cryo-micrographs [85]. Moreover the molecular crowding in the cytoplasm further complicates the required template matching [86], and the clear identification of molecules smaller than 500 kDa is likely to remain challenging [18,87]. Labeling strategies with electron-dense markers (e.g., gold labels) have been developed to help overcome this limitation [79], but despite constant progress [88], these methods often involve harsh preparative treatment of the cells. Additionally, cryo-ET is, currently limited to samples that do not exceed a thickness of about 500 nm [89] and only offers a field of view of about 2 μm^2 [90]. As a consequence most eukaryotic cells cannot be investigated *in toto* and the studies are limited to small cells and thin cell peripheries if no sectioning methods are applied [90]. Several different sectioning approaches have been developed for cellular ET [91], including the sectioning of vitrified cells under cryo-conditions [49]. The cryo-sectioning of vitrified cells and the handling and characterization of cellular cryo-sections, though, is still technically demanding and prone to artifacts [92]. Despite its limitations cryo-ET is the most powerful technique to investigate the spatial organization of the proteome with nanometer resolution in single cells.

Although the field of single cell proteomics is advancing at an enormous pace, there is no ultimate single technique that can cope with the sheer complexity of a proteome. This challenging task requires a correlative approach combining different techniques, linking different kinds of data and exploring novel approaches and combinations.

1.3 References

[1]   Barkai, N. & Shilo, B.-Z. **Variability and robustness in biomolecular systems.** *Mol. Cell* 28, 755-760, (2007).

[2]   Raj, A. & van Oudenaarden, A. **Nature, nurture, or chance: stochastic gene expression and its consequences.** *Cell* 135, 216-226, (2008).

[3]   Rao, C. V., Wolf, D. M. & Arkin, A. P. **Control, exploitation and tolerance of intracellular noise.** *Nature* 420, 231-237, (2002).

[4]   Raser, J. M. **Noise in gene expression : Origins, consequences, and control.** *Science* 309, 2010-2013, (2005).

[5]   Lestas, I., Vinnicombe, G. & Paulsson, J. **Fundamental limits on the suppression of molecular fluctuations.** *Nature* 467, 174-178, (2010).

[6]   Elowitz, M. B., Levine, A. J., Siggia, E. D. & Swain, P. S. **Stochastic gene expression in a single cell.** *Science* 297, 1183-1186, (2002).

[7]   Blake, W. J., Kærn, M., Cantor, C. R. & Collins, J. J. **Noise in eukaryotic gene expression.** *Nature* 422, 633-637, (2003).

[8]   Eldar, A. & Elowitz, M. B. **Functional roles for noise in genetic circuits.** *Nature* 467, 167-173, (2010).

[9]   Wakamoto, Y., Dhar, N., Chait, R., Schneider, K., Signorino-Gelo, F. *et al.* **Dynamic persistence of antibiotic-stressed mycobacteria**. *Science* 339, 91-95, (2013).

[10]   Sharma, S. V., Lee, D. Y., Li, B., Quinlan, M. P., Takahashi, F. *et al.* **A chromatin-mediated reversible drug-tolerant state in cancer cell subpopulations.** *Cell* 141, 69-80, (2010).

[11]   Balázsi, G., van Oudenaarden, A. & Collins, J. J. **Cellular decision making and biological noise: from microbes to mammals.** *Cell* 144, 910-925, (2011).

[12]   Canham, M. a., Sharov, A. a., Ko, M. S. H. & Brickman, J. M. **Functional heterogeneity of embryonic stem cells revealed through translational amplification of an early endodermal transcript.** *PLoS Biol.* 8, e1000379, (2010).

[13]   Chang, H. H., Hemberg, M., Barahona, M., Ingber, D. E. & Huang, S. **Transcriptome-wide noise controls lineage choice in mammalian progenitor cells.** *Nature* 453, 544-547, (2008).

[14]   Eldar, A., Chary, V. K., Xenopoulos, P., Fontes, M. E., Losón, O. C. *et al.* **Partial penetrance facilitates developmental evolution in bacteria.** *Nature* 460, 510-514, (2009).

[15]   Bahar, R., Hartmann, C. H., Rodriguez, K. a., Denny, A. D., Busuttil, R. a. *et al.* **Increased cell-to-cell variation in gene expression in ageing mouse heart.** *Nature* 441, 1011-1014, (2006).

[16]   Pujadas, E. & Feinberg, A. P. **Regulated noise in the epigenetic landscape of development and disease.** *Cell* 148, 1123-1131, (2012).

[17]   Schermelleh, L., Heintzmann, R. & Leonhardt, H. **A guide to super-resolution fluorescence microscopy.** *J. Cell Biol.* 190, 165-175, (2010).

[18]   Kourkoutis, L. F., Plitzko, J. M. & Baumeister, W. **Electron microscopy of biological materials at the nanometer scale.** *Annu. Rev. Mater. Res.* 42, 33-58, (2012).

[19]   Ohi, M., Li, Y., Cheng, Y. & Walz, T. **Negative staining and image classification - powerful tools in modern electron microscopy.** *Biol. Proced. Online* 6, 23-34, (2004).

[20]   Mironov, A. A. & Beznoussenko, G. V. **Correlative microscopy: a potent tool for the study of rare or unique cellular and tissue events.** *J. Microsc.* 235, 308-321, (2009).

[21]   van Rijnsoever, C., Oorschot, V. & Klumperman, J. **Correlative light-electron microscopy (CLEM) combining live-cell imaging and immunolabeling of ultrathin cryosections.** *Nat. Methods* 5, 973-980, (2008).

[22]   Jiang, H., Song, C., Chen, C.-C., Xu, R., Raines, K. S. *et al.* **Quantitative 3D imaging of whole, unstained cells by using X-ray diffraction microscopy.** *Proc. Natl. Acad. Sci. U. S. A.* 107, 11234-11239, (2010).

[23]   Stewart, M. P., Toyoda, Y., Hyman, A. a. & Müller, D. J. **Tracking mechanics and volume of globular cells with atomic force microscopy using a constant-height clamp.** *Nat. Protoc.* 7, 143-154, (2012).

[24]   Klepárník, K. **Recent advances in the combination of capillary electrophoresis with mass spectrometry: from element to single-cell analysis.** *Electrophoresis* 34, 70-85, (2013).

[25]   Fritzsch, F. S. O., Dusny, C., Frick, O. & Schmid, A. **Single-cell analysis in biotechnology, systems biology, and biocatalysis.** *Annu. Rev. Chem. Biomol.* 3, 129-155, (2012).

[26]   Yun, H., Kim, K. & Lee, W. G. **Cell manipulation in microfluidics.** *Biofabrication* 5, 022001, (2013).

[27]   Di Carlo, D., Tat, H., Tse, K. & Gossett, D. R. **Introduction: Why Analyze Single Cells?** in: Single-Cell Analysis: Methods and Protocols, *Methods in Molecular Biology*, Vol. 853, Ch. 1, Springer Science+Business Media, (2012).

[28]   Lecault, V., White, A. K., Singhal, A. & Hansen, C. L. **Microfluidic single cell analysis: from promise to practice.** *Curr. Opin. Chem. Biol.* 16, 381-390, (2012).

[29]   Szita, N., Polizzi, K., Jaccard, N. & Baganz, F. **Microfluidic approaches for systems and synthetic biology.** *Curr. Opin. Biotechnol.* 21, 517-523, (2010).

[30]   Wang, D. & Bodovitz, S. **Single cell analysis: the new frontier in 'omics'.** *Trends Biotechnol.* 28, 281-290, (2010).

[31]   Breslauer, D. N., Lee, P. J. & Lee, L. P. **Microfluidics-based systems biology.** *Mol. Biosyst.* 2, 97-112, (2006).

[32]   Westerhoff, H. V. **Systems biology left and right.** *Methods Enzymol.* 500, 3-11, (2011).

[33]   Amantonico, A., Urban, P. L. & Zenobi, R. **Analytical techniques for single-cell metabolomics: state of the art and trends.** *Anal. Bioanal. Chem.* 398, 2493-2504, (2010).

[34]   Kalisky, T. & Quake, S. R. **Single-cell genomics.** *Nat. Methods* 8, 311-314, (2011).

[35]   Schmid, A., Kortmann, H., Dittrich, P. S. & Blank, L. M. **Chemical and biological single cell analysis.** *Curr. Opin. Biotechnol.* 21, 12-20, (2010).

[36]   Trouillon, R., Passarelli, M. K., Wang, J., Kurczy, M. E. & Ewing, A. G. **Chemical analysis of single cells.** *Anal. Chem.* 85, 522-542, (2013).

[37]   Wu, M. & Singh, A. K. **Single-cell protein analysis.** *Curr. Opin. Biotechnol.* 23, 83-88, (2012).

[38]   Ma, C., Fan, R., Ahmad, H., Shi, Q., Comin-Anduix, B. *et al.* **A clinical microchip for evaluation of single immune cells reveals high functional heterogeneity in phenotypically similar T cells.** *Nat. Med.* 17, 738-743, (2011).

[39]   Lubeck, E. & Cai, L. **Single-cell systems biology by super-resolution imaging and combinatorial labeling.** *Nat. Methods* 9, 743 - 750, (2012).

[40]   Spits, C., Le Caignec, C., De Rycke, M., Van Haute, L., Van Steirteghem, A. *et al.* **Whole-genome multiple displacement amplification from single cells.** *Nat. Protoc.* 1, 1965-1970, (2006).

[41]   Lizardi, P. M., Huang, X., Zhu, Z., Bray-Ward, P., Thomas, D. C. *et al.* **Mutation detection and single-molecule counting using isothermal rolling-circle amplification.** *Nat. Genet.* 19, 225-232, (1998).

[42]   Dean, F. B., Nelson, J. R., Giesler, T. L. & Lasken, R. S. **Rapid amplification of plasmid and phage DNA using Phi 29 DNA polymerase and multiply-primed rolling circle amplification.** *Genome Res.* 11, 1095-1099, (2001).

[43]   Zhang, K., Martiny, A. C., Reppas, N. B., Barry, K. W., Malek, J. *et al.* **Sequencing genomes from single cells by polymerase cloning.** *Nat. Biotechnol.* 24, 680-686, (2006).

[44] Babic, A., Lindner, A. B., Vulic, M., Stewart, E. J. & Radman, M. **Direct visualization of horizontal gene transfer.** *Science* 319, 1533-1536, (2008).

[45] Hinkle, D., Glanzer, J., Sarabi, A., Pajunen, T., Zielinski, J. *et al.* **Single neurons as experimental systems in molecular biology.** *Prog. Neurobiol.* 72, 129-142, (2004).

[46] Mardis, E. R. **The impact of next-generation sequencing technology on genetics.** *Trends Genet.* 24, 133-141, (2008).

[47] Le, T. T., Harlepp, S., Guet, C. C., Dittmar, K., Emonet, T. *et al.* **Real-time RNA profiling within a single bacterium.** *Proc. Natl. Acad. Sci. U. S. A.* 102, 9160-9164, (2005).

[48] Levsky, J. M., Shenoy, S. M., Pezo, R. C. & Singer, R. H. **Single-cell gene expression profiling.** *Science* 297, 836-840, (2002).

[49] Al-Amoudi, A., Chang, J.-J., Leforestier, A., McDowall, A., Salamin, L. M. *et al.* **Cryo-electron microscopy of vitreous sections.** *EMBO J.* 23, 3583-3588, (2004).

[50] Rubakhin, S. S., Romanova, E. V., Nemes, P. & Sweedler, J. V. **Profiling metabolites and peptides in single cells.** *Nat. Methods* 8, S20-29, (2011).

[51] Rubakhin, S. S. & Sweedler, J. V. **Quantitative measurements of cell-cell signaling peptides with single-cell MALDI MS.** *Anal. Chem.* 80, 7128-7136, (2008).

[52] Waanders, L. F., Chwalek, K., Monetti, M., Kumar, C., Lammert, E. *et al.* **Quantitative proteomic analysis of single pancreatic islets.** *Proc. Natl. Acad. Sci. U. S. A.* 106, 18902-18907, (2009).

[53] Zhang, H. & Jin, W. **Single-cell analysis by intracellular immuno-reaction and capillary electrophoresis with laser-induced fluorescence detection.** *J. Chromatogr. A* 1104, 346-351, (2006).

[54] Bouchet-Marquis, C. & Hoenger, A. **Cryo-electron tomography on vitrified sections: a critical analysis of benefits and limitations for structural cell biology.** *Micron* 42, 152-162, (2011).

[55] Henderson, G. P., Gan, L. & Jensen, G. J. **3-D ultrastructure of *O. tauri*: electron cryotomography of an entire eukaryotic cell.** *PloS ONE* 2, e749, (2007).

[56] Medalia, O., Beck, M., Ecke, M., Weber, I., Neujahr, R. *et al.* **Organization of actin networks in intact filopodia.** *Curr. Biol.* 17, 79-84, (2007).

[57]   Sun, X. & Jin, W. **Catalysis-electrochemical determination of zeptomole enzyme and its application for single-cell analysis.** *Anal. Chem.* 75, 6050-6055, (2003).

[58]   Ni, Q., Titov, D. V. & Zhang, J. **Analyzing protein kinase dynamics in living cells with FRET reporters.** *Methods* 40, 279-286, (2006).

[59]   Heinemann, M. & Zenobi, R. **Single cell metabolomics.** *Curr. Opin. Biotechnol.* 22, 26-31, (2011).

[60]   Masujima, T. **Live single-cell mass spectrometry.** *Anal. Sci.* 25, 953-960, (2009).

[61]   Wurm, M., Schöpke, B., Lutz, D., Müller, J. & Zeng, a.-P. **Microtechnology meets systems biology: the small molecules of metabolome as next big targets.** *J. Biotechnol.* 149, 33-51, (2010).

[62]   Kovarik, M. L. & Allbritton, N. L. **Measuring enzyme activity in single cells.** *Trends Biotechnol.* 29, 222-230, (2011).

[63]   Nielsen, L. J., Olsen, L. F. & Ozalp, V. C. **Aptamers embedded in polyacrylamide nanoparticles : A tool for *in vivo* metabolite sensing.** *ACS Nano* 4, 4361-4370, (2010).

[64]   Okumoto, S. **Imaging approach for monitoring cellular metabolites and ions using genetically encoded biosensors.** *Curr. Opin. Biotechnol.* 21, 45-54, (2010).

[65]   Whitmore, C. D., Olsson, U., Larsson, E. A., Hindsgaul, O., Palcic, M. M. *et al.* **Yoctomole analysis of ganglioside metabolism in PC12 cellular homogenates.** *Electrophoresis* 28, 3100-3104, (2007).

[66]   Zong, C., Lu, S., Chapman, a. R. & Xie, X. S. **Genome-wide detection of single-nucleotide and copy-number variations of a single human cell**. *Science* 338, 1622-1626, (2012).

[67]   Metzker, M. L. **Sequencing technologies - the next generation.** *Nat. Rev. Genet.* 11, 31-46, (2010).

[68]   Dunn, W. B. **Mass spectrometry in systems biology an introduction.** *Methods Enzymol.* 500, 15-35, (2011).

[69]   Benesch, J. L. P. & Robinson, C. V. **Mass spectrometry of macromolecular assemblies: preservation and dissociation.** *Curr. Opin. Struct. Biol.* 16, 245-251, (2006).

[70]   Hernández, H. & Robinson, C. V. **Determining the stoichiometry and interactions of macromolecular assemblies from mass spectrometry.** *Nat. Protoc.* 2, 715-726, (2007).

[71] Han, X., Aslanian, A. & Yates, J. R. **Mass spectrometry for proteomics.** *Curr. Opin. Chem. Biol.* 12, 483-490, (2008).

[72] Gstaiger, M. & Aebersold, R. **Applying mass spectrometry-based proteomics to genetics, genomics and network biology.** *Nat. Rev. Genet.* 10, 617-627, (2009).

[73] Bantscheff, M., Schirle, M., Sweetman, G., Rick, J. & Kuster, B. **Quantitative mass spectrometry in proteomics: a critical review.** *Anal. Bioanal. Chem.* 389, 1017-1031, (2007).

[74] Martens, L. **Bioinformatics challenges in mass spectrometry-driven proteomics** in: Gel-Free Proteomics, *Methods in Molecular Biology*, Vol. 753, 359-371, Humana Press, (2011).

[75] Dovichi, N. J., Hu, S., Michels, D., Mao, D. & Dambrowitz, A. **Single Cell Proteomics** in: Proteomics for Biological Discovery, Ch. 12, 225-245, John Wiley & Sons, Inc., (2006).

[76] Beck, M., Claassen, M. & Aebersold, R. **Comprehensive proteomics.** *Curr. Opin. Biotechnol.* 22, 3-8, (2011).

[77] Picotti, P., Bodenmiller, B., Mueller, L. N., Domon, B. & Aebersold, R. **Full dynamic range proteome analysis of *S. cerevisiae* by targeted proteomics.** *Cell* 138, 795-806, (2009).

[78] Kühner, S. E. A. **Proteome organization in a genome-reduced bacterium**. *Science* 326, 1235-1240, (2009).

[79] Nickell, S., Kofler, C., Leis, A. P. & Baumeister, W. **A visual approach to proteomics**. *Nat. Rev. Mol. Cell Biol.* 7, 225-230, (2006).

[80] Dubochet, J., Adrian, M., Chang, J. J., Homo, J. C., Lepault, J. *et al.* **Cryo-electron microscopy of vitrified specimens.** *Q. Rev. Biophys.* 21, 129-228, (1988).

[81] Ben-Harush, K., Maimon, T., Patla, I., Villa, E. & Medalia, O. **Visualizing cellular processes at the molecular level by cryo-electron tomography.** *J. Cell Sci.* 123, 7-12, (2010).

[82] Lucić, V., Förster, F. & Baumeister, W. **Structural studies by electron tomography: from cells to molecules.** *Annu. Rev. Biochem.* 74, 833-865, (2005).

[83] Best, C., Nickell, S. & Baumeister, W. **Localization of protein complexes by pattern recognition.** *Methods Cell Biol.* 79, 615-638, (2007).

[84]   Beck, M., Topf, M., Frazier, Z., Tjong, H., Xu, M. *et al.* **Exploring the spatial and temporal organization of a cell's proteome.** *J. Struct. Biol.* 173, 483-496, (2011).

[85]   Yahav, T., Maimon, T., Grossman, E., Dahan, I. & Medalia, O. **Cryo-electron tomography: gaining insight into cellular processes by structural approaches.** *Curr. Opin. Struct. Biol.* 21, 670-677, (2011).

[86]   Beck, M., Malmström, J. a., Lange, V., Schmidt, A., Deutsch, E. W. *et al.* **Visual proteomics of the human pathogen *Leptospira interrogans*.** *Nat. Methods* 6, 817-823, (2009).

[87]   Leis, A., Rockel, B., Andrees, L. & Baumeister, W. **Visualizing cells at the nanoscale.** *Trends Biochem. Sci.* 34, 60-70, (2009).

[88]   Kireev, I., Lakonishok, M., Liu, W., Joshi, V. N., Powell, R. *et al.* ***In vivo* immunogold labeling confirms large-scale chromatin folding motifs**. *Nat. Methods* 5, 311-313, (2008).

[89]   Diebolder, C. A., Koster, A. J. & Koning, R. I. **Pushing the resolution limits in cryo electron tomography of biological structures.** *J. Microsc.* 248, 1-5, (2012).

[90]   Mader, A., Elad, N. & Medalia, O. **Cryoelectron tomography of eukaryotic cells.** *Methods Enzymol.* 483, 245-265, (2010).

[91]   Hoenger, A. & Bouchet-Marquis, C. **Cellular tomography.** *Adv. Protein Chem. Struct. Biol.* 82, 67-90, (2011).

[92]   Al-Amoudi, A., Studer, D. & Dubochet, J. **Cutting artefacts and cutting process in vitreous sections for cryo-electron microscopy.** *J. Struct. Biol.* 150, 109-121, (2005).

2 "Lyse and spread" visual proteomics

2.1 Framework and objective of this thesis

The work presented in this thesis was carried out in the framework of a project that aims to establish an alternative and complementary approach to single cell proteomics. An overview of the overall project, concerning its major concepts, ongoing work and future plans, is given in this section. The objective of this thesis was to develop, evaluate and establish the basic microfluidic modules of the new sample preparation pipeline described below.

2.2 The basic idea

A new approach to visual proteomics based on lossless sample deposition and scanning transmission electron microscopy (STEM) was proposed in 2009 [1]. STEM offers the possibility to determine the mass of single biomacomolecules in heterogeneous samples [2] and to directly correlate this information to the size and the shape of the investigated particle [3]. Consequently, STEM is as an ideal instrument to aid protein identification. The new visual proteomics method was suggested to complement both proteomic studies by ET and the various sectioning techniques used in EM as well as to work in synergy with MS [1,4]. The basic idea of the approach is to lyse individual eukaryotic cells and spread their cellular components onto EM grids in a lossless manner. Microfluidic technologies were proposed as a suitable toolbox to implement the required sample preparation workflow, from cell lysis to sample deposition. A microfluidic sample preparation procedure offers the potential to provide samples of single cell proteomes that are suitable for structural analysis by negative stain TEM and mass analysis by STEM and MS. Subsequent data analysis aims to link the information about structure and mass and, thereby, provide additional information to characterize the proteome and interactome of single cells and detect variations between cells.

2.3 The overall research concept

The objective and scope of the overall project is to establish a new visual approach to analyze the proteome of a single cell based on the idea outlined above. The implementation includes the development of a microfluidic pipeline to prepare single cell samples for the analysis of their protein content by negative stain TEM, STEM, MS and other techniques. The

microfluidic setup and its control software must be easily adaptable to semi-automated high-throughput operation. Similarly, data acquisition must utilize existing and/or newly developed semi-automated high-throughput methods in the future. Ensuing data acquisition, registration and analysis is envisaged to result in correlative datasets facilitating data interpretation and providing new insights into the proteome of single eukaryotic cells.
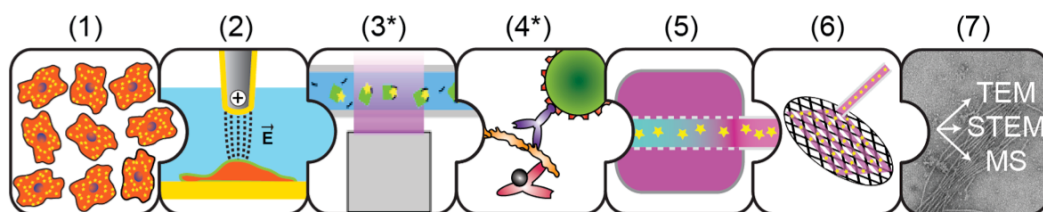
2.3.1   The microfluidic pipeline

Figure 2-1: *Schematic representation of the microfluidic pipeline showing the basic and optional (*) modules. (1) Cell culturing module: Adherent eukaryotic cell cultures are grown on a transparent support that allows LM observation. (2) Single-cell lysis module: Individual cells growing on a transparent and functionalized conductive layer can be targeted and lysed by a microcapillary electrode. After cell lysis all the cellular components can be aspirated into the microcapillary. (3) Crosslinking module (optional): A generic crosslinking reaction that can be triggered by light to stabilize weak interactions in protein complexes. (4) Protein separation module (optional): Two different strategies can be applied to reduce the complexity of the sample. First, a generic approach to introduce some kind of order into complex samples, e.g., CE or LC (not shown). Second, a targeted approach to fish out specific proteins with antibodies and label them for quantitative EM. (5) Conditioning module: Microdyalysis can be used to condition the sample for a specific analysis method, e.g., desalting for STEM, mixing with negative stain for TEM or mixing with matrix for MALDI-MS. (6) Hand-over module: A microcapillary can be used to micropattern sub-microliter sample volumes onto EM grids or other sample carriers. (7) Data acquisition by TEM, STEM or MS.*

The aim is to develop a modular and versatile pipeline (Fig. 2-1, modules 1-6), utilizing microfabrication as well as microfluidic and microcapillary techniques, to couple live cell imaging and single cells lysis to various sample preparation methods for different analysis techniques. The invasive approach of cell lysis will offer straightforward access to the cellular content and the potential to combine microfluidic modules for the implementation of sample preparation steps such as crosslinking, separation, labelling, conditioning and hand-over. The modules 1, 2, 5 and 6 have been developed during the course of this thesis and first concept studies for module 3 have been performed.

To date many platforms manipulate cells in flow-through configurations and thus depend on the cells being in suspension [5]. Consequently, these devices are not well suited to the use of standard adherent cell cultures or living tissue, as the cells have to be detached or otherwise extracted for further processing. Evaluating existing single cell lysis techniques [6] according to their ability to target individual adherent cells *in situ*, in particular eukaryotic cells, indicates that electroporation is the most suitable approach. The use of a freely positionable microcapillary electrode allows individual cells of adherent cultures grown on a conductive support to be targeted from the top, and permits fast and tunable cell lysis and sample aspiration [7,8]. Attached cells can be grown in confined areas on a transparent conductive layer, using standard cell culturing techniques (module 1). This allows the lysis and aspiration procedure to be monitored from below by optical microscopy (module 2). Moreover the implementation of this approach on an inverted optical microscope offers the possibility for long-term live cell imaging, fluorescence based experiments and the correlation of LM information with the subsequently derived EM or MS data from the lysate. For the preparation of the collected minute sample volumes the combination of up to four other pipeline modules is foreseen (modules 3–6). The optional crosslinking module (module 3) will be employed to stabilize and conserve weak interactions between proteins if needed. Ideally this stabilization step will feature a fast and generic crosslinking process that can be triggered at a specific time point. Light inducible reactions offer the greatest potential to be integrated into the microfluidic pipeline and several possible candidates have been identified and are being investigated in terms of integrability [9,10]. The second optional module (module 4) aims to reduce the complexity of the sample. This protein separation module will provide targeted and/or unbiased methods to separate the proteins and protein complexes present. A targeted approach is geared towards the extraction of a specific protein from complex samples for quantitative EM analysis. The procedure being developed is based on antibodies immobilized on trapped magnetic beads via a photocleavable crosslinker [11]. This will enable the extraction and recovery of untagged proteins from crude cell lysate. Furthermore the captured target protein offers the possibility to fish for potential binding partners and an additional labeling step can be applied to aid their detection and identification. Other techniques that introduce some kind of order into complex protein mixtures without *a priori* knowledge, e.g., CE and LC, also have the potential to be integrated at this position in the pipeline. The nature of the following conditioning step depends on the desired analysis method. Thus the sample-conditioning module (module 5) is designed to be adaptable to meet a range of requirements. It utilizes micro-dialysis in a flow-through configuration. The

principle of dialysis offers the variability to realize various sample conditioning strategies and without loss and dilution. A hollow micro-dialysis fiber, passing through a reservoir, allows dialysis of the flowing sample against a buffer in the reservoir. This conditioning module can be used to mix the sample with negative stain solution for TEM analysis or to desalt the sample for STEM mass measurements. Moreover it offers the potential to produce MS samples by dialysis against a matrix solution for subsequent MALDI experiments. In a final step before the analysis the processed sample has to be transferred to a sample carrier. The handover module (module 6) is designed to efficiently deposit minute sample volumes onto sample carriers such as EM grids or MS targets. An effective and unbiased sample transfer is essential to address complex and/or low concentration samples like in SCA. Therefore the deposition approach is geared to distribute and dry down submicrolitre volumes of preprocessed sample, to circumvent further processing steps, such as washes or blotting, after application to the sample carrier. The procedure aims to increase the sample transfer efficiency and prevent preferential adsorption, which can distort the representation of the sample constituents on the sample carrier.

The microfluidic pipeline outlined above will provide a new sample preparation approach for the analysis of single eukaryotic cells based on TEM and STEM analysis. Combination with LM as well as the feasibility to adapt the sample preparation and sample carriers to different analytical techniques will facilitate data correlation and interpretation. Importantly, the modularity of the pipeline not only provides the opportunity to use different module combinations, but also allows the straightforward integration of additional modules to expand the potential applications.

2.3.2 Instrument control and data registration

The goal of making high-throughput correlative measurements demands a software framework that allows data-registration and storage in a generalized and coordinated way. The software developed to meet these demands, openBEB[1], is plugin-based and used for instrument control as well as for raw-data registration, [11]. This software is designed to allow easy integration of existing or new instrument modules and fast annotation and visualization of raw data. A macro language, exhibiting an open modular structure, allows the control and coordination of the individual independent pipeline modules and parallel processes. Furthermore, openBEB complements openBIS[2] a robust and scalable database system developed for

---

[1] open Biology Experiment Browser; see: www.openBEB.org

[2] open Biology Information System; see: http://www.cisd.ethz.ch/software/openBIS

experimental systems-biology [12]; the local cache of the experimental data maintained by openBEB can be directly synchronized with openBIS.

2.3.3 Proteomic data acquisition

Structural investigations can be performed on negatively stained samples imaged with a TEM. In conjunction with various image processing techniques, this method allows to obtain structural details and 3D information of proteins or protein complexes down to about 20Å [13]. Moreover a microscope equipped with a 96 EM grid revolver [14] can be used for semi-automated high-throughput imaging of separated and/or labeled negatively stained samples, adding the possibility for quantitative studies [15]. Mass measurements can be performed either by STEM or MS. STEM allows the mass of individual proteins (>100kDa) and protein complexes to be determined and links this mass information to the shape of their 2D projections [16]. This mass-to-shape relationship may prove essential to link more accurate mass determination by MS to the structural information obtained from negatively stained samples [4].

2.3.4 Data analysis

The data analysis required for visual proteomics will be developed stepwise, initially focusing on one or a few target proteins or complexes, known to be involved in a specific process *a priori*. The interpretation of the raw data is expected to be possible directly, without any further data processing, either because the structure of the targets is distinctive or by the labeling techniques presently under development (module 4). However, for a throughout detection and a precise quantification an automatic detection of target structures must be established. This software will be developed in python and, whenever possible, will use existing software solutions, such as EMAN2 [17] or MolMatch [18]. Visual proteomics assigns structures by feature or template matching. Similar methods were originally developed for the visual proteomics analysis of electron microscopy tomograms of small cells [19,20] and will be adapted and extended in the future. Labeling techniques, performed directly in the cell lysate or using the protein-separation module (module 4) will complement this image analysis and confirm the assignments made (Fig. 2-2, pathway A).

The following procedure will be used to search for target proteins in the raw data (Fig. 2-2, pathway B): (i) Target selection: Specific target proteins and their ultrastructures will be selected. All available information about the stability, structure, structural variation and changes of oligomeric state will be catalogued for each. (ii) Assemble template galleries: Structural

information for every target protein or protein complex, respectively, will be collected and used to calculate projections, which will be stored as template galleries. Such templates can be calculated from atomic coordinate files (PDBs) or obtained from available EM structures (eg., structures can be obtained from the EMDB data base[3]); the available 3D information will be carefully normalized before the required projection gallery is determined. These libraries and galleries will be organized so that they can be managed by openBEB and stored and visualized by openBIS over an internet browser. (iii) Template Matching: Templates from the galleries will be cross-correlated with EM images of the cell lysate to search for similar regions. The correlation pattern will be normalized and thresholded to define regions of interest (ROIs). A ROI will be allotted to the template with the highest cross-correlation coefficient and thus assigned to a specific protein. (iv) Figure of Merit: The template assignment will be characterized by scoring the match; the algorithms required for this will be developed.

The targeted approach outlined above is the most simple, and different strategies will be needed for discovery driven experiments. The images could first be segmented, eg. by a hierarchical image segmentation [21,22], to extract protein-complexes and particles belonging to different size ranges. These segmented objects could then be classified according to their size and shape. Subsequently, particles belonging to a specific class could be averaged to obtain a higher SNR for template matching (Fig. 2-2, pathway C). Further, the lower resolution mass-linked shape information obtained by STEM of unstained samples could be correlated to the class averages obtained by negative stain TEM of corresponding samples, to aid protein identification. This pathway does not need *a priori* information and offers the possibility to detect *de novo* components associated with the biological experiment.

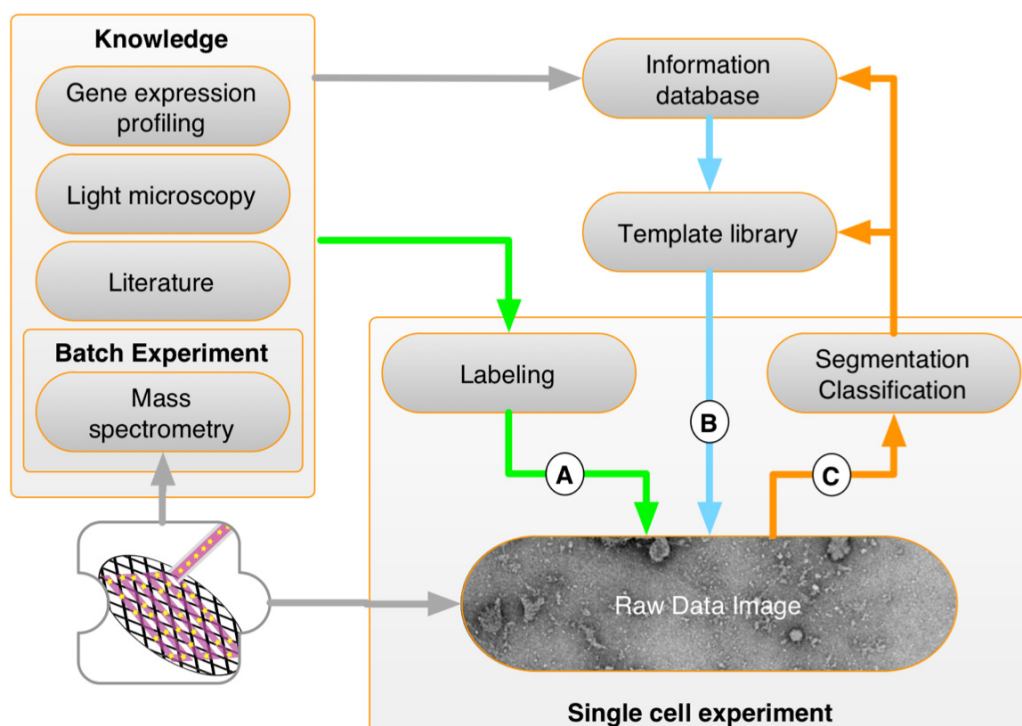[3] EM Data Bank; see: http://emdatabank.org/

Figure 2-2: *General overview of possible data-analysis pathways in "lyse and spread" visual proteomics. (A) Green: labeling techniques can be used to identify proteins in the cell lysate. (B) Blue: A visual template library can be built from existing knowledge. This library can be used to scan raw images for these known structures. (C) Orange: The raw-image is segmented, and the individual structures are aligned and classified during several rounds. Averages of the classification classes are obtained and can be compared to known structures.*

2.4 References

[1]   Engel, A. **Scanning transmission electron microscopy: Biological applications** in: Advances in Imaging and Electron Physics, Vol. 159, Ch. 9, 357-386, Elsevier Inc., (2009).

[2]   Engel, A. **Molecular weight determination by scanning transmission electron microscopy**. *Ultramicroscopy* 3, 273-281, (1978).

[3]   Müller, S. A., Aebi, U. & Engel, A. **What transmission electron microscopes can visualize now and in the future.** *J. Struct. Biol.* 163, 235-245, (2008).

[4]   Engel, A. **Assessing biological samples with scanning probes** in: Single Molecule Spectroscopy in Chemistry, Physics and Biology, *Springer Series in Chemical Physics.*, Vol. 96, Ch. 21, 417-431, Springer, Berlin Heidelberg, (2010).

[5]   Yun, H., Kim, K. & Lee, W. G. **Cell manipulation in microfluidics.** *Biofabrication* 5, 022001, (2013).

[6]   Brown, R. B. & Audet, J. **Current techniques for single-cell lysis.** *J. R. Soc. Interface* 5, S131-138, (2008).

[7]   Han, F., Wang, Y., Sims, C. E., Bachman, M., Chang, R. *et al.* **Fast electrical lysis of cells for capillary electrophoresis.** *Anal. Chem.* 75, 3688-3696, (2003).

[8]   Nashimoto, Y., Takahashi, Y., Yamakawa, T., Torisawa, Y.-S., Yasukawa, T. *et al.* **Measurement of gene expression from single adherent cells and spheroids collected using fast electrical lysis.** *Anal. Chem.* 79, 6823-6830, (2007).

[9]   Fancy, D. A. & Kodadek, T. **Chemistry for the analysis of protein–protein interactions: rapid and efficient cross-linking triggered by long wavelength light**. *Proc. Natl. Acad. Sci. U. S. A.* 96, 6020-6024, (1999).

[10]   Gomes, A. F. & Gozzo, F. C. **Chemical crosslinking with a diazirine photoactivatable crosslinker investigated by MALDI and ESI MS/MS**. *J. Mass Spectrom.* 45, 892-899, (2010).

[11]   Ramakrishnan, C., Bieri, A., Enimanev, K., Stahlberg, H., Rinn, B. *et al.* **openBEB: Open biological experiment browser for correlative measurements.** *Manuscript under revision*, (2013).

[12]   Bauch, A., Adamczyk, I., Buczek, P., Elmer, F.-J., Enimanev, K. *et al.* **openBIS: a flexible framework for managing and analyzing complex data in biology research.** *BMC Bioinformatics* 12, 468, (2011).

[13]   Ohi, M., Li, Y., Cheng, Y. & Walz, T. **Negative staining and image classification - powerful tools in modern electron microscopy.** *Biol. Proced. Online* 6, 23-34, (2004).

[14]   Coudray, N., Hermann, G., Caujolle-Bert, D., Karathanou, A., Erne-Brand, F. *et al.* **Automated screening of 2D crystallization trials using transmission electron microscopy: a high-throughput tool-chain for sample preparation and microscopic analysis.** *J. Struct. Biol.* 173, 365-374, (2011).

[15]   Giss, D., Kemmerling, S., Dandey, V., Stahlberg, H. & Braun, T. **Exploring the Interactome: Microfluidic Isolation of Proteins and Interacting Partners for Quantitative Analysis by Electron Microscopy.** *Manuscript in preparation*, (2013).

[16]   Müller, S., Wolpensinger, B., Angenitzki, M., Engel, A., Sperling, J. *et al.* **A supraspliceosome model for large nuclear ribonucleoprotein particles based on mass determinations by scanning transmission electron microscopy**. *J. Mol. Biol.* 283, 383-394, (1998).

[17]   Tang, G., Peng, L., Baldwin, P. R., Mann, D. S., Jiang, W. *et al.* **EMAN2: an extensible image processing suite for electron microscopy**. *J. Struct. Biol.* 157, 38-46, (2007).

[18]   Förster, F. **Quantitative Analysis of Macromolecules in Cryoelectron Tomograms using Correlation Methods** Dissertation, Technical University of Munich, Munich, (2005).

[19]   Förster, F., Han, B.-G. & Beck, M. **Visual proteomics.** *Methods Enzymol.* 483, 215-243, (2010).

[20]   Lucić, V., Förster, F. & Baumeister, W. **Structural studies by electron tomography: from cells to molecules.** *Annu. Rev. Biochem.* 74, 833-865, (2005).

[21]   Adiga, U., Baxter, W. T., Hall, R. J., Rockel, B., Rath, B. K. *et al.* **Particle picking by segmentation: a comparative study with SPIDER-based manual particle picking.** *J. Struct. Biol.* 152, 211-220, (2005).

[22]   Coudray, N., Buessler, J.-l., Kihl, H. & Urban, J.-p. **Multi-scale and First Derivative Analysis for Edge Detection in TEM Images.** in: A Campilho & M Kamel eds. ICIAR, *LNCS*, Vol. 4633, 1005-1016, Springer-Verlag Berlin Heidelberg, (2007).

3   Connecting μ-fluidics to electron microscopy

Connecting μ-fluidics to electron microscopy

Simon Kemmerling[1], Jörg Ziegler[1], Gabriel Schweighauser[1], Stefan A. Arnold[1],
Dominic Giss[1], Shirley A. Müller[1], Philippe Ringler[1], Kenneth N. Goldie[1],
Nils Goedecke[2], Andreas Hierlemann[2], Henning Stahlberg[1], Andreas Engel[1,3]
and Thomas Braun[1,*]

[1] Center for Cellular Imaging and Nano Analytics (C-CINA), Biozentrum, Universität Basel, Basel, Switzerland

[2] Bio Engineering Laboratory (BEL), Department of Biosystems Science and Engineering (D-BSSE), ETH Zurich, Basel, Switzerland

[3] Department of Pharmacology, Case Western Reserve University, Cleveland, USA

* Corresponding Author: thomas.braun@unibas.ch

Keywords: Electron microscopy, microfluidics, single-molecule analysis, mass and shape, systems biology

3.1 Abstract

A versatile methodology for electron microscopy (EM) grid preparation enabling total content sample analysis is presented. A microfluidic-dialysis conditioning module to desalt or mix samples with negative stain solution is used, combined with a robotic writing table to micro-pattern the EM grids. The method allows heterogeneous samples with minute volumes to be processed at physiological pH for structure and mass analysis, and allows the preparation characteristics to be finely tuned.

3.2 Introduction

Systems biology aims to quantify the molecular elements of a biological system, to determine their interactions and to integrate this information into network models [1]. The development of comprehensive models requires experimental information about the spatial and temporal arrangements of the network components as well as their structure, a challenge that required a multi-resolution approach and the combination of different techniques [2,3]. Cryo-electron tomography (cryo-ET) is the ultimate technique to reveal the spatial organisation of protein structures and macromolecular complexes in single cells [4,5]. Currently cryo-ET is restrained by several limitations, such as the size of the cell that can be analysed (maximum diameter of ~2 μm) [6], and by problems in data segmentation and in the template matching required for protein recognition (restricted to relatively large protein complexes) [7]. Indeed, many target structures can only be recognised if labelled with electron-dense markers [8], which, despite recent progress [9], often involves harsh preparative treatment of the cells. Furthermore, while ET delivers structural and spatial information, correlation of these with other methods such as mass spectroscopy (MS) [10] is difficult. A complementary approach is to physically lyse the cells and to subsequently write the entire sample onto electron microscopy (EM) grids for structure analysis by transmission EM (TEM), or mass analysis by scanning TEM (STEM). Ultimately, the use of microfluidic techniques offers the potential to analyse a single cell by making it possible to investigate protein ultrastructures and membrane fragments in lysates [11].

Here we present a lossless sample deposition method for EM (Fig. 3-1), which allows the handling of minute sample volumes and immobilization of the total sample content on EM grids to obtain, for example, the full cell inventory. This methodology is combined with a microfluidic sample-conditioning module. The constellation provides a new staining technique for

heavy metal salts (negative stain) for TEM as well as specific desalting for mass measurements by STEM.
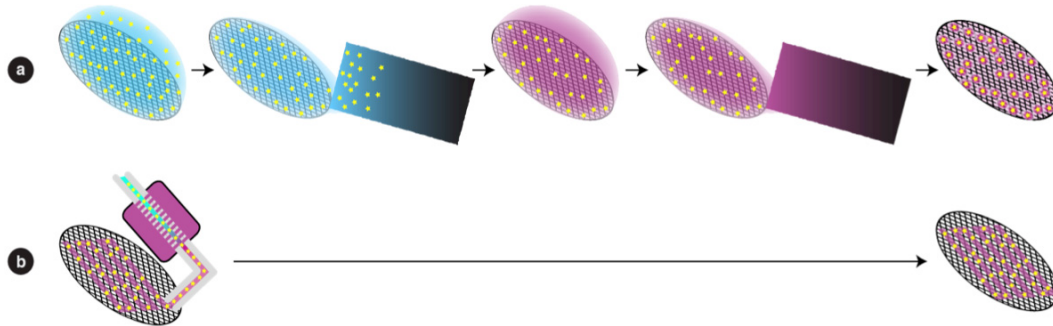

Figure 3-1: *Principles of negative staining for EM. (a) Classical negative staining by hand: The sample is absorbed to the carbon film of an EM grid and the grid is blotted to remove the excess sample solution. The absorption time and the specific absorption properties of the sample components determines the fraction of the sample that is immobilized. A wash and blot cycle sometimes follows (not shown). The grid is then incubated with the negative stain solution of choice, followed by another blotting step to remove excess stain solution. The grid is left to air-dry before investigation in the electron microscope. With this method only a specific sub-fraction of the sample is immobilized on the grid. (b) The here developed microfluidic negative staining approach: A very small amount (0.1-0.3 μl) of stain-mixed sample is applied to the grid via a nozzle of 50 μm inner diameter. The grid is then air-dried without any blotting. With this method the entire sample is immobilized on the grid. Additionally, the micro-precision of the writing process allows a meander-type micro-pattern of stained sample to be created on the carbon film.*

3.3 Materials and Methods

3.3.1 Stain preparation

The reservoir of the sample-conditioning module (Fig. 3-2a) was filled with different commonly used negative stains prepared in the following way: *Phosphothungstic acid (PTA$_{7.0}$)*: Sodium-phosphotungstate tribasic hydrate (Riedel-de Haen, Switzerland) was dissolved in double-distilled water (ddH$_2$O) to give a 1% or 2% (w/v) final concentration. The pH of the aqueous solution was adjusted to 7.0 using 1M potassium hydroxide; *Ammonium molybdate (AM$_{6.5}$)*: Ammonium molybdate (Aldrich, Switzerland) was dissolved in ddH$_2$O to give a aqueous solution with a final concentration of 0.5% (w/v) at pH 6.5; *NanoVan® (NV$_{8.0}$)*: The 2% ready to use methylamine vanadate (Nanoprobes, USA) solution at pH 8.0 was diluted with ddH$_2$O to give a final concentration of 1% (w/v*); NanoW® (NW$_{6.8}$)*: The 2% ready to use methylamine tungstate (Nanoprobes, USA) solution at pH 6.8 was diluted with ddH$_2$0 to give a final concentration of 1% (w/v); *Uranyl acetate (UA$_{4.5}$)*:

Uranyl acetate was dissolved in ddH$_2$O to give a final concentration of 0.25% (w/v) at pH 4.5; *Buffered uranyl acetate (UA$_{7.0}$)*: To prepare UA at pH 7, the above 0.25% (w/v) uranyl acetate solution was mixed with an equal volume of a 20 mM oxalic acid solution. The pH was adjusted using 3% ammonium hydroxide, added slowly while stirring [12]. This resulted in a 0.12% UA solution at pH 7.0.

3.3.2   Test samples

Several samples were used for the initial tests and as a proof of concept: The chosen test samples apoferritin (AF; from equine spleen; Sigma, Switzerland) and tobacco mosaic virus (TMV; kindly supplied by Ruben Diaz-Avalos, New York Structural Biology Center, USA) are well characterized, and TMV is used as a standard for mass calibration in scanning transmission electron microscopy (STEM). The used test-samples were composed as follows: (1) A mixture of 0.05 mg/ml AF and 0.1 mg/ml TMV in phosphate buffered saline pH 7.4 (PBS; P4417, Sigma-Aldrich, Switzerland). (2) 0.05 mg/ml AF in PBS. (3) 0.1 mg/ml TMV in quartz-ddH$_2$O. (4) Baby Hamster Kidney (BHK) cell lysate in PBS (see next section).

3.3.3   BHK cell culture and lysis

Attached Baby Hamster Kidney (BHK21; ECACC 85011433) cells were grown for 48 h in a polystyrene T75-flask containing 30 ml of DHI-5 medium (see end of section) at 37 °C, 100% air humidity, and 5% CO$_2$. To harvest the cells the medium was removed and the flask was washed with 7 ml of PBS. To detach the cells from the flask surface, 3 ml of trypsin-EDTA were added and the cells were incubated for 5 min at 37 °C. Afterwards, 7 ml of DHI-5 medium were added and the detached cells were mixed using a pipet. 0.5 ml of the cell suspension was left in the flask and again incubated with 30 ml of fresh media for 48 h to obtain the next batch. The rest of the cell suspension was centrifuged twice and washed with PBS (48 g, 2 min). The pellet was dissolved in 2 ml of PBS. In an Eppendorf tube 200 µl of this cell suspension were further diluted with 800 µl of PBS and the cells were lysed by sonification for 2 min at 25 kHz while cooling.

DHI-5 medium is a mixture of DMEM (Dulbecco`s Modified Eagels Medium; D6171, Sigma, Switzerland), HamF12 (Nutrient Mixture F-12Ham; N8641, Sigma, Switzerland), and IMDM (Iscove`s Modified Dulbecco`s Medium, I3390, Sigma, Switzerland) media (1:1:2), supplemented with 5% FCS (Fetal Bovine Serum, E7524, Sigma, Switzerland) and complemented with non essential amino acids (MEM Non essential amino acid solution, M7145, Sigma, Switzerland), L-glutamine (L-Glutamine Solution, G7513,

Sigma, Switzerland) and Vitamins (RPMI1640 Vitamins Solution, R7256, Sigma, Switzerland).

3.3.4 Microfluidic setup

Samples were specifically treated and then deposited on carbon films covering 200 and 400 mesh Ni-TEM grids or on the special grids used for mass measurement (see below). This was achieved using a custom-built modular microfluidic setup (Fig. 3-2a) consisting of a syringe pump, a 10-port 2-position valve, a custom-built sample conditioning module, a custom-built hand-over module, with functionalized nozzle, xyz-stage and several HPLC consumables (fused silica capillaries, PTFE tubing and connectors; BGB-analytic, Switzerland). The whole system is driven by the syringe pump (KDS210; Ismatec SA, Switzerland) and the sample is injected via a sample loop on the valve (Valco 10-port 2-position valve; BGB-analytic, Switzerland). All electronic components of the apparatus are controlled by a LabView-based custom-made software system (supp. Fig. 3-1), which features a macro language for flexible automation by coordination of the different modules. On request we will provide the software and the construction plans.

3.3.5 Sample-conditioning module

The sample-conditioning module consists of a custom-build reservoir that holds about 5 ml of solution (dialysis reservoir); either stain solution (for negative stain TEM) or 100 mM ammonium acetate prepared using quartz-ddH$_2$0 (desalting). About 10-12 cm of a 13 kDa cut off cellulose fiber (Spectra/Pro® microdialysis fibers ID=200 µm; Spectrum Laboratories, USA) that holds 3-4 µl of sample at one time spans this reservoir. When the sample is pumped through this conditioning module at a rate of 2 µl/min, the dialysis time is about 2 min.

3.3.6 Hand-over module and grid preparation

The hand-over module deposits sub-microlitre sample volumes on EM grids by contact writing and can be programmed to automatically prepare a series of grids. The Ni-TEM grids are held in place by magnets and their carbon films are activated with atmospheric pressure helium cold-plasma (piezobrush® PZ1, Polyscience AG Switzerland) immediately before sample application. Initial tests showed that a 4 sec treatment at a distance of 1 cm from the plasma source gives comparable results to the conventional glow discharge [13], without destroying of the carbon film. A fully controllable micro-mechanical device (Physik Instrumente xyz micro-precision translation stages; Dyneos AG, Switzerland) brings a thin nozzle that is connected by micro-capillaries to the sample-conditioning module, in close

proximity to the EM grid (Fig. 3-2b). After liquid contact, the grids are moved under the nozzle with sub-micrometer precision to create a micro-pattern of the sample on carbon in the form of a thin wet film. In this way 0.1-0.3 µl of stained or specifically desalted sample are 'written' on the grid, which is then air-dried. The degree of wetting obtained can be tuned by modifying the plasma treatment, and the writing can be optimized for the sample by adjusting the writing parameters. A defined combination of grid hydrophobicity (defined by plasma treatment parameters), writing speed, and surface tension of the applied solution (can be changed by the addition with ethanol traces), allowed a continuous line about 13 mm long and 200 to 300 µm wide to be written (Fig. 3-2c).
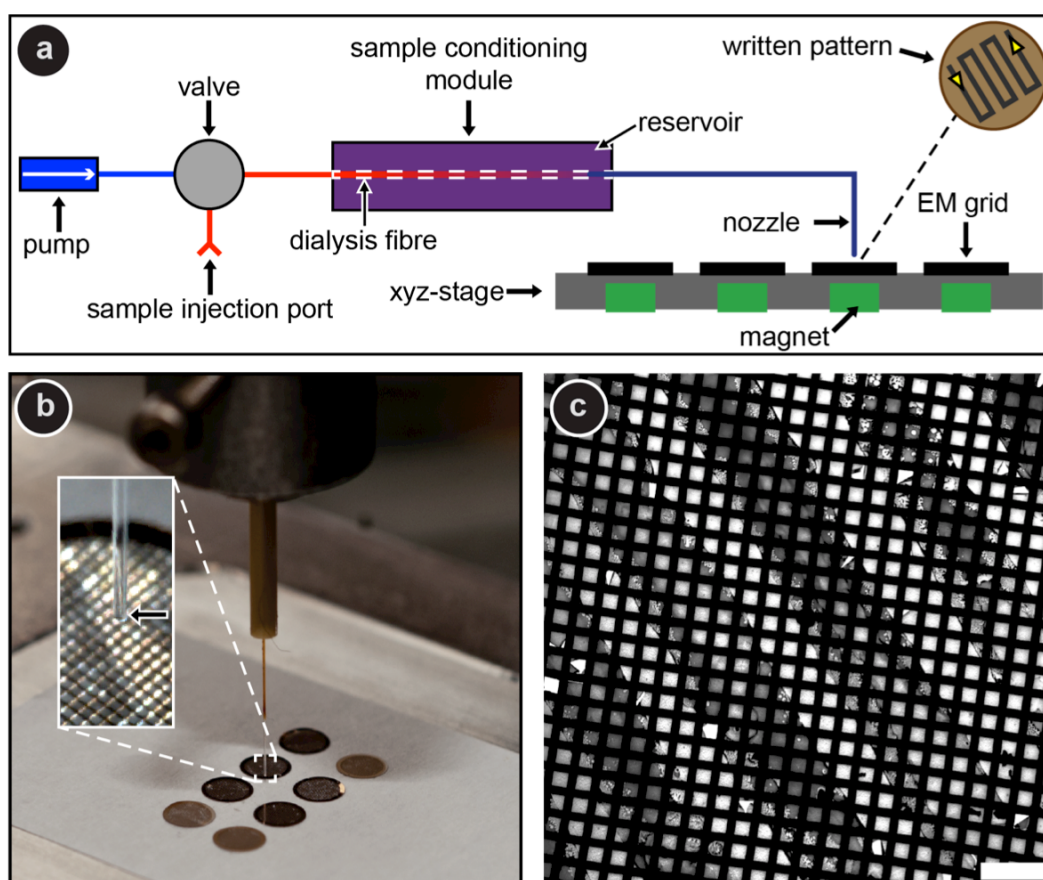

Figure 3-2: Sample-conditioning module and micro-patterning device. (a) Schematic representation of the main components and the meander-type writing pattern. (b) Nozzle positioned above an EM grid on the xyz-stage. Inset: enlarged view; the arrow indicates the nozzle tip. (c) TEM image of a micro-patterned grid showing a section of the six 200-300-µm-wide lines of a PTA$_{7.0}$ stained sample (diagonal dark grey lines) written on an EM grid (black) and the empty carbon film in between (light grey). Scale bar: 200 µm

3.3.7   Nozzle preparation

Commercially available fused silica capillaries (Polymicro) were used to make the nozzles. These were processed in the following way to optimize the liquid handling and direct the fluid onto the EM grids. The first 0.5-1.0 cm of the polyimide coating of the fused silica capillaries was stripped away using hot chromosulfuric acid [14]. Afterwards, the nozzle was extensively rinsed with ddH$_2$O to remove all traces of the acid. The fused silica was then cleaned by successively dipping the capillaries into ddH$_2$O, ethanol and acetone for 10 min while shaking. Subsequently, the fused silica surface was activated by a 1 min treatment with cold atmospheric pressure helium plasma (piezobrush® PZ1, Polyscience AG Switzerland). Immediately after plasma treatment the capillary tips were dipped into a silanization solution (~5% dimethyldichlorosilane in heptane; Silanization Solution 1, 85126, Fluka, Switzerland) for 1 h and baked at 90 °C for 4 h. The stripped and silanized capillaries have an inner nozzle diameter of 50 mm.

3.3.8   Scanning transmission electron microscopy

A Vacuum Generators (East Grinstead, U.K.) HB-5 STEM interfaced to a modular computer system (Tietz Video and Image Processing Systems) was used. All samples were prepared on thin carbon films spanning gold sputtered, carbon-coated, 200-mesh-per-inch, gold-plated copper grids [15]. The aim was to determine whether samples leaving the microfluidics setup were clean and suitable for mass evaluation. After extensive rinse cycles for maintenance of the set-up, the sample dialysis reservoir was filled with quartz-ddH$_2$O. A stock solution of TMV in quartz-ddH$_2$O was then passed through the conditioning module (micro-dialysis time of 2 min) and written to STEM microscopy grids by the hand-over module. The control grid, which also served as mass standard, was manually prepared in the conventional manner i.e., a 5ml droplet of the same TMV stock was adsorbed to a STEM grid, blotted and washed on 8 droplets of 100mM ammonium bicarbonate solution prepared with quartz-ddH$_2$O, blotting after each step. All grids were allowed to air-dry. Series of digital 512 x 512 pixel, dark-field images were recorded from the grids at an acceleration voltage of 80 kV and a nominal magnification of 200,000x. The recording dose used varied between 290 and 635 electrons/nm^2. The images were evaluated with the MASDET program package as described previously [16]. All mass-per-length (MPL) data were corrected for beam-induced mass-loss. The results from the control grid (mass standard) gave the instrumental scale factor, which was correspondingly applied to all measurements. The MPL data from the test grid were binned into a histogram and described by a Gaussian curve. The average MPL and standard deviation (SD) were also calculated and compared

to the expected value of, 133 kDa/nm^2 [15], and to the SD of the control grid results, respectively.

3.4 Results

The apparatus enables micro-patterning of EM grids with stained or desalted samples. It consists of two main units, (a) a sample-conditioning module for staining or desalting (or an inline combination of both), and (b) a hand-over module for micro-patterning the sample onto the grids (Fig. 3-2a). The instrument is designed for a prospective degree of automation and controlled by custom-written software (supp. Fig. 3-1). In the first step the sample is conditioned using the micro-dialysis principle. This method was chosen because it is easy to integrate and because of its multiple application potential. In this sample-conditioning module, the sample flows through a cellulose fibre capillary (13 kDa cut-off) that extends through a reservoir of either negative stain solution or a volatile buffer (e.g., ammonium acetate or ammonium bicarbonate) in quartz double-distilled water (ddH$_2$O). Dialysis occurs as the sample liquid flows through the chamber, to either add the negative stain solution or remove undesired salts. The sample flow rate defines the dialysis time and can be adapted in a range from seconds to minutes. Liquid contact writing is then used to deposit the sample on EM grids supporting a thin carbon film that was rendered partially hydrophilic by activation with a atmospheric pressure, helium, cold plasma. Initial tests indicated that grids treated in this way were no different to those processed using the conventional glow discharge technique [13]. Piezo-driven plasma generation was chosen, as it is easier to integrate in an automated setup. The hand over unit is a micro-mechanical positioning device that brings a thin nozzle in close proximity to the grid. After liquid contact has been established, the grid is moved under the nozzle at sub-micrometer precision to create a meander-type micro-pattern of the sample on its carbon film (Fig. 3-2b and c). When this is finished, the nozzle is quickly moved up and down as the next grid is positioned (the time required is operator defined; minimum 0.5 sec). At present, a series of 26 grids can be written in sequence.

We have tested this new grid preparation method with a range of commonly used negative stains [17], namely phosphotungstic acid at pH 7.0 (PTA$_{7.0}$), ammonium molybdate at pH 6.5 (AM$_{6.5}$), NanoVan® at pH 8.0 (NanoV$_{8.0}$), NanoW® at pH 6.8 (NanoW$_{6.8}$), and uranyl acetate at pH 4.5 (UA$_{4.5}$) and pH 7.0 (UA$_{7.0}$), and compared the results with grids prepared by conventional negative staining/blotting methods. Due to the effective staining behaviour of this method only half or even less (2 min micro-dialysis against 0.5% -1%) of the concentrations normally applied were used. A mixture of tobacco mosaic virus (TMV) and apoferritin (AF) in phosphate

buffer system (PBS; 10 mM phosphate buffer, 2.7 mM KCl, 137 mM NaCl, pH 7.4) was employed to investigate the staining quality (Fig. 3-3 left column, and supp. Fig. 3-2), while complete cell lysates of baby hamster kidney (BHK) cells allowed the staining behaviour for heterogeneous samples to be assessed (Fig. 3-3 right column, and supp. Fig. 3-3). UA, one of the most commonly used negative stains employed in conventional negative stain EM, caused sample aggregation in our new method at pH 4.5 and pH 7.0 (supp. Fig. 3-4) and was not investigated further. Uranyl formate was not considered for testing as a similar fixative effect has been reported [17]. The other stains examined gave excellent results for both test samples. When used at significantly lower concentrations than in classical staining methods, these stains provided good contrast in the EM and clearly revealed structural details. With the exception of UA$_{4.5}$, all of the stains were stabilized at physiological or close to physiological pH. When BHK cell lysates were examined in an analogous procedure, ultrastructural details, such as membrane fragments packed with proteins, filaments and individual proteins were all clearly resolved in the TEM with no sign of aggregation (supp. Fig. 3-5).

A STEM mass measurement achieves an accuracy of ± 5 – 10% depending on the sample and, working from an image, directly links the mass data to shape information [11]. Initial tests made with TMV clearly showed that the modular microfluidic setup is capable of preparing the stringently clean grids required for these measurements (Fig. 3-4a). The carbon film of the written, air-dried grids of TMV in quartz-ddH$_2$O dialysed against quartz-ddH$_2$O was clean. Further, the mass-per-length measured for TMV was within 1.5% of that measured for the control grids, which were manually prepared in the conventional way and imaged in the same data acquisition session (Fig. 3-4b). Mass measurements require the removal of all non-volatile buffer components [15]. The classic way to do this specific desalting, is to wash the grid several times with quartz-ddH$_2$O or a volatile buffer e.g., ammonium acetate or bicarbonate, directly after sample adsorption. With the new grid preparation method, the required desalting is achieved before adsorption by dialysis. To avoid drastic pH changes and sample aggregation (supp. Fig. 3-6), this can be made against a volatile buffer, which allows the pH to be kept as close as possible to physiological at all stages. Changes in the lateral aggregation of TMV after dialysis against ammonium bicarbonate illustrate the effect, and document the efficiency of the sample–conditioning module (supp. Fig. 3-6).

apoferritin and TMV   BHK cell lysate
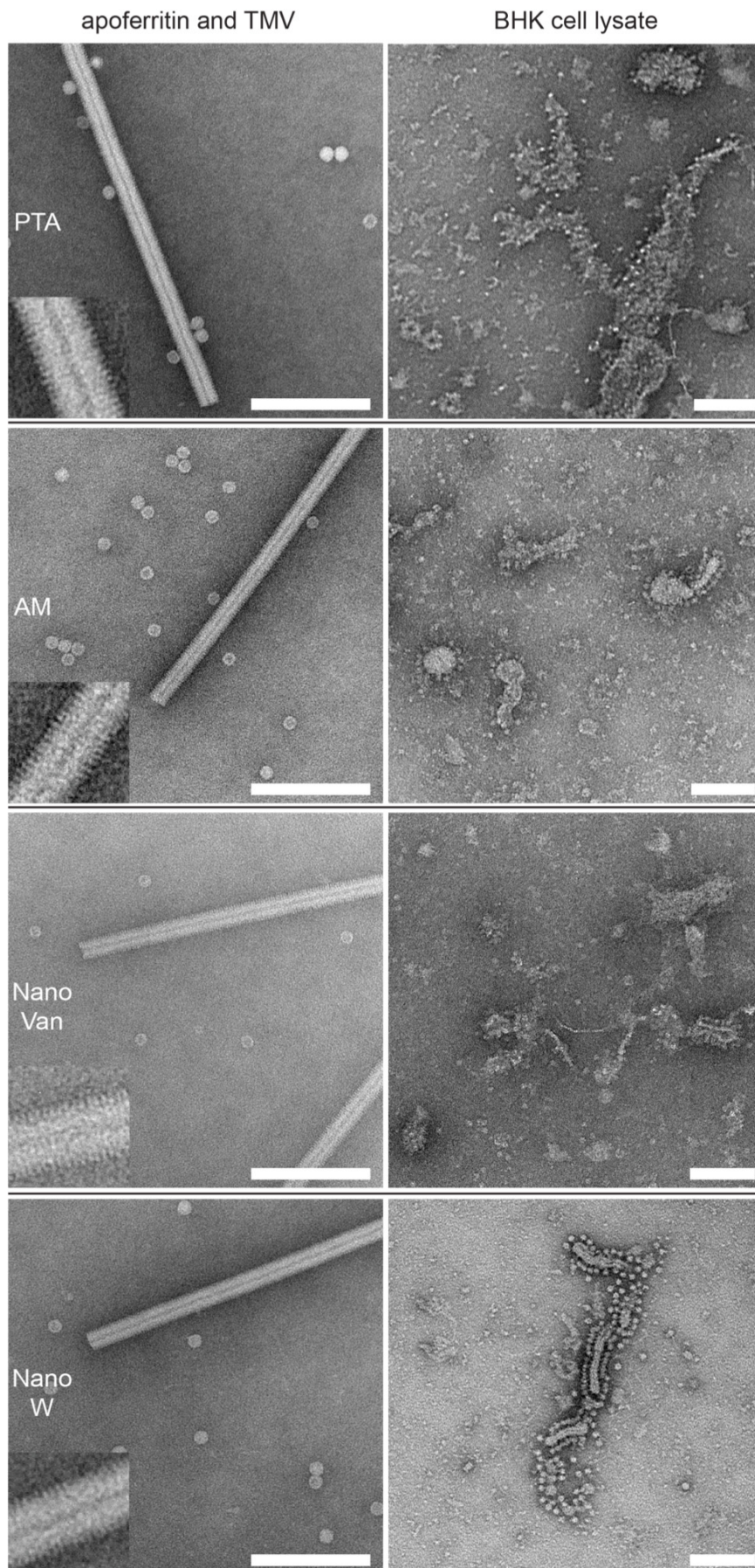

PTA

AM

Nano
Van

Nano
W

Figure 3-3: Gallery of TEM images. This selection shows TEM images of the two test samples prepared with the setup and different stains. (Left column) Mixture of AF and TMV. For all negative stains the central channel and the 23 Å repeat of TMV and the sub-structure of the AF is visible. (Right column) BHK cell lysate showing typical membrane structures with integrated membrane proteins that exhibit the shape of ATPases. (Rows) Samples in PBS were conditioned with 1% PTA$_{7.0}$, 0.5% AM$_{6.5}$, 1% NanoV$_{8.0}$, and 1% (left) or 2% (right) NanoW$_{6.8}$. Scale bars: 100 nm; insets depict three-fold enlarged regions of the TMV. (for more images see supplementary Fig. 2-2 and 2- 3).
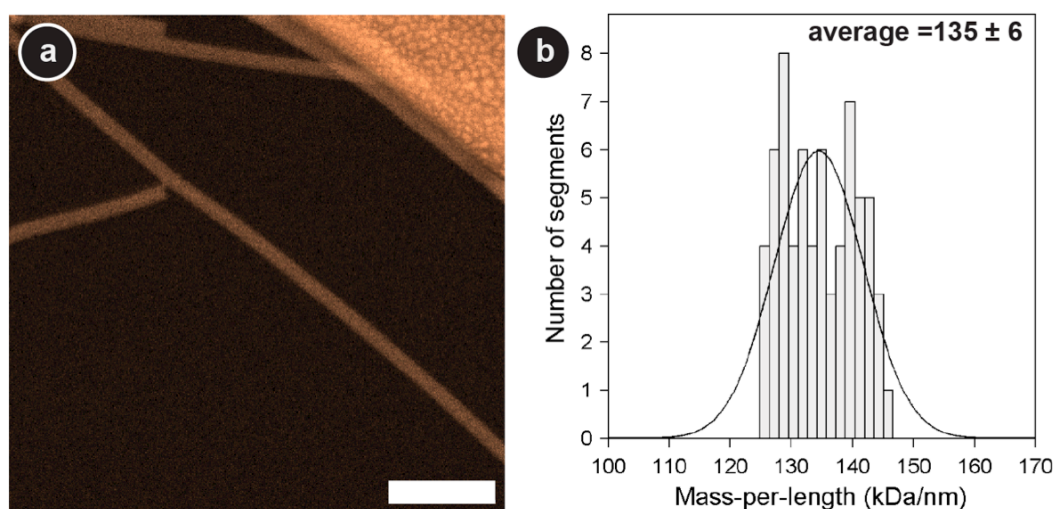

Figure 3-4: Mass measurement of TMV by STEM to test the preparation quality and cleanliness delivered by the microfluidic setup. (a) STEM dark-field image of unstained, air-dried TMV written on a STEM microscopy grid for mass measurement. TMV (0.1 mg/ml) in quartz-ddH$_2$O was dialysed against quartz-ddH$_2$O for 2 min in the sample preparation module and written on the grid. The thin carbon film beneath the TMV rods is clean (uniform dark regions). A small segment of the gold-sputtered, perforated thick carbon layer supporting this film is also visible (bright irregular region upper right). (b) Mass-per-length histogram of correspondingly written TMV. After scaling according to the mass standard, the determined average mass-per-length, 135 ± 6 kDa/nm, is within 1.5% of the expected value, 133 kDa/nm [15]. Further, the standard deviation of the data set is comparable to that of the mass standard, ± 4 kDa/nm, which was prepared in the conventional way (see Materials and Methods). Scale bar: 100 nm.

3.5 Discussion

Negative stain TEM is a standard technique used in most electron microscopy laboratories involved in biology or biomedicine. In classical negative staining techniques for EM, a drop of sample (3 – 7 μl) is applied to the EM grid, which is then washed and stained. Each step is followed by a

blotting procedure to remove excess liquid (Fig. 3-1a). Consequently, only a fraction of the sample and the stain remains on the grid. The amount of sample remaining depends on the adsorption, washing and blotting times, is often not reproducible and the relative protein concentrations may be distorted by preferential adsorption of specific sample sub-fractions. Instead, our newly developed method adds the stain via dialysis prior to immobilization on the EM grid. Only 0.1-0.3 µl of the stain-mixed sample are required and no washing or blotting steps are involved (Fig. 3-1b). This allows a much higher proportion (close to 100%) of the initial sample to be deposited on the EM grid, so that the true relative ratios between the different sample constituents are maintained (supp. Fig. 3-7). Moreover the stain density is controlled by the heavy metal concentration in the reservoir and the flow rate and can be easily tuned (Fig. 3-5).
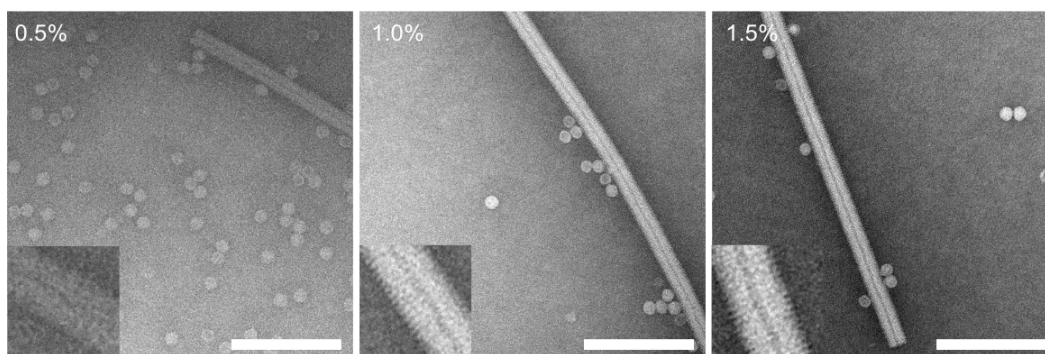

Figure 3-5: *Fine-tuning of the stain density. Representative images of samples conditioned with different $PTA_{7.0}$ concentrations, clearly showing the different stain densities. This demonstrates that easy and reproducible stain density fine-tuning is possible to adapt too different samples or to reveal different details of the same sample. Combined with several applicable stains with distinct properties this offers the potential to individually optimize the staining for a certain sample or certain sample details. The mixture of AF and TMV in PBS was conditioned with 0.5%, 1% or 1.5% of $PTA_{7.0}$ Scale bars: 100nm; insets depict three-fold enlarged regions of the TMV.*

In our hands, the automated procedure is more reproducible than manual staining, especially for "difficult" stains such as AM, NanoW® and PTA. This new method without any blotting or washing steps also results in a more effective staining even at lower stain concentrations, because all the stain in the solution dries down on the grid. Under these conditions, even stains with weak electron scattering properties provide good contrast; the contrast is significantly higher than that achieved manually. Furthermore, the stain seems to be homogenously distributed around the particles, a fact that might be important for subsequent data analysis steps, such as alignments. Both the contrast and the stain distribution attained with low scattering stains, may be favourably influenced by the preincubation of the protein complexes before

adsorption to the grid surface as the stain has more time to penetrate the fine structures of the proteins. However, the resolution still appears to be limited by the grain size of the stain. Visually, AM seems to exhibit an excellent balance between stain roughness, contrast and "dynamic range" (supp. Fig. 3-5c). Moreover their tolerance to phosphate buffers, the most frequently used buffers in biochemistry and cell biology, and the possibility to adapt their pH makes AM and PTA applicable to a broad spectrum of samples.

In the future, the hand-over module will be developed to allow grid preparation for higher resolution techniques such as cryo-EM where the ice thickness is a critical, contrast-determining property. To this end, the grid temperature will be kept at the thaw point to avoid evaporation/ condensation of the liquid during writing. Subsequently, the grid will be shot into liquid ethane. Alternatively, it will be freeze-dried to allow improved mass measurements by STEM.

The microfluidic sample preparation platform presented here has the potential to become an important tool not only for systems biology but also for EM in general, which demands reproducible, quantitative sample grid preparation and assessment. The new technique allows lossless grid preparation from small sample volumes at physiological pH, inline negative staining for TEM imaging as well as desalting for mass measurements, excellent and tuneable staining characteristics also for stains with weak electron scattering properties, and automated grid preparation. Further, the possibility of micro-patterning EM grids will allow a more systematic and convenient analysis of complex samples in the future. Combined with microfluidic methods for cell lysis, protein separation and labelling, this method for total cell content analysis for structure and mass, offers the potential to optimally complement other experimental system biology techniques such as MS [18] and ET [19,20]. Importantly, the raw images must be analyzed by feature matching methods [7,20,21] to obtain quantitative information. To aid the analysis, a visual library will be constructed containing the projections of *a priori* target molecules. The raw data images recorded from samples prepared in a lossless manner, will be segmented by a hierarchical algorithm [22,23] and the various particles present classified according to their size and shape. A shape matching will also allow the link to be made between negative stain and STEM images, combining the higher resolution and high contrast of the TEM projections with the mass obtained from unstained samples by STEM. Finally, cross-correlation techniques will be used to assign the TEM projections to the most probable match in the visual library [20].

The outlined automated sample preparation technique opens the way for a new visual proteomics approach. Ultimately it will allow the total content of

a single cell or miniscule tissue region to be examined by EM. It will then become possible to assemble complete ultrastructural libraries from cells or tissues. The method will make the structural study of the various cellular components on single molecule level possible. We foresee this technique as a valuable tool to study complex biological systems complementing other systems-biological methods.

## Acknowledgements

3.6 Supplemental material
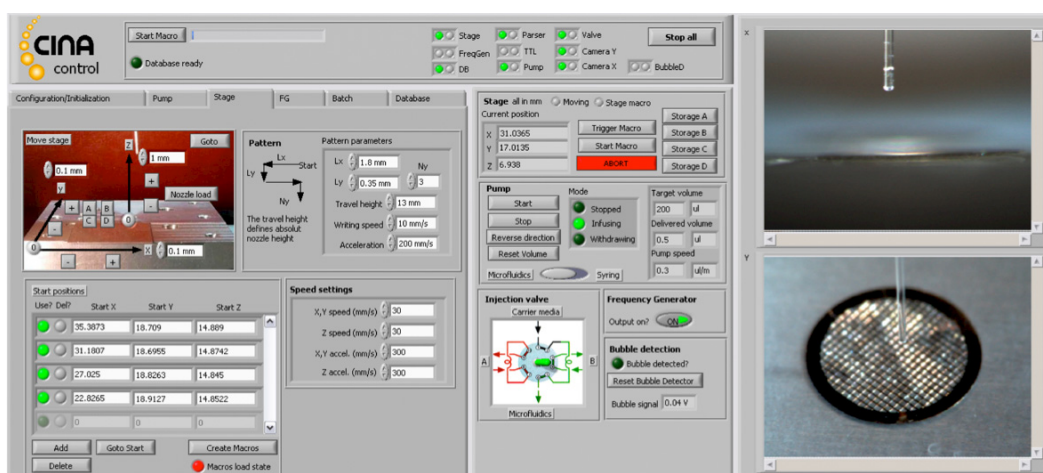
Supplementary Figure 3-1: *Graphical user interface of the LabView-based control software: This self-written software allows all setup components to be controlled and examined. It shows the status of all components and two cameras installed at different angles deliver live images of the nozzle and the grid being processed, respectively. The parameters controlling the components can either be set individually or via a macro language that was integrated to facilitate automation.*
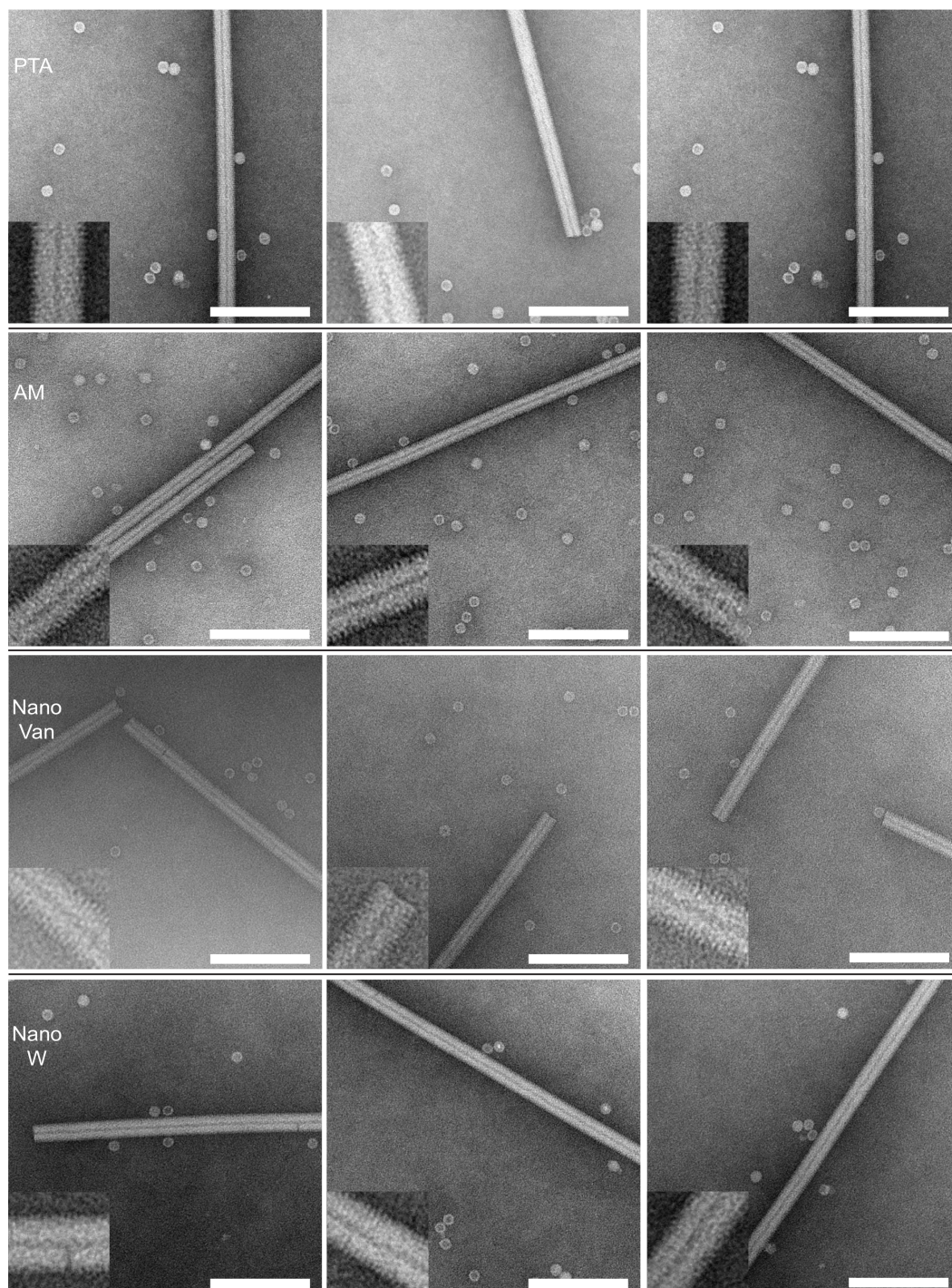
***Supplementary Figure 3-2****: Further examples of negatively stained TMV and AF samples. For all four stains the ultrastructure of TMV and AF is well preserved and the surrounding background shows a smooth fine grain. Samples were conditioned with 1% PTA$_{7.0}$, 0.5% AM$_{6.5}$, 1% NanoV$_{8.0}$, and 1% NanoW$_{6.8}$. Scale bars: 100 nm; the insets depict three-fold enlarged regions of the TMV.*
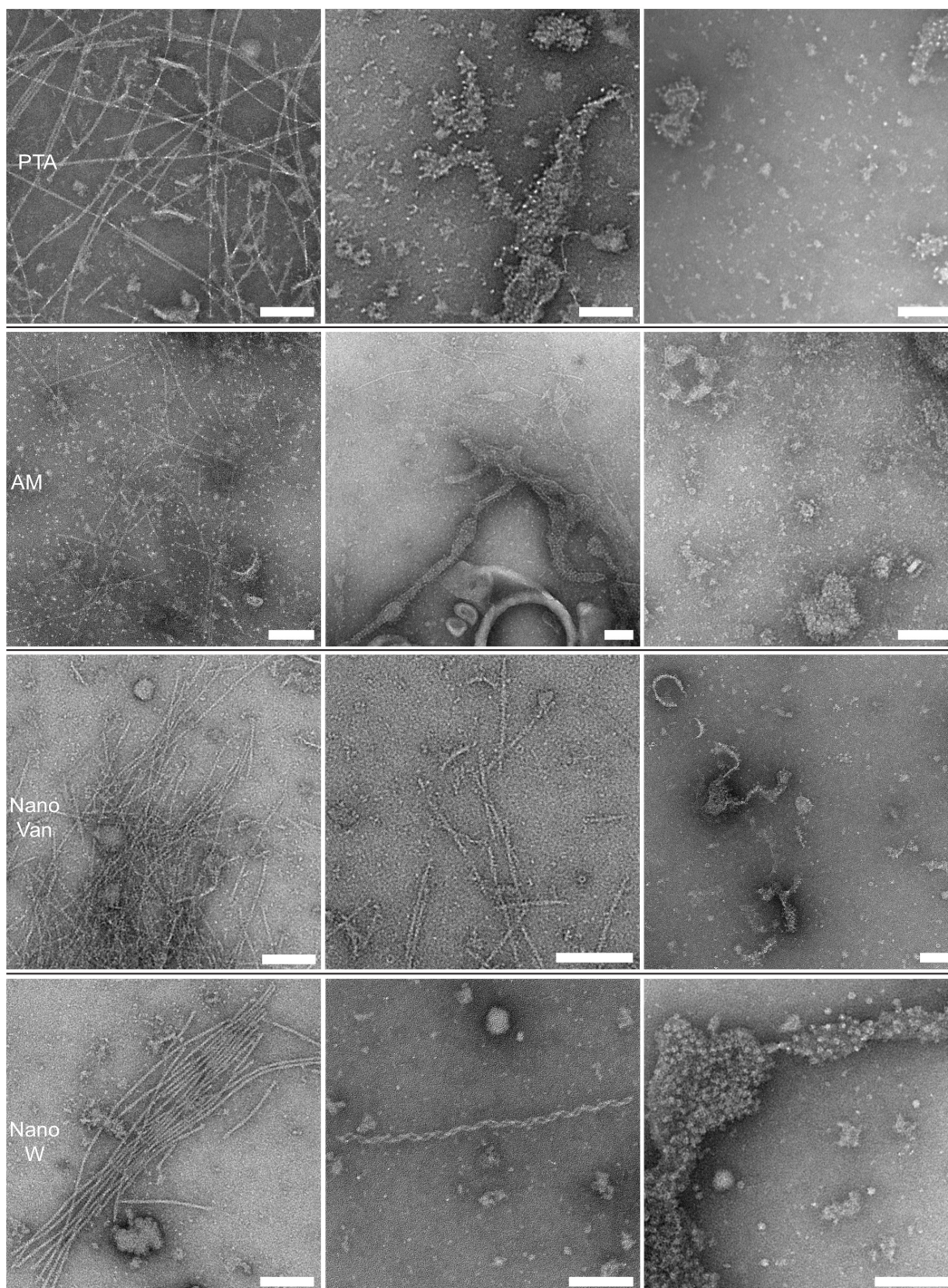
Supplementary Figure 3-3: *Further examples of negatively stained BHK lysate for the four different stains, revealing structures resembling actin filaments (e.g. top left) and protein-packed membranes (e.g. top center). Samples were conditioned with 2% PTA$_{7.0}$, 0.5% AM$_{6.5}$, 1% NanoV$_{8.0}$, and 2% NanoW$_{6.8}$. Scale bars: 100 nm.*
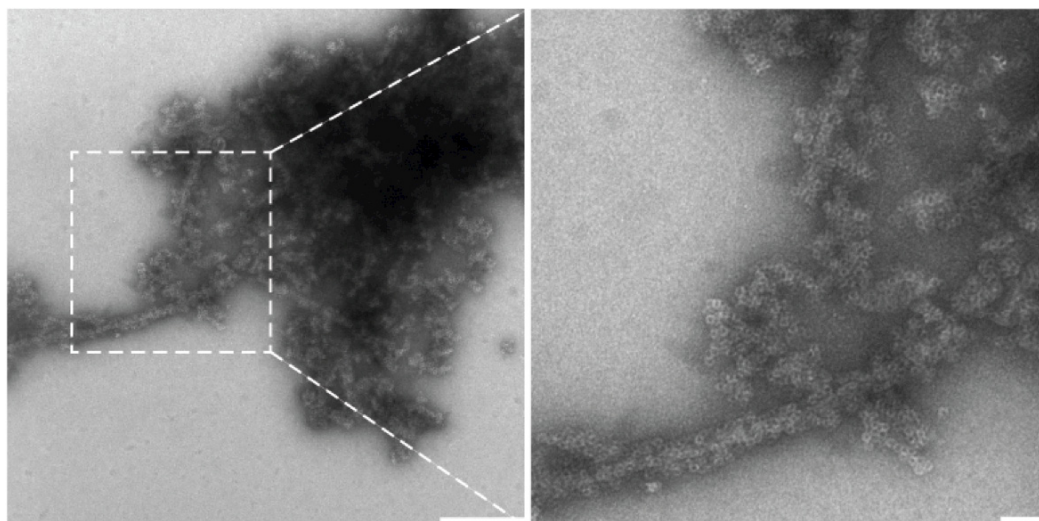
Supplementary Figure 3-4: *UA staining results. A TEM image of aggregated TMV and AF conditioned with 0.25 % $UA_{4.5}$. An enlarged view of the marked region is shown on the right. Other experiments showed, that there is serious precipitation when $UA_{4.5}$ is mixed with the sample at concentrations above 0.5 % and dried down on the grid (data not shown), even if the buffer does not contain phosphate; the sample was in HEPES or ddH$_2$O. Decreasing the UA concentration to 0.25% or below prevented the formation of precipitates, but the fixation property of UA caused sample aggregation when stain and sample were mixed prior to immobilization on the grid. Furthermore, buffering the UA solution at a concentration of 0.25% or below at pH 7 could not prevent this sample aggregation. Scale bars: (left) 250 μm; (right) 50μm.*
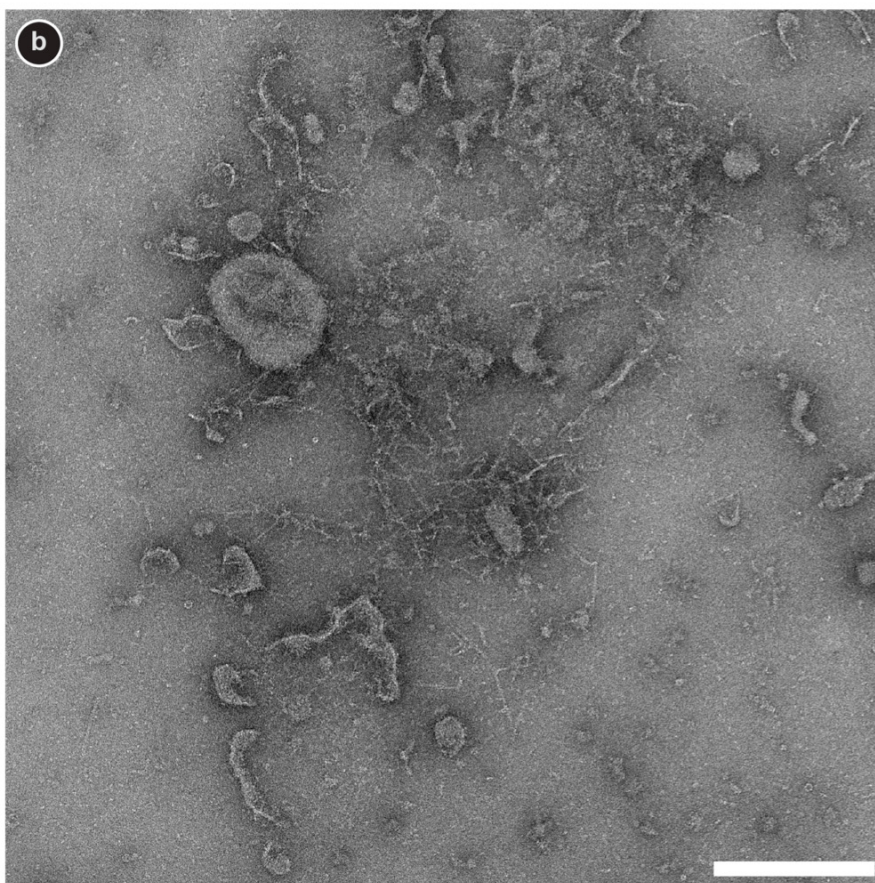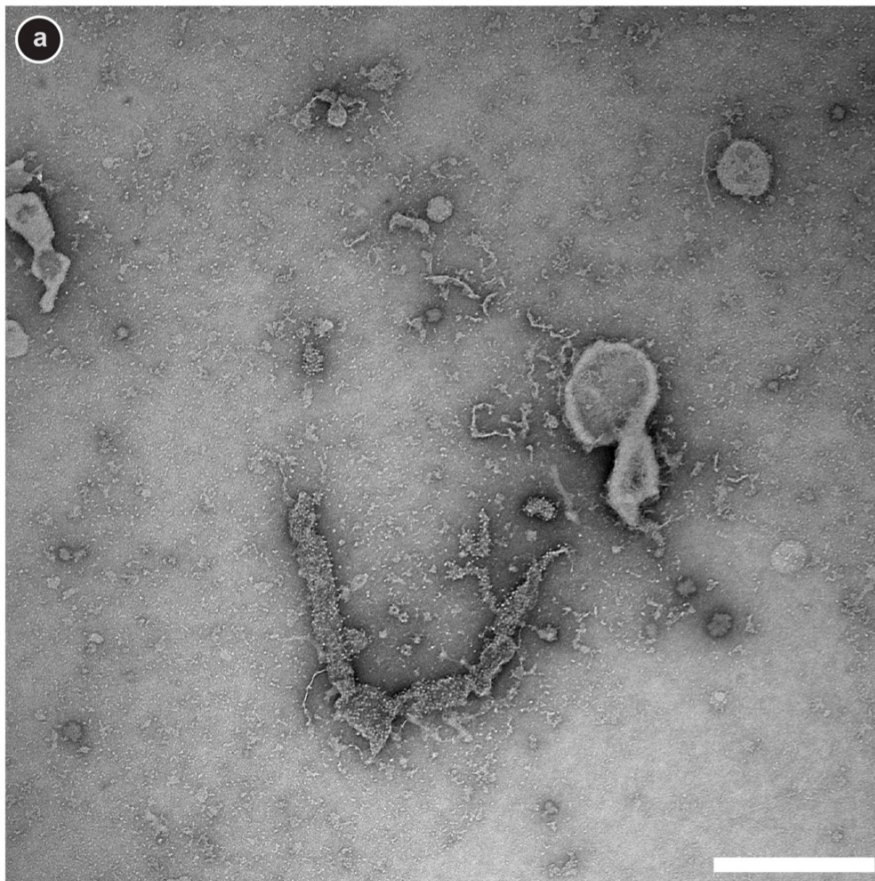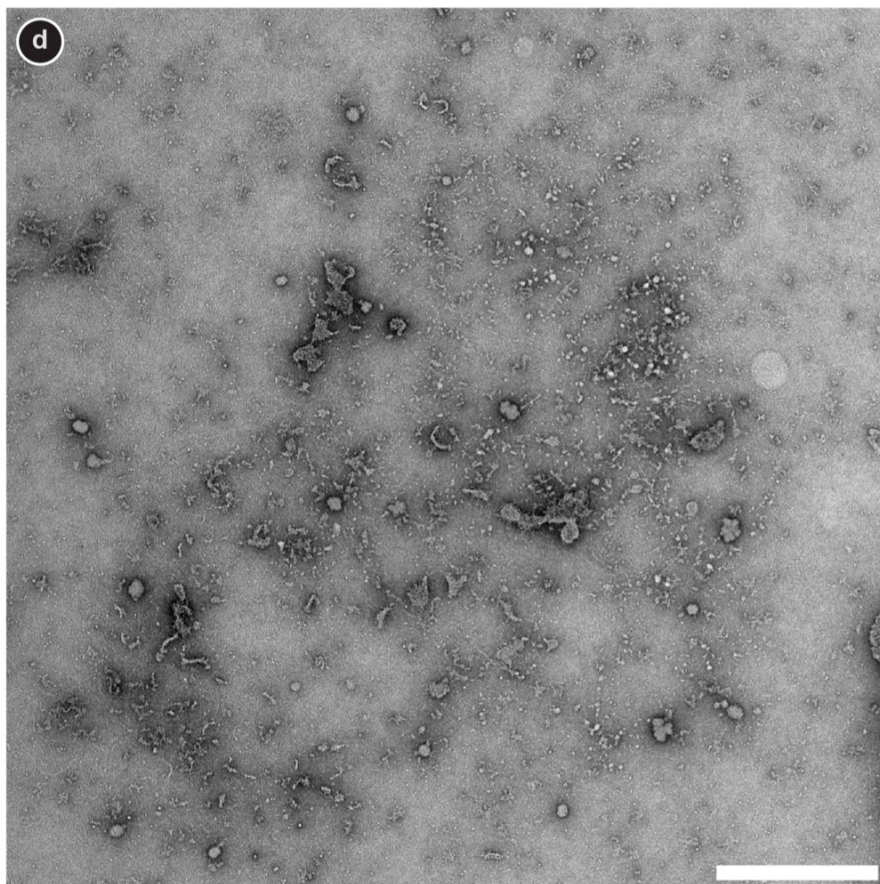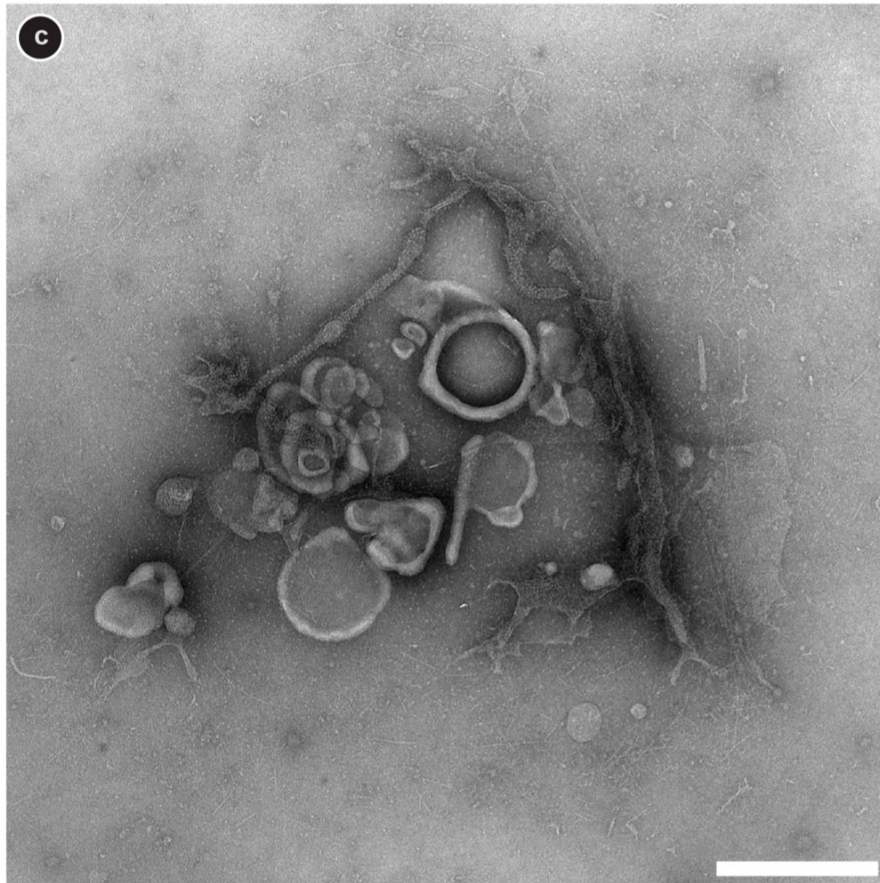
Supplementary Figure 3-5: *Images of BHK cell lysate demonstrating the absence of aggregation. The overview images show soluble proteins, membrane patches and filaments; there is no sign of aggregation. The sample in PBS was conditioned with (a) 2% PTA$_{7.0}$. (b) 0.5% AM$_{6.5}$. (c)1% NanoV$_{8.0}$. (d) 2% NanoW$_{6.8}$. Scale bars: 500 nm.*
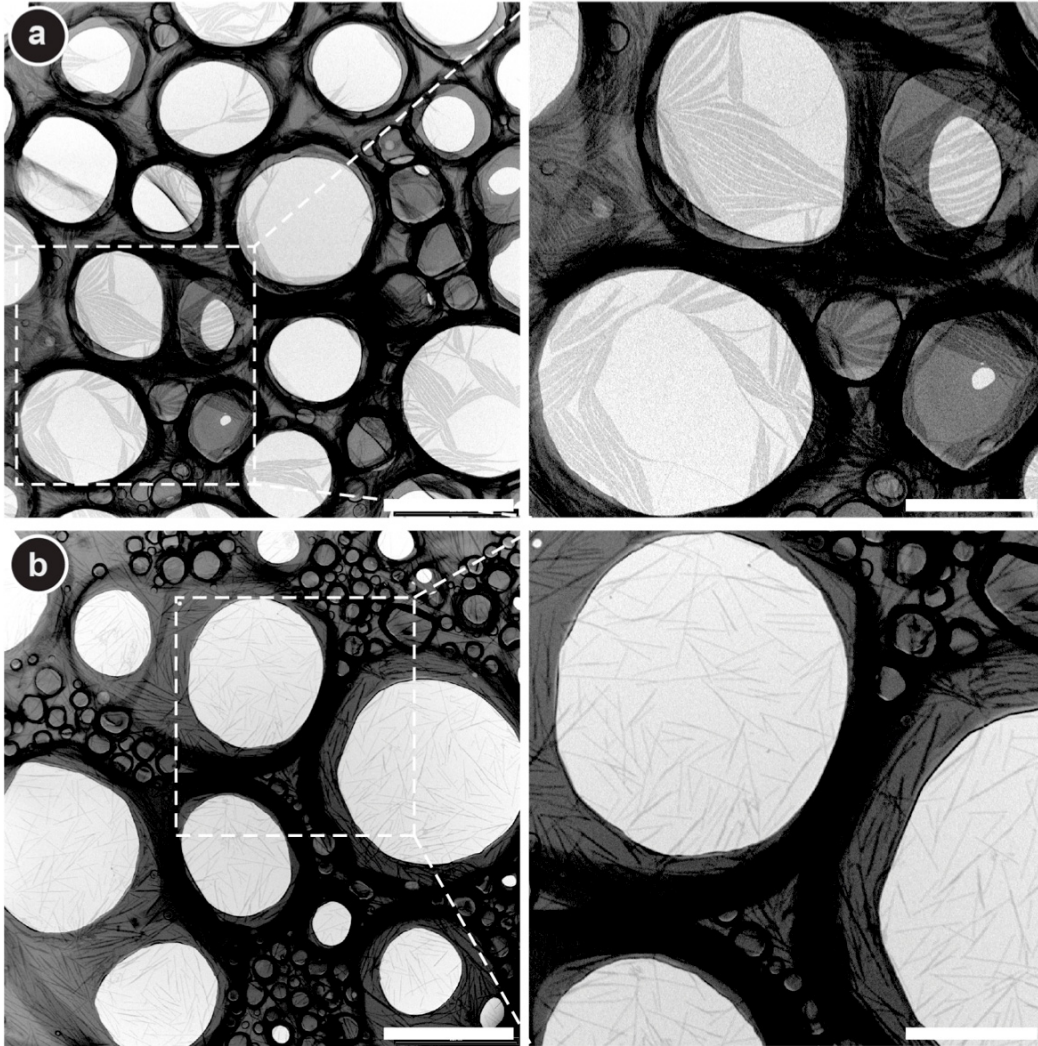

Supplementary Figure 3-6: *TEM images of unstained TMV written on STEM grids after passage through the sample preparation module: (a) TMV in quartz-ddH$_2$0, after micro-dialysis against quartz-ddH$_2$0. The rods tend to aggregate, which would hinder mass determination; only a few are well separated from their neighbors. (b) TMV in quartz-ddH$_2$0, after micro-dialysis against 100 mM ammonium bicarbonate buffer. The rods are homogeneously distributed over the grid and generally well separated. The marked change in aggregation shows that conditioning was effective. The results illustrate that even robust samples like TMV benefit from solutions that are buffered close to physiologic pH. Scale bars: (left column) 500 µm; (right column) 250 µm.*
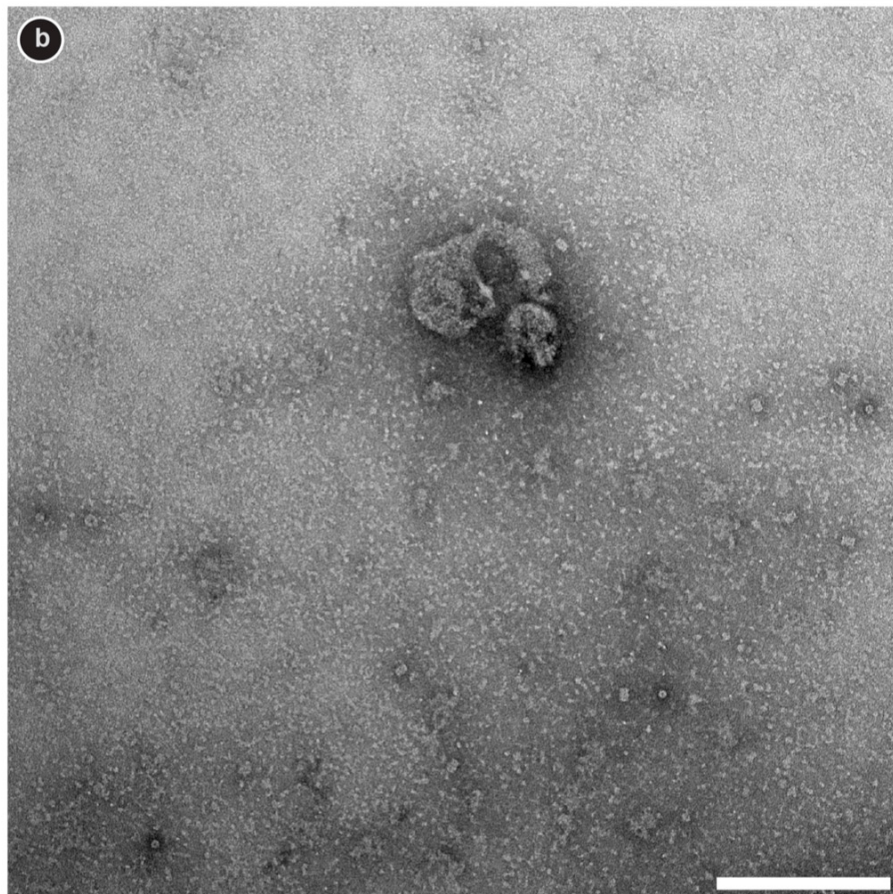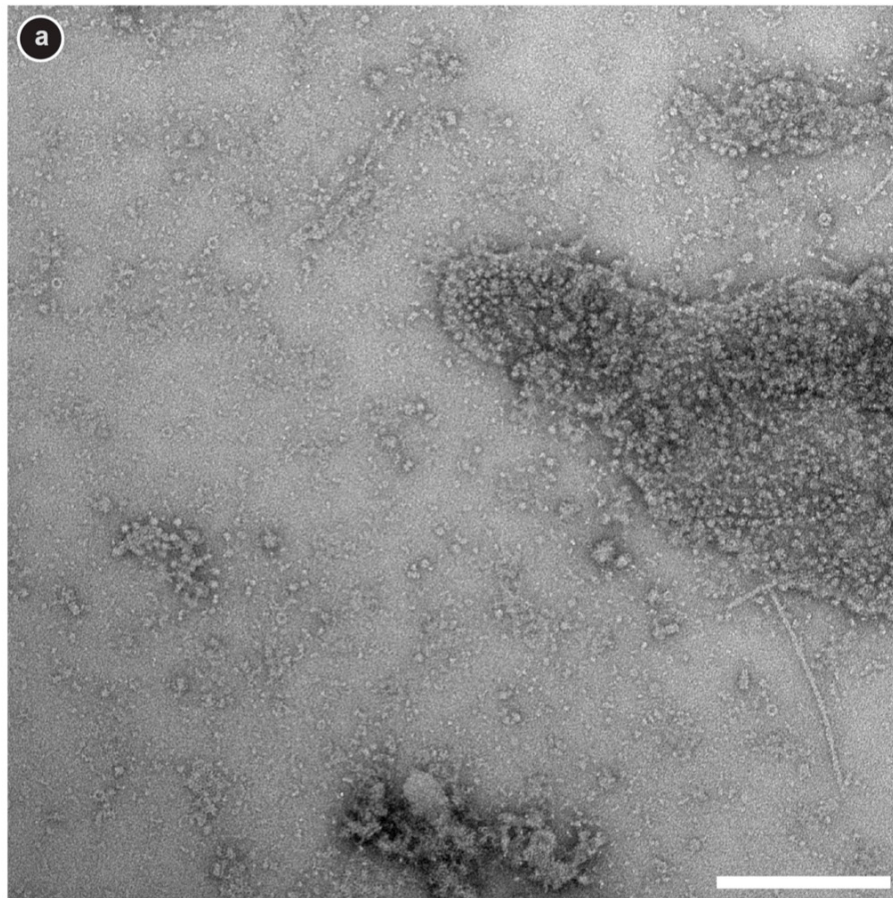
Supplementary Figure 3-7: *Comparison of manual and automated grid preparation. Representative overview images of lysate from heat-shocked (46°C for 60min) BHK cells. (a) Prepared with the setup and conditioned with 1% NanoW$_{6.8}$. (b) Manually prepared (1 min sample adsorption followed by four wash steps of 5 sec) and stained with 2% NanoW$_{6.8}$ (two times 5 µl of stain for 10 sec). Besides the heat-shock proteins that can be observed with both preparation methods the setup preparation method reveals more sample constituents. Large "protein packed" membrane patches as well as filaments are abundant and clearly visible with structural details. These components were not observed when the grids were prepared by hand. Scale bars: 200 nm.*

3.7 References

[1]   Aderem, A. **Systems biology: its practice and challenges**. *Cell* 121, 511-513, (2005).

[2]   Aloy, P. & Russell, R. B. **Structural systems biology: modelling protein interactions**. *Nat. Rev. Mol. Cell Biol.* 7, 188-197, (2006).

[3]   Kherlopian, A. R., Song, T., Duan, Q., Neimark, M. a., Po, M. J. *et al.* **A review of imaging techniques for systems biology**. *BMC Syst. Biol.* 2, 74-74, (2008).

[4]   Ben-Harush, K., Maimon, T., Patla, I., Villa, E. & Medalia, O. **Visualizing cellular processes at the molecular level by cryo-electron tomography.** *J. Cell Sci.* 123, 7-12, (2010).

[5]   Lučić, V., Förster, F. & Baumeister, W. **Structural studies by electron tomography: from cells to molecules.** *Annu. Rev. Biochem.* 74, 833-865, (2005).

[6]   Leis, A., Rockel, B., Andrees, L. & Baumeister, W. **Visualizing cells at the nanoscale.** *Trends Biochem. Sci.* 34, 60-70, (2009).

[7]   Bohm, J., Frangakis, A. S., Hegerl, R., Nickell, S., Typke, D. *et al.* **Toward detecting and identifying macromolecules in a cellular context: template matching applied to electron tomograms.** *Proc. Natl. Acad. Sci. U. S. A.* 97, 14245-14250, (2000).

[8]   Nickell, S., Kofler, C., Leis, A. P. & Baumeister, W. **A visual approach to proteomics**. *Nat. Rev. Mol. Cell Biol.* 7, 225-230, (2006).

[9]   Kireev, I., Lakonishok, M., Liu, W., Joshi, V. N., Powell, R. *et al.* ***In vivo* immunogold labeling confirms large-scale chromatin folding motifs**. *Nat. Methods* 5, 311-313, (2008).

[10]   Aebersold, R. & Mann, M. **Mass spectrometry-based proteomics**. *Nature* 422, 198-207, (2003).

[11] Engel, A. **Assessing biological samples with scanning probes** in: Single Molecule Spectroscopy in Chemistry, Physics and Biology, *Springer Series in Chemical Physics.*, Vol. 96, Ch. 21, 417-431, Springer, Berlin Heidelberg, (2010).

[12] Hayat, M. A. **Principles and Techniques of Electron Microscopy. Biological Applications**. 4th ed., Cambridge University Press, Cambridge (2000).

[13] Aebi, U. & Pollard, T. D. **A glow discharge unit to render electron microscope grids and other surfaces hydrophilic**. *J. Electron Microsc. Tech.* 7, 29-33, (1987).

[14] Matthewson, M. J., Kurkjian, C. R. & Hamblin, J. R. **Acid stripping of fused silica optical fibers without strength degradation**. *Journal of Lightwave Technology* 15, 490-497, (1997).

[15] Müller, S. A., Goldie, K., Burki, R., Haring, R. & Engel, A. **Factors influencing the precision of quantitative scanning transmission electron microscopy**. *Ultramicroscopy* 46, 317-334, (1992).

[16] Krzyžánek, V., Müller, S. A., Engel, A. & Reichelt, R. **MASDET-A fast and user-friendly multiplatform software for mass determination by dark-field electron microscopy**. *J. Struct. Biol.* 165, 78-87, (2009).

[17] Bremer, A., Henn, C., Engel, A., Baumeister, W. & Aebi, U. **Has negative staining still a place in biomacromolecular electron microscopy?** *Ultramicroscopy* 46, 85-111, (1992).

[18] Picotti, P., Bodenmiller, B., Mueller, L. N., Domon, B. & Aebersold, R. **Full dynamic range proteome analysis of *S. cerevisiae* by targeted proteomics.** *Cell* 138, 795-806, (2009).

[19] Bárcena, M. & Koster, A. J. **Electron tomography in life science**. *Semin. Cell Dev. Biol.* 20, 920-930, (2009).

[20] Förster, F., Han, B.-G. & Beck, M. **Visual proteomics.** *Methods Enzymol.* 483, 215-243, (2010).

[21] Huang, Z. & Penczek, P. A. **Application of template matching technique to particle detection in electron micrographs**. *J. Struct. Biol.* 145, 29-40, (2004).

[22] Adiga, U., Baxter, W. T., Hall, R. J., Rockel, B., Rath, B. K. *et al.* **Particle picking by segmentation: a comparative study with SPIDER-based manual particle picking.** *J. Struct. Biol.* 152, 211-220, (2005).

[23]   Coudray, N., Buessler, J.-l., Kihl, H. & Urban, J.-p. **Multi-scale and First Derivative Analysis for Edge Detection in TEM Images.** in: A Campilho & M Kamel eds. ICIAR, *LNCS*, Vol. 4633, 1005-1016, Springer-Verlag Berlin Heidelberg, (2007).

4   Ionic liquids as matrices in microfluidic sample deposition for high-mass MALDI-MS

Ionic liquids as matrices in microfluidic sample deposition for high-mass matrix-assisted laser desorption/ionization mass spectrometry

Simon Weidmann[1], Simon Kemmerling[2], Stefanie Mädler[1,3],
Henning Stahlberg[2], Thomas Braun[2], Renato Zenobi[1,*]

[1] Department of Chemistry and Applied Biosciences, ETH Zurich, CH-8093 Zurich, Switzerland.

[2] Center for Cellular Imaging and Nanoanalytics, University of Basel, CH-4058 Basel, Switzerland.

[3] Current address: Centre for Research in Mass Spectrometry, York University, Toronto, ON M3J 2R7, Canada.

* Corresponding Author: zenobi@org.chem.ethz.ch

S.K. has developed the microfluidic deposition device shown in Figure 3.1 and supervised the spotting experiments performed with this setup.

4.1 Abstract

Sample preparation for MALDI-MS via a microfluidic deposition device using ionic liquid matrices addresses several problems of standard protocols with crystalline matrices, such as the heterogeneity of sample spots due to the co-crystallization of sample and matrix, and the limited capability for high-throughput analysis. Since ionic liquid matrices do not solidify during the measurement, the resulting sample spots are homogeneous. The use of these matrices is also beneficial for automated sample preparation, since crystallization of the matrix is avoided, and thus no clogging of the spotting device can occur. The applicability of ionic liquids to the analysis of biomolecules with high molecular weights, up to ≈ 1 MDa is shown, as well as a good sensitivity (5 fmol) for recombinant human fibronectin, a protein with a molecular weight of 226 kDa. Microfluidic sample deposition of proteins with high molecular weights will in the future allow parallel sample preparation for MALDI-MS and for electron microscopy.

4.2 Introduction

Since its invention in the early 1980s by Karas and Hillenkamp [1], matrix-assisted laser desorption/ionization mass spectrometry (MALDI-MS) has developed into a very powerful analytical method, especially for the analysis of biomolecules such as oligonucleotides [2,3], peptides and proteins [2,4]. One of the main features of MALDI is the incorporation of the sample into a suitable matrix. The matrix normally co-crystallizes with the sample, and also serves to absorb the laser wavelength that is used to desorb and ionize the sample/matrix mixture [5-7]. However, the crystallization process is not homogeneous when using solid matrices and the sample incorporation is therefore not homogeneous, either. This often leads to the formation of regions within a sample where the signal intensity is much larger than elsewhere. This well-documented "sweet spot" effect obscures the relation between the measured signal intensity and the sample concentration present. A homogeneous sample preparation is one approach to overcome this problem. For example, special crystallization conditions that lead to smaller and therefore more homogeneous crystals can be applied [4,8,9]. Another possibility is the use of liquid matrices, e.g., ionic liquids where the acidic proton of the matrix is replaced by another cation such as an ammonium or a phosphonium moiety [10]. Depending on the cation used, the matrix can remain liquid or become solid, but in any case will present a much more homogeneous environment [10], in which the sample is more evenly distributed. It has already been shown that ionic liquids can be used as

matrices in MALDI [10-15]. Due to the homogeneous sample distribution, the mass spectra obtained are more reproducible compared to the ones using solid matrices [12,15].

Besides determining the chemical identity of components within a sample, it is also important to analyze the associated spatial distribution pattern. Since its introduction by Caprioli et al. [16] MALDI-MS imaging became an important tool to investigate proteins and peptides [17-20] or lipids in tissue [21,22] sections. One of the crucial points in MS imaging is a fast and reproducible deposition of matrix over large sample areas. Several different approaches for automation, such as acoustic matrix deposition [23], electric field mediated deposition [24], piezo-electric dispensing [25], ink-jet printing [26,27], or spotting robots [28,29] have been published, although all of the deposition methods mentioned are applied to low-mass samples only. The analysis of the intact proteome of tissue sections has several advantages compared to the commonly used approach, where the proteins are digested before MS imaging: the information on the protein is directly available without database search of the fragments, and since no waiting time for digestion is needed, and spreading or leaking of compounds into neighboring compartments is minimized. Only few examples of imaging of proteins with molecular weights exceeding 50 kDa have been published [30,31]. The samples for these experiments were prepared either manually [30,31] or using an automated sprayer [31]. Development of a matrix spotting method suitable for high-mass MALDI would allow the profiling and imaging of compounds such as proteins or protein complexes with masses higher than 100 kDa.

Among the methods mentioned above, the simplest way to prepare such samples is by the use of a robotic spotting device. However, plugging of the capillary or the spotting nozzle due to crystallization of the matrix, or sample loss inside components of the spotting device due to adhesion of the sample to the tubing/capillaries (if delivered via the spotting device) are known to cause problems [23]. The use of ionic liquid matrices in such a spotting device would therefore be beneficial; however, this has never been shown.

In this paper, a microfluidic sample delivery set-up for spotting liquid MALDI matrices is presented. It has also been developed for compatibility with automated deposition on electron microscopy (EM) grids [32]. In contrast to the work published by Benesch and coworkers, where deposition is achieved in vacuo after mass separation and soft landing on an EM grid [33], the whole proteome is deposited without prior mass separation in our approach. In conjunction with cell lysis and loss-less sample transport [32], "visual proteomics" is one of the long-term goals [34]: complete lysis of few cells allows for the preparation of minute amounts of sample, either by

"smearing" of the whole proteome onto an EM grid, or by aliquoting the lysate onto MALDI targets. Since the very same sample could be analyzed in parallel by electron microscopy and high-mass MALDI, information about the shape and the mass of the proteome of cells could be obtained, and individual proteins could be identified according to these parameters. If a sufficiently large number of EM images can be recorded, 3D reconstruction of the protein shape should also become possible.

Until now, the highest molecular weight molecules that has been measured by MALDI using ionic liquid matrices is immunoglobulin G (molecular weight of 146 kDa)[12]; the heaviest ion ever detected in this fashion was the nonspecific trimer of urease (molecular weight of 270 kDa)[11]. The goal of this work is to show the capability of ionic liquids as matrices for the analysis of biomolecules with even higher molecular weights (up to 1 MDa), and to prove that the use of ionic liquid matrices does not compromise sensitivity, as demonstrated by determining the limit of detection for samples with masses well above 100 kDa with manual sample preparation, as well as in combination with microfluidic sample deposition. The use of such a combination would potentially allow for extending MALDI imaging or profiling of biomolecules with higher masses and therefore provide insight into biological pathways within tissue. The development of a spotting device, which can be used to prepare electron microscopy grids as well as MALDI plates, is useful for future investigations of the cell content, e.g. fast identification of proteins by both methods.

The suitability of ionic liquids for the analysis of biomolecules with high molecular weights is shown here. Sensitivity restriction is not compromised, and improved homogeneity of the sample spots is observed. In conjunction with a microfluidic spotting device, this rapid, sensitive and reproducible sample preparation method paves the road towards visual proteomics.

4.3 Experimental

4.3.1 Materials

Sinapinic acid (SA), α-cyano-4-hydroxycinnamic acid (CHCA), trimethylamine solution (43%), triethylamine, pyridine, and bovine serum albumin (BSA) were purchased from Fluka (Buchs, Switzerland). Trifluoroacetic acid (TFA) was purchased from Acros Organics (Geel, Belgium). N-methyl-N-isopropyl-N-tertbutyl-amine (MIT-amine), phosphate buffered saline tablets (pH 7.4), acetonitrile, immunoglobulin G (IgG) and immunoglobulin M (IgM) were obtained from Sigma-Aldrich (Buchs, Switzerland). Bovine thyroglobulin (Tg bov) was purchased from Morphosys AbD (Düsseldorf, Germany), and recombinant human fibronectin (rh Fn)

from R&D Systems Europe (Abingdon, UK). The water used was of nanopure quality (18.2 MΩ cm^{-1}) and prepared using a NANOpure water purification system (Barnstead, IA, USA).

4.3.2 Sample preparation

Lyophilized rh Fn was reconstituted in PBS at a concentration of 100 μg mL^{-1}. Tg bov was used as delivered. The ionic liquid matrices were synthesized by a procedure similar to that published by Zabet-Moghaddam et al. [15]. After addition of an equimolar amount of amine to a 10 mg mL^{-1} solution of sinapinic acid in acetonitrile/water (2:1, v:v) containing 0.1% TFA, and subsequent sonication for 10 minutes, the sample was mixed with the freshly prepared ionic liquid matrix in a 1:1 (v:v) ratio and vortexed. 0.5 - 1 μL of the sample mixture was deposited on a 384 spot stainless steel MALDI plate and the solvents were allowed to evaporate.

4.3.3 Spotting device

Besides manual sample deposition, automated deposition with a self-built spotting device [32] was also performed. The spotting device (Fig. 4-1) consists of a syringe pump (KDS210, Ismatec SA, Switzerland), equipped with a gas-tight syringe (Vici AG International, Schenkon, Switzerland) containing nanopure water, a ten-port valve for sample injection (Valvo 10-port 2-position valve; BGB Analytik AG, Böckten, Switzerland) and a fused silica capillary as nozzle for the deposition of the sample. For accurate deposition of the sample onto the MALDI plate, a plate holder was constructed and mounted on a xyz translation stage. A commercial MALDI plate was cut in half and positioned on the sample holder, where it was held in place by two magnets. To place the nozzle correctly with respect to the plate, its position was observed with two cameras positioned at different angles for precise alignment in all three directions. The coordinates of the spot positions were stored in a list before the deposition, for a faster access during the deposition. The pump, the valve, and the stage were controlled via software programmed in LabView (National Instruments, Austin TX, USA). The protein samples were mixed with an ionic liquid matrix and injected into a 5 μL PEEK-loop attached to the ten-port valve. From another PEEK-loop with a volume of 10 μL, 5 μL of air were injected into the spotting capillary before and after the sample. This procedure allows the separation of the sample into several aliquots and protects the samples from dilution by surrounding water and cross contamination of different samples[35]. In the future, different samples might be injected sequentially into different bubbles. A flow rate of 5 μL min^{-1} was chosen for all steps that were necessary to create the sample bubble. To deposit the spot on the plate, a droplet was "grown" on the nozzle to a

volume of 0.5 µL with a flow rate of 1 µL min^{-1}. The plate was then lifted close to the nozzle (but without making contact), such that just the drop made contact to the plate, where it remained after retraction of the plate. To avoid carry-over of sample or matrix solution, the capillaries, the sample loops and the nozzle were rinsed with water at a flow rate of 5 µL min^{-1} after every series of deposition. The nozzle was also dipped into a water reservoir to get rid of possible contaminations on the outer part of the capillary.
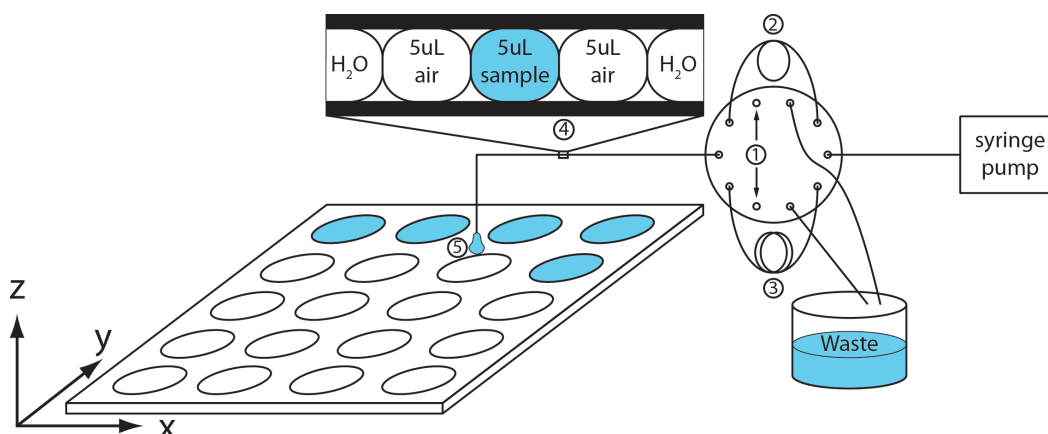

Figure 4-1: *Schematic drawing of the spotting device. The sample and the air bubble were introduced via the injection port (1) into the 5 µL (2) and the 10 µL loop (3), respectively. The sample was separated from the surrounding solvent with a 5 µL air bubble on both sides in the capillary (4). The droplet of the sample was formed at the tip of the nozzle (5) to a final volume of 0.5 µL and deposited by lifting the MALDI plate close to the nozzle.*

4.3.4 Mass Spectrometry

A MALDI ToF/ToF mass spectrometer (4800 Plus, AB SCIEX, Darmstadt, Germany) equipped with a frequency-tripled Nd:YAG laser (355 nm) was used. The laser power is reported in arbitrary units ranging from 0 to 7000. An acceleration voltage of 20 kV was applied. In one run, the same sample spot was measured several times with identical conditions. One of these measurements consisted of 200 to 500 shots that were accumulated and averaged to obtain a mass spectrum. The laser shots were distributed in a randomized pattern over the whole sample spot. To allow for measurements in the high mass region, the system was equipped with a special high mass detector (HM2tuvo, CovalX, Zürich, Switzerland) based on ion-to-secondary ion-to-electron conversion. The detector voltages for the first and second conversion dynodes were -2.5 kV and -20kV, respectively. Calibration was performed using proteins with known masses such as BSA or IgG and extrapolated to a higher m/z range. The data was recorded using software from the manufacturer (4000 Series Explorer V.3.5.3, AB SCIEX, Darmstadt,

Germany) and exported as a text file to OriginPro 8.5.0 (OriginLab Corporation, Northampton MA, USA), where the data were smoothed with the provided Savitzky-Golay algorithm.

4.4 Results and discussion

Ionic liquids have been successfully used as MALDI matrices for a broad range of analytes such as amino acids [15], DNA oligomers [13], peptides [10,11] and proteins with molecular weights up to approximately 146 kDa per monomer [10-12]. Since sinapinic acid usually shows the best performance for the analysis of high-mass proteins, especially in the mass range over 100 kDa, we chose sinapinate as the anion for the ionic liquids. Different amines were tested as counter cations. For comparison, an ionic liquid consisting of N-methyl-N-isopropyl-N-tertbutyl amine in combination with CHCA was also used. Using this matrix, the trimer of urease with a total molecular weight of 270 kDa has previously been detected [11].

When investigating complex samples such as lysates or mixtures with unknown compounds with MALDI-MS, sensitivity is a key aspect. To determine the sensitivity, a dilution series with rh Fn was generated with either PBS buffer or water as the solvent. These freshly prepared diluted samples were mixed in a 1:1 (v:v) ratio with the matrix under investigation and analyzed by MALDI-MS. The sample is detected mainly as protonated species, but sodiated species cannot be excluded entirely. Due to the limited resolution of the instrument in this m/z range the different species cannot be distinguished. The limit of detection was taken to be the lowest concentration where the signal of the singly charged monomer (226 kDa) was still visible with a signal-to-noise ratio of 3:1 (Fig. 4-2). The observed limit of detection was found to depend on the solvent used for dilution as well as on the matrix. The limits of detection for solid sinapinic acid as matrix were determined as 15 fmol or 7.5 fmol of rh Fn diluted in water or PBS, respectively (data not shown). When using an ionic liquid matrix consisting of trimethylammonium and sinapinate, the limit of detection was 5 fmol when using either water or PBS as solvent. This is in the same range, or even slightly lower, compared to using a solid matrix. Therefore, no drawbacks arise concerning the sensitivity when ionic liquids are used as matrix instead of sinapinic acid.
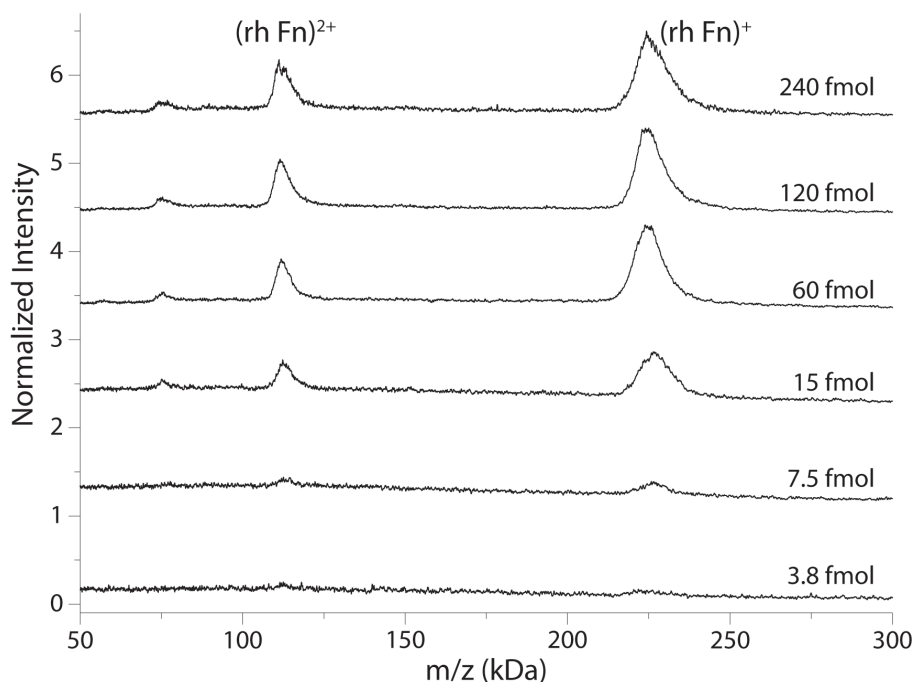
Figure 4-2: *Determination of the limit of detection for rh Fn. The limit of detection is defined to be the concentration where the singly charged fibronectin monomer (226 kDa) is still detectable with a signal-to-noise ratio of 1:3, which is in this example 7.5 fmol rh Fn per spot, whereas the next lower amount of 3.8 fmol did not yield a signal.*

Besides the sensitivity, the homogeneity of the sample spot also plays an important role. Measuring a sample spot many times generally leads to decreasing signal intensity in MALDI, since the sample is gradually depleted by laser ablation. If the sample is distributed evenly and the laser shots are distributed randomly over the whole spot, the signal intensity should decrease monotonically. If sweet spots exist, the signal decrease might not be monotonic but more random. For example, if in the first measurements of a run the sweet spots are missed, but hit in a later measurement, the signal intensity will increase again. To compare the behavior of an ionic liquid and a solid matrix, IgG was measured using an MIT-amine ionic liquid matrix as well as solid sinapinic acid. Both matrices were prepared at a concentration of 10 mg mL^{-1} in 2:1 acetonitrile:water (v/v). An equal volume of matrix and sample was mixed and spotted eight times with a volume of 0.5 µL per spot. Each of the eight spots was analyzed by ten series of 500 shots in a randomized pattern with a laser power of 4600 a.u. Eight replicates of the ten series were averaged and plotted. Figure 4-3 shows that the signal intensity of the experiment with the solid matrix does not decrease steadily, but reaches a maximum intensity in the fourth run. This somewhat unexpected finding is probably due inhomogeneity in crystallization, that may lead to accumulation of salts or other impurities in different layers of the crystallized sample, and exposure of the highest sample concentration once the laser has

removed some of these layers. In contrast, the use of ionic liquids leads to a steadily decreasing signal. This observation allows the design of an automated run with a reduced number of laser shots and thus shorter overall measurement time, since the signal intensity is monotonically decaying. When performing a series of measurements manually, it is also possible to search for a sweet spot to obtain the best signal possible. However, if the laser beam is "parked" on such a sweet spot it will soon become depleted and yield no signal anymore. If a large number of measurements is needed, for example in MALDI imaging, manual acquisition of spectra is very time consuming or impossible and therefore, automated acquisition is highly beneficial [18].
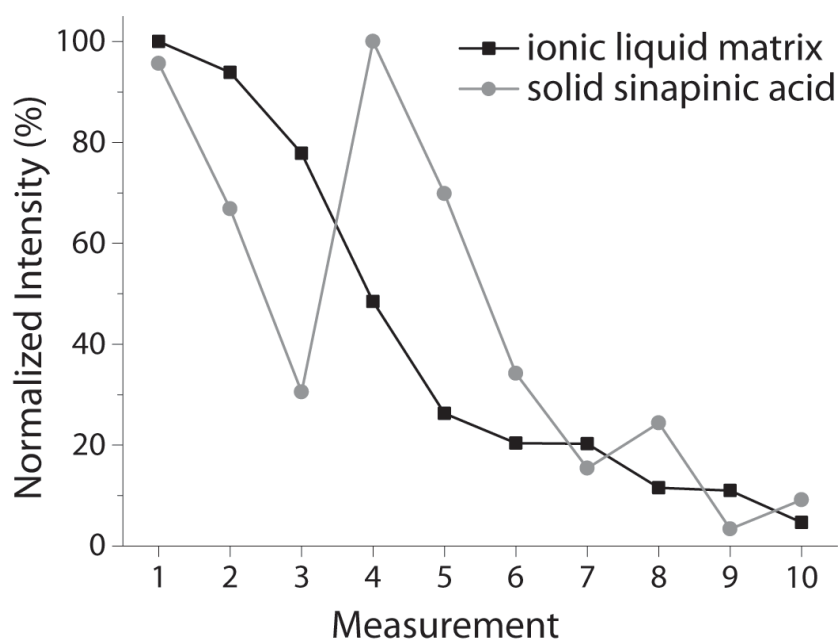
Figure 4-3: *Comparison between the signal intensity of the rh Fn monomer measured either in solid sinapinic acid (grey) or in ionic liquid consisting of sinapinate and trimethylammonium (black). The steady signal decay when using the ionic matrix shows the homogeneous distribution of the sample within the spot. The decrease is caused by depletion of sample during the measurement. The grey curve shows much more fluctuations in signal intensity, therefore leading to the conclusion that the sample was not distributed homogeneously but forming sweet spots.*

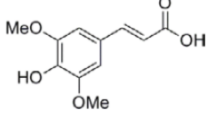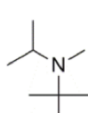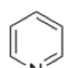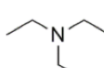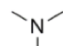| Sinapinic acid		MIT-amine 10.90[12]	Pyridine 5.23	Triethylamine 10.75	Trimethylamine 9.80
	$pK_a{}^{36}$ PA [kJ mol^{-1}][36]	NA	930	981.8	948.9
Protein	MW (kDa)				
Immunoglobulin M	1000	0	**	0	*
Bovine thyroglobulin	660	0	0	0	*
Recombinant human fibronectin	226	0	*	0	**
Immunoglobulin G	148	*	**	**	***

Table 4-1: *Summary of the different proteins and ionic liquids that were investigated. The pK$_a$ and the proton affinity (PA) of the used amines are specified, where available. The quality of the obtained spectra is indicated with a three star ranking system, where three stars indicate the optimum. No signal obtained is indicated with a "0". As can be seen, there are proteins that seem to work with every matrix (IgG) and matrices, which are able to ionize all the proteins (trimethylamine).*

In table 4-1, results for all four proteins measured with different cations are summarized. This table shows that the choice of the amine cation is crucial for the success of a measurement. Some proteins seem to possess properties that render them rather easy to ionize (e.g. IgG) while others are only ionizable with a certain combination of cation and anion of the liquid matrix. Moreover, ammonium cations which work for a certain organic acid as counterion, such as MIT-amine in combination with CHCA [11], do not necessarily work well with others. The reason for these findings might be that the size of the cation, which decreases from left to right in table 1, hampers the protonation of the amine by the sinapinic acid molecule and this leads to a mixture of ionic liquid matrix and sinapinic acid. The amine might get protonated during the MALDI process and therefore reduce the ionization yield of the sample. In a study published by Crank and Armstrong [11], the pK$_a$ and the proton affinities were identified as two major factors determining the ability of a cation to form ionic liquid matrices that work well. They observed a trend that the cation needs a pK$_a$ ≥ 11 and a proton affinity > 930 kJ mol^{-1} to form a matrix that performs well in MALDI. We found that in addition, the sample itself influences the success of the experiment: the two cations that worked well for the analysis of IgM, pyridine and trimethylamine, do not fulfill the requirements concerning pK$_a$. Similar results were obtained by Mank et al. [12] where IgG was detected using tributylamine as cation (pK$_a$ = 9.9) [11]. However, all these cations have a proton affinity ≥ 930 kJ mol^{-1} and thus fulfill the second requirement [36]. In general it could be shown that ionic matrices are applicable for the

analysis of biomolecules with very high molecular weights, and present a suitable alternative to conventional solid matrices.

To allow for the analysis of high-mass biomolecules, e.g. in a cell lysate, the suitability of a spotting device, such as the one shown in figure 4-1, in combination with ionic liquids as matrices needs to be verified. The spotting device used in this work is compatible with commercially available 384 spot MALDI plates that were cut in half. For reasons of the limited travel range of the xyz stage, only eleven rows with eight spots each were accessible. Typically, 0.5 µL of sample were deposited with a flow rate of 1 µL min^{-1}. If the time needed for movements of the sample plate is taken into account, an overall spotting time of only ca. 45 s per spot is currently required. The accessible range of the MALDI plate can be spotted in about 1 h. The accessible range could easily be increased by replacing the currently used stage motors with motors with greater travel distances, large enough to cover the whole 384-spot plate.

Two proteins that are considered to be "difficult" due to their high masses were chosen as test samples. They were deposited in the same way as described above, using the spotting device. In case of rh Fn, a matrix made from trimethylamine solution and sinapinic acid was used, for IgM the matrix consisted of SA and pyridine. 10 µL of the sample/matrix mixture was injected with the gas-tight syringe into the spotting device (Fig. 4-1). High-mass protein samples were then spotted onto the stainless steel MALDI plate and analyzed (Fig. 4-4) with 200 shots at a laser power of 5100 a.u. The fused silica nozzle could be used for 48 consecutive runs without any signs of plugging. This shows the advantages of ionic liquids over conventional matrices, where plugging was observed [23]. The protein peaks were easily detected and assigned. The width of the signal of IgM is caused by the microheterogeneity in the primary amino acid sequence and the glycosylations that are present. The spotting device is able to handle samples with such high masses without losing the sample in the tubing due to adhesion. Furthermore, no cross contamination was observed. Although the use of ionic liquids for MALDI imaging has already been shown [22], this was never extended to biomolecules with high masses. With the approach introduced in this work, imaging of these compounds might become feasible and allow further insight into the distribution of proteins and similar samples within tissues.

The setup presented here enables the parallel preparation of EM grids [32] and MALDI-MS targets using a microfluidic platform. Since the handover of the sample is lossless, even the preparation of tiny sample amounts becomes possible. In a next step, the sample preparation will become online, which means that the sample and the matrix is mixed within the microfluidic

device and therefore the sample amount needed is reduced even further. During this step, other sample pretreatment, such as desalting, dilution, or buffer exchange can be performed as well. In the future, this workflow could allow for the analysis of cell lysates, where the samples of interest are only present in limited quantity. Complete automation of the whole spotting procedure allows rapid preparation of the targets. Therefore, information about the content of cells concerning the shape and the mass of the compounds could be gained and probably changes in the expression of certain proteins could be monitored.
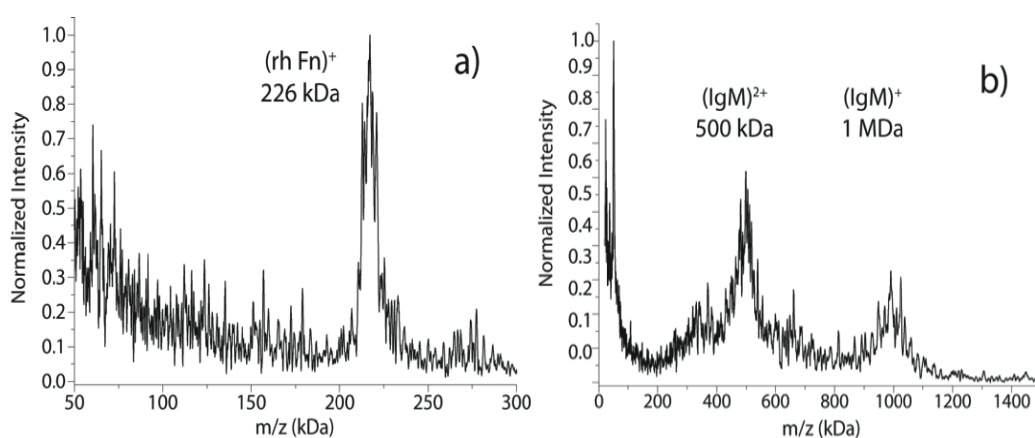
Figure 4-4: The spectra of recombinant human fibronectin (a) and Immunoglobulin M (b) were recorded from spots deposited using an automated spotting device. For rh Fn an ionic matrix produced from trimethylamine and sinapinic acid was used. The spectrum of IgM was recorded using sinapinic acid as anion as well, but pyridine as counterion.

4.5 Conclusions

In this work, we could show that ionic liquids are useful for the analysis of high mass biomolecules and that the deposition of ionic liquid matrices with a spotting device proves to be useful for the preparation of MALDI samples. The process of sample deposition can either be automated or is controlled manually. Since the same spotting device can be used for preparation of both, MALDI samples and EM grids, analysis of the same sample with respect to mass and shape is possible.

Furthermore, it was possible to show the suitability of these matrices for high-throughput MALDI-MS, especially considering the fact that the benefits do not lead to disadvantages such as lower sensitivity. This fact is indeed crucial for the success of the presented combination, since a low limit of detection allows extending the range of applications and might in the future allow for the survey of reactions or events along a time axis. To achieve this

goal, it is necessary to continue the developments of the existing system and combine it, for example, with a continuous feed of matrix. This would allow skipping the sample preparation in vials and enabling online sample processing.

4.6 References

[1]   Karas, M. & Hillenkamp, F. **Laser Desorption Ionization of Proteins with Molecular Masses Exceeding 10 000 Daltons**. *Anal. Chem.* 60, 2299-2301, (1988).

[2]   Hillenkamp, F. & Peter-Katalinic, J. **MALDI MS - A Practical Guide to Instrumentation, Methods and Application**. WILEY-VCH Verlag GmbH und Co. KGaA, Weinheim (2007).

[3]   Jurinke, C., Oeth, P. & van den Boom, D. **MALDI-TOF mass spectrometry - A versatile tool for high-performance DNA analysis**. *Mol. Biotechnol.* 26, 147-163, (2004).

[4]   Cohen, S. L. & Chait, B. T. **Influence of Matrix Solution Conditions on the MALDI-MS Analysis of Peptides and Proteins**. *Anal. Chem.* 68, 31-37, (1996).

[5]   Zenobi, R. & Knochenmuss, R. **Ion formation in MALDI mass spectrometry**. *Mass Spectrom. Rev.* 17, 337-366, (1998).

[6]   Knochenmuss, R. **Ion formation mechanisms in UV-MALDI**. *Analyst* 131, 966-986, (2006).

[7]   Karas, M., Glückmann, M. & Schäfer, J. **Ionization in matrix-assisted laser desorption/ionization: singly charged molecular ions are the lucky survivors**. *J. Mass Spectrom.* 35, 1-12, (2000).

[8]   Sadeghi, M. & Vertes, A. **Crystallite size dependence of volatilization in matrix-assisted laser desorption ionization**. *Appl. Surf. Sci.* 127-129, 226-234, (1998).

[9]   Jaskolla, T. W., Karas, M., Roth, U., Steinert, K., Menzel, C. *et al.* **Comparison Between Vacuum Sublimed Matrices and Conventional Dried Droplet Preparation in MALDI-TOF Mass Spectrometry**. *J. Am. Soc. Mass Spectrom.* 20, 1104-1114, (2009).

[10] Armstrong, D. W., Zhang, L.-K., He, L. & Gross, M. L. **Ionic Liquids as Matrixes for Matrix-Assisted Laser Desorption/Ionization Mass Spectrometry**. *Anal. Chem.* 73, 3679-3686, (2001).

[11] Crank, J. A. & Armstrong, D. W. **Towards a Second Generation of Ionic Liquid Matrices (ILMs) for MALDI-MS of Peptides, Proteins, and Carbohydrates**. *J. Am. Soc. Mass Spectrom.* 20, 1790-1800, (2009).

[12] Mank, M., Stahl, B. & Boehm, G. **2,5-Dihydroxybenzoic Acid Butylamine and Other Ionic Liquid Matrixes for Enhanced MALDI-MS Analysis of Biomolecules**. *Anal. Chem.* 76, 2938-2950, (2004).

[13] Carda-Broch, S., Berthod, A. & Armstrong, D. W. **Ionic matrices for matrix-assisted laser desorption/ionization time-of-flight detection of DNA oligomers**. *Rapid Commun. Mass Spectrom.* 17, 553-560, (2003).

[14] Tholey, A. & Heinzle, E. **Ionic (liquid) matrices for matrix-assisted laser desorption/ionization mass spectrometry—applications and perspectives**. *Anal. Bioanal. Chem.* 386, 24-37, (2006).

[15] Zabet-Moghaddam, M., Heinzle, E. & Tholey, A. **Qualitative and quantitative analysis of low molecular weight compounds by ultraviolet matrix-assisted laser desorption/ionization mass spectrometry using ionic liquid matrices**. *Rapid Commun. Mass Spectrom.* 18, 141-148, (2004).

[16] Caprioli, R. M., Farmer, T. B. & Gile, J. **Molecular imaging of biological samples: Localization of peptides and proteins using MALDI-TOF MS**. *Anal. Chem.* 69, 4751-4760, (1997).

[17] Chaurand, P., Stoeckli, M. & Caprioli, R. M. **Direct profiling of proteins in biological tissue sections by MALDI mass spectrometry**. *Anal. Chem.* 71, 5263-5270, (1999).

[18] Stoeckli, M., Farmer, T. B. & Caprioli, R. M. **Automated mass spectrometry imaging with a matrix-assisted laser desorption ionization time-of-flight instrument**. *J. Am. Soc. Mass Spectrom.* 10, 67-71, (1999).

[19] Stoeckli, M., Chaurand, P., Hallahan, D. E. & Caprioli, R. M. **Imaging mass spectrometry: A new technology for the analysis of protein expression in mammalian tissues**. *Nat. Med.* 7, 493-496, (2001).

[20] Grey, A. C., Chaurand, P., Caprioli, R. M. & Schey, K. L. **MALDI Imaging Mass Spectrometry of Integral Membrane Proteins from Ocular Lens and Retinal Tissue**. *J. Proteome Res.* 8, 3278-3283, (2009).

[21] Chan, K., Lanthier, P., Liu, X., Sandhu, J. K., Stanimirovic, D. *et al.* **MALDI mass spectrometry imaging of gangliosides in mouse brain using ionic liquid matrix**. *Anal. Chim. Acta* 639, 57-61, (2009).

[22] Meriaux, C., Franck, J., Wisztorski, M., Salzet, M. & Fournier, I. **Liquid ionic matrixes for MALDI mass spectrometry imaging of lipids**. *J. Proteomics* 73, 1204-1218, (2010).

[23] Aerni, H.-R., Cornett, D. S. & Caprioli, R. M. **Automated acoustic matrix deposition for MALDI sample preparation**. *Anal. Chem.* 78, 827-834, (2006).

[24] Ericson, C., Phung, Q. T., Horn, D. M., Peters, E. C., Fitchett, J. R. *et al.* **An automated noncontact deposition interface for liquid chromatography matrix-assisted laser desorption/ionization mass spectrometry**. *Anal. Chem.* 75, 2309-2315, (2003).

[25] Önnerfjord, P., Ekström, S., Bergquist, J., Nilsson, J., Laurell, T. *et al.* **Homogeneous sample preparation for automated high throughput analysis with matrix-assisted laser desorption/ionisation time-of-flight mass spectrometry**. *Rapid Commun. Mass Spectrom.* 13, 315-322, (1999).

[26] Meier, M. A. R., de Gans, B.-J., van den Berg, A. M. J. & Schubert, U. S. **Automated multiple-layer spotting for matrix-assisted laser desorption/ionization time-of-flight mass spectrometry of synthetic polymers utilizing ink-jet printing technology**. *Rapid Commun. Mass Spectrom.* 17, 2349-2353, (2003).

[27] Baluya, D. L., Garrett, T. J. & Yost, R. A. **Automated MALDI matrix deposition method with inkjet printing for imaging mass spectrometry**. *Anal. Chem.* 79, 6862-6867, (2007).

[28] Canelle, L., Pionneau, C., Marie, A., Bousquet, J., Bigeard, J. *et al.* **Automating proteome analysis: improvements in throughput, quality and accuracy of protein identification by peptide mass fingerprinting**. *Rapid Commun. Mass Spectrom.* 18, 2785-2794, (2004).

[29] Baeumlisberger, D., Rohmer, M., Arrey, T. N., Mueller, B. F., Beckhaus, T. *et al.* **Simple Dual-Spotting Procedure Enhances nLC-MALDI MS/MS Analysis of Digests with Less Specific Enzymes**. *J. Proteome Res.* 10, 2889-2894, (2011).

[30] Leinweber, B. D., Tsaprailis, G., Monks, T. J. & Lau, S. S. **Improved MALDI-TOF Imaging Yields Increased Protein Signals at High Molecular Mass**. *J. Am. Soc. Mass Spectrom.* 20, 89-95, (2009).

[31] van Remoortere, A., van Zeijl, R. J. M., van den Oever, N., Franck, J., Longuespee, R. *et al.* **MALDI Imaging and Profiling MS of Higher Mass Proteins from Tissue**. *J. Am. Soc. Mass Spectrom.* 21, 1922-1929, (2010).

[32] Kemmerling, S., Ziegler, J., Schweighauser, G., Arnold, S. A., Giss, D. *et al.* **Connecting µ-fluidics to electron microscopy.** *J. Struct. Biol.* 177, 128-134, (2012).

[33] Benesch, J. L. P., Ruotolo, B. T., Simmons, D. A., Barrera, N. P., Morgner, N. *et al.* **Separating and visualising protein assemblies by means of preparative mass spectrometry and microscopy**. *J. Struct. Biol.* 172, 161-168, (2010).

[34] Engel, A. **Assessing biological samples with scanning probes** in: Single Molecule Spectroscopy in Chemistry, Physics and Biology, *Springer Series in Chemical Physics.*, Vol. 96, Ch. 21, 417-431, Springer, Berlin Heidelberg, (2010).

[35] Linder, V., Sia, S. K. & Whitesides, G. M. **Reagent-loaded cartridges for valveless and automated fluid delivery in microfluidic devices**. *Anal. Chem.* 77, 64-71, (2005).

[36] Haynes, W. M. **CRC Handbook of Chemistry and Physics**. 92th ed., CRC Press/Taylor and Francis, Boca Raton, FL, USA (Internet Version 2012).

5 Single-cell lysis for visual analysis by electron microscopy

Simon Kemmerling[1, #], Stefan A. Arnold[1, #], Benjamin A. Bircher[1], Nora Sauter[1], Carlos Escobedo[2], Gregor Dernick[3], Andreas Hierlemann[2], Henning Stahlberg[1] and Thomas Braun[1,*]

[1] Center for Cellular Imaging and Nano Analytics (C-CINA), Biozentrum, University of Basel, Basel, Switzerland.

[2] Department of Biosystems Science and Engineering (D-BSSE), ETH Zurich, Basel, Switzerland.

[3] Discovery Technologies, Pharma Research and Early Development (pRED), F. Hoffmann-La Roche AG, Basel, Switzerland

[#] Authors contributed equally.

[*] Corresponding Author: thomas.braun@unibas.ch

5.1 Abstract

The stochastic nature of biological systems makes the study of individual cells a necessity in systems biology. Yet, handling and disruption of single cells and the analysis of the relatively low concentrations of their protein components still challenges available techniques. Transmission electron microscopy (TEM) allows for the analysis of proteins at the single-molecule level. Here, we present a system for single-cell lysis under light microscopy observation, followed by rapid uptake of the cell lysate. Eukaryotic cells were grown on conductively coated glass slides and observed by light microscopy. A custom-designed microcapillary electrode was used to target and lyse individual cells with electrical pulses. Nanoliter volumes were subsequently aspirated into the microcapillary and dispensed onto an electron microscopy grid for TEM inspection. We show, that the cell lysis and preparation method conserves protein structures well and is suitable for visual analysis by TEM.

5.2 Introduction

The aim of systems biology is to understand the emergence of biological functions from interaction networks [1]. This requires knowledge of the intracellular players and their interconnections, for which an inventory of the individual components of the system, i.e. the transcriptome, the proteome, the metabolome and, finally, the interactome, has to be assembled. Such an inventory will strongly vary from cell to cell, as the stochastic nature of biological processes leads to "biological noise" [2,3]. This makes the study of individual systems, e.g., single cells, a necessity [4].

Genome sequencing [5] and expression profiling [6] are far advanced, and amplification techniques are ready to be applied to single cells [7]. The analysis of the metabolism of a biological system profits from the experience and advances of analytical chemistry [8]; for example, mass spectrometry (MS) can be used to identify metabolites with single-cell sensitivity [9]. Moreover, excellent imaging techniques, such as light- and electron microscopy (EM) or X-ray diffraction imaging, are available for structural analyses.

However, proteomic studies at the single-cell level are hampered by the low expression level of many proteins and the lack of amplification techniques. Although powerful and valuable techniques, such as MS [10] and cryo-electron tomography (cryo-ET) [11-13], are applied for single-cell proteomic studies, such studies still remain a challenging task, especially for

eukaryotic cells [14-16]. Thus, adjuvant techniques utilizing novel or hybrid approaches are beneficial to further untangle the complexity of single-cell protein networks.

A combination of microfluidics and TEM was suggested as an alternative and complementary approach to investigate the protein content of single eukaryotic cells [17,18]. The idea is to physically lyse single cells and spread the entire sample onto EM grids for structural analysis by transmission electron microscopy (TEM), or mass measurements by scanning TEM (STEM). This "lyse and spread" approach provides access to EM imaging at a higher signal-to-noise ratio (SNR) than when in the cellular background, and enables a more straightforward correlation of structural information with mass data. A prerequisite of this envisaged approach is a targeted lysis of individual cells and an efficient preparation of their lysate for TEM analysis.

A variety of different techniques for single-cell lysis exists today, and most of them have been implemented in microfluidic systems [19]. Many of these systems utilize the principle of electroporation [20,21] to lyse detached or suspended cells in flow-through configurations, whereas only a few report on electrical lysis of "standard" adherent eukaryotic cells in cultures [22,23]. However, despite their popularity none of these systems has been utilized to prepare samples of a single-cell lysate for electron microscopy.

Here, we present a system for the electrical lysis of individual adherent eukaryotic cells and subsequent preparation of minute sample volumes for negative-stain TEM. The setup includes a custom-designed microcapillary electrode (Fig. 5-1), which targets and lyses individual cells observed in a light microscope. Immediately after lysis, the cell-fragments are aspirated into the microcapillary, deposited on an EM grid and negatively stained. This method offers the potential for an alternative approach to analyze proteins and protein complexes from individual eukaryotic cells.

5.3 Materials and Methods

5.3.1 Instrument setup

The principle and basic design of the system developed for the electrical lysis of single cells is shown in figure 5-1A. The system is designed for use with an inverted optical microscope (OM; Zeiss Axiovert 40C). The microscope is equipped with a custom-built stage that has a customized mounting frame on the objective guide. The latter accommodates an indium tin oxide (ITO)-coated glass slide (ground electrode and sample platform) and can be moved manually in the xy-plane. Miniaturized Petri dishes on the surface of the glass slide (see below) allow cell cultures to be grown. A

tapered gold-coated microcapillary that serves as second electrode can be positioned in close proximity above the glass slide. The upper un-tapered end of the microcapillary is inserted in a steel adapter and electrically connected with silver paint (Fig. 5-1B). The insulating holder of the adapter is attached to a stepper motor (PI M-126.PD2, Physik Instrumente, Germany) mounted on top of an xy-platform on the microscope stage. This platform allows the microcapillary tip to be centered above the objective lens of the OM. The stepper motor moves the capillary in the z-direction. The other end of the steel adapter holding the capillary is connected via a PEEK (poly(ether-ether-ketone)) tube (inner diameter (ID) 250 µm) to a pressure reservoir (Fig. 5-1). The tube is intercepted by a solenoid valve (LVFA0550310H, The Lee Company, USA) that is controlled by the computer through an NI USB-6009 module. A pressure controller (PCNC-0001-00, Seyonic, Switzerland) is used to apply positive or negative pressure to the system via the pressure reservoir. A function generator (33220A, Agilent, Switzerland) delivers a voltage signal, which is amplified 20 times by a linear voltage amplifier (F20A, FLC Electronic AB, Sweden). The output of the linear amplifier is electrically connected to the capillary, and the conductive glass slide is grounded. All electronic components of the system are controlled by a LabVIEW-based, custom-made software (supp. Fig. 5-1). A camera (GC750 GigE, Prosilica, USA), mounted on the microscope, enables live-cell imaging and video recording. The next version of the control software will be available as an open-source plug-in for the openBEB (open biological experiment browser) system (www.openBEB.org).

5.3.2 Microcapillaries

Fused-silica (FS) microcapillaries (outer diameter (OD) 350 µm, ID 250 µm, Polymicro) were cut to a length of 10-15 cm. The polymer coating in the middle was removed over a length of 1-2 cm, using hot chromic-sulfuric acid (102499, Merck, Switzerland). Afterwards, the microcapillaries were rinsed thoroughly with double distilled H_2O (ddH_2O), followed by isopropanol and subsequently pulled with a laser-based micropipette puller (Sutter Instruments, P2000) to obtain a taper with a 30-50 µm ID at the tip. The tapered microcapillaries were plasma-cleaned before the sputter-deposition of a 2 nm Ti adhesive layer, followed by a 50-100 nm Au layer on their outer surface to increase conductivity. Coating was successively performed from two opposite sides at an angle of 45 degrees to obtain a closed conductive layer around the microcapillaries.
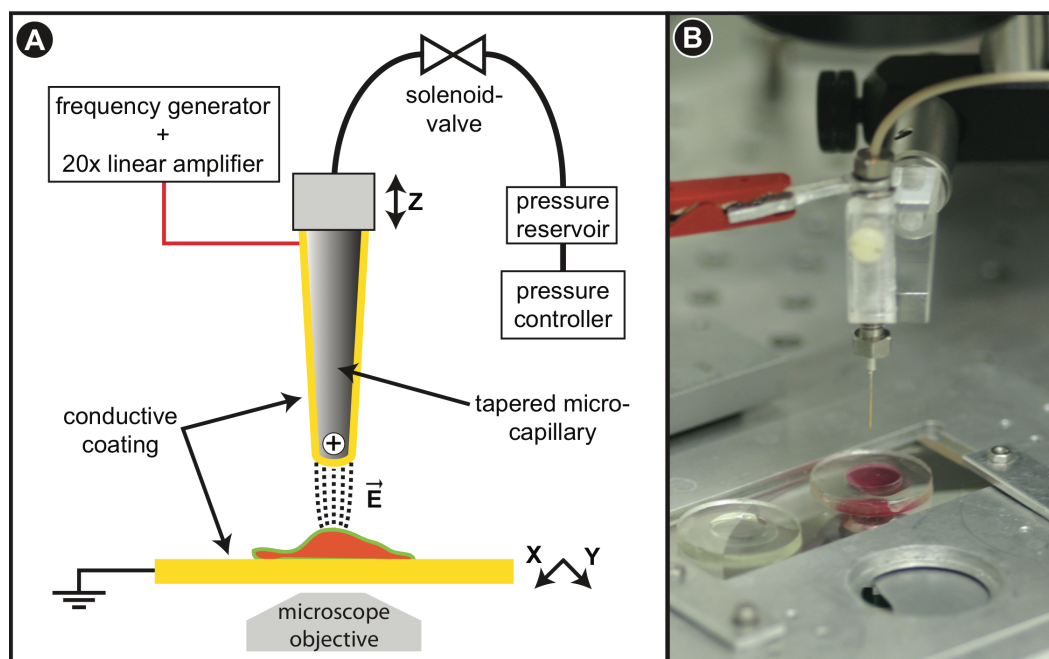
Figure 5-1*: Single-cell lysis instrumentation. (A) Schematic representation of the single-cell lysis setup, which is mounted on an inverted optical microscope. A camera allows for live-cell imaging. The stepper motor approaches the gold-coated microcapillary to the ITO-coated glass slide, where individual cells can be targeted. The function generator sends a voltage pulse to the capillary tip to lyse the cell. Meanwhile, the pressure controller builds up a negative pressure on the closed solenoid valve. Upon cell lysis, the valve is opened for a defined period of time, and the cell lysate is aspirated into the capillary. (B) Lysis microcapillary and cell culture slide. The upper end of the gold-coated microcapillary is inserted into a steel adapter and electrically connected with silver paste. The other end of the steel adapter is attached to a piece of PEEK tubing that connects the microcapillary to the pressure controller via a pressure reservoir. The microcapillary is positioned above a grounded, ITO-coated, glass slide with a PDMS ring on its surface. Slide and ring form a mini Petri dish that can be filled with cell culture medium (red).*

5.3.3   Miniaturized Petri dishes on conducting glass slides

Commercially available ITO-coated glass slides (Diamond Coatings UK, 8-12 Ω/square) were used as a conductive substrate for cell culturing. These slides have a silver electrode at each end for electrical connections. They were washed and sonicated in detergent solution (1% Alconox, Alconox Inc., USA), rinsed with ddH2O and stored in ethanol until use.

PDMS (poly(dimethylsiloxane), Dow Corning SYLGARD 184) rings with an ID of 1 cm and a height of 2-3 mm, were fabricated and reversibly bonded onto glass slides to form sample wells with a volume of about 250 μl. These miniaturized Petri dishes allowed cells to be grown and kept in a physiological buffer solution during the experiment. An ITO glass slide with a PDMS ring filled with cell culture medium is shown in figure 5-1B.

5.3.4   Cell culture

Adherent baby hamster kidney fibroblasts (BHK21; ECACC 85011433) were cultured in polystyrene T75-flasks containing 30 ml DHI-5 medium (see below) at 37 °C and 5% carbon dioxide. To split the cells, the medium was removed, and the flask was washed with 10 ml of 37 °C warm PBS w/o calcium and magnesium (Dulbecco's Phosphate Buffered Saline, D8537, Sigma, Switzerland). To detach the cells, 3 ml of trypsin-EDTA solution (0.05% Trypsin, 0.53 mM EDTA; 25300-054, Invitrogen, Switzerland) were added, and the cells were incubated at 37 °C for 5 min. The detached cells were diluted with 7 ml of 37 °C warm DHI-5 medium and homogenized using a pipette. 0.5 ml of the homogenized cell suspension and 30 ml of fresh media were returned to the flask for further cultivation. The rest of the cell suspension was used for experiments or disposed. A miniaturized Petri dish was filled with approximately 250 µl of medium, and 1-2 µl of cell suspension were added. The cells were incubated on the glass slide base of this dish for 1-2 days at 37 °C and 5% CO_2.

DHI-5 medium is a 1:1:2 mixture of DME (Dulbecco's Modified Eagles Medium; D6171, Sigma, Switzerland), HamF12 (Nutrient Mixture F-12Ham; N8641, Sigma, Switzerland), and IMDM (Iscove's Modified Dulbecco's Medium; I3390, Sigma, Switzerland) media, supplemented with 5% FCS (Fetal Bovine Serum; E7524, Sigma, Switzerland) and complemented with non-essential amino acids (MEM non-essential amino acid solution; M7145, Sigma, Switzerland), L-glutamine (L-glutamine solution; G7513, Sigma, Switzerland), and vitamins (RPMI1640 vitamins solution; R7256, Sigma, Switzerland).

For the single-cell lysis experiments, the medium was removed from the sample well, and the cells were washed twice with 37 °C warm PBS (Dulbecco's Phosphate Buffered Saline; D8662, Sigma, Switzerland), ISB (isotonic sucrose buffer: 0.25 M sucrose, Bio-Rad, 161-0720; 5 mM HEPES pH 7.4, AppliChem A3724) or HEPES buffer (0.15 M NaCl; 20 mM HEPES pH 7.4; 5.5 mM KCl; 2 mM $CaCl_2$; 1 mM $MgCl_2$). The cells remained in the wash buffer solution during the experiment.

5.3.5   Cell lysis

Live BHK21 cells were lysed in situ in PBS, HEPES or ISB buffer. During the experiments, the conductive glass slide hosting the cell culture was electrically grounded, and the microcapillary was connected to a function generator. The miniaturized Petri dish, formed by a PDMS ring and the glass slide, was positioned on the OM stage. An individual cell was then selected and centered in the field of view with the help of the microscope. Next, the tip of the gold-coated microcapillary was immersed in the buffer solution,

brought in close proximity to the conductive surface of the glass slide (distance ≈ 20 μm) using the stepper motor and aligned directly above the targeted cell by moving the microscope stage. A camera mounted on the microscope allowed for live-imaging of the individual cells and their surroundings during the following lysis procedure. After aligning the microcapillary tip above a targeted cell, a burst of five to ten DC square pulses with amplitudes of 6-10 V and a frequency of 10 kHz (pulse duration: 50 μs) was applied to the gold-coated microcapillary using the function generator. This generated a strong electric field (3-5 kV/cm) across the selected cell and resulted in cell lysis. Note, for the compensation of electrode aging, higher voltages were applied in rare cases (maximally 20 V). Right after the burst, the solenoid valve was opened towards the partially evacuated pressure reservoir (Fig. 5-1A) and remained open for a defined period of time, aspirating sub-microliter volumes (200–400 nl) of lysate and buffer into the microcapillary. The amount of sample aspirated was controlled by the pressure difference (-50 to -600 mbar) and the opening time of the solenoid valve (50-400 ms). To transfer the sample, an EM grid was clamped by tweezers and centered under the microcapillary. The tip of the microcapillary was approached close to the surface of the grid by the stepper motor. The aspirated sample was then dispensed directly onto the carbon film of the grid by applying a positive pressure to the microcapillary.

Single-cell lysis and aspiration experiments were also performed with fluorescently stained HEK293 cells (see supplementary material and supplemental movies 1 and 2).

5.3.6 Electron microscopy

Loaded sample grids were incubated for 60 sec - 20 min in a humidity chamber to prevent desiccation. Grids with adsorption times of longer than 3 min were washed on four drops of ddH$_2$O and blotted once at the end and air-dried. All samples were negatively stained with two 5 μl drops of 2% uranyl acetate (UA) or 2% ammonium molybdate (AM) and imaged in a Phillips CM10 electron microscope operated at 80 kV. The images were recorded on a 2k x 2k CCD camera (Olympus SIS, Münster, Germany).

5.3.7 Enzyme activity assay

Horseradish peroxidase (HRP) conjugated goat anti-mouse IgG (8.5 mg/ml, A2554, Sigma, Switzerland) was diluted to a concentration of 4.25 μg/ml in PBS. 3 μl of the sample was placed onto an ITO coated glass slide, and the microcapillary electrode was placed in the drop, about 20 μm above the glass slide. Different voltages (0 V, 4-18 V in 2 V steps and 22 V), each

with a burst count of 5 and a single pulse length of 50 µs were applied. 2 µl were removed from the treated sample droplet, diluted to 8.5 ng/ml in PBS, and the enzymatic activity of HRP was analyzed by enhanced chemiluminescence (ECL) on a dot plot (Amersham ECL Prime Western Blotting Detection Reagent; RPN2232, GE Healthcare, UK).

5.4 Results

The single-cell lysis setup (Fig. 5-1) allows for live-cell imaging, lysis of single adherent eukaryotic cells, rapid aspiration of the lysate, and transfer of the sample onto EM grids. This is demonstrated using adherent BHK21 cells.

The adherent cells were individually lysed in situ in buffer solution, while the process was monitored by means of optical microscopy. To achieve lysis, a gold-coated microcapillary tip was positioned in close proximity to and directly above the selected BHK21 cell growing on the ITO coated glass slide inside of a miniaturized Petri dish (Fig. 5-1B). The distance between the capillary tip and the conductive surface of the glass slide was approximately 20 µm; there was no direct cell contact. As documented by light microscopy, the electric field, generated across the cell by a burst of five to ten 50 µs DC square pulses with amplitudes of 6-10 V applied to the microcapillary electrode, was sufficient to reproducibly and efficiently lyse the BHK21 cells in PBS or HEPES buffer (Fig. 5-2A-C). Electrical pulses alone were sufficient to achieve lysis as indicated by a necrotic morphology of the targeted cells, nevertheless, cells were not completely disrupted, and cell fragments stayed in place if not aspirated (Fig. 5-2A and supp. Fig. 5-2A). Moreover, aspiration alone was not sufficient to lyse, disrupt or detach cells.

As demonstrated, only the targeted cell is lysed and neighboring cells remain unaffected, due to the small electrode dimensions and when conductive buffers are used (Fig. 5-2A-C and supp. Fig. 5-2A-D). This findings are supported by finite-element analysis (FEA) results, which show that a high electric field is only generated in very close proximity to the cell, between the microcapillary tip and the ITO support (Fig. 5-3A). Further, adaptation of the electrical parameters to obtain a higher peak-voltage and longer pulse duration allowed the cells to be lysed in low-conductivity, isotonic sucrose buffers, but in this case neighboring cells were also affected (supp. Fig. 5-2E and F).

FEA was also used to estimate the maximal temperature increase by Joule heating due to five 50 µs DC square pulses with amplitudes of 10 V. This estimation predicts a maximal local temperature of 34 °C for a time span of less than 1 ms (Fig. 5-3B and supp. Fig. 5-3 and 5-4). The average cell

temperature stays below 30 °C throughout the overall time span used for simulation. To experimentally study the effects of the short temperature increase, the enzymatic activity of horseradish peroxidase (HRP) after applying electrical pulses was quantified. HRP is known to be irreversibly impaired by exposition to increased temperatures ([24] and supp. Fig. 5-5). Figure 5-3C shows the normalized activity of HRP after exposing 3 µl droplets to electrical pulses of different voltages. The effect was measured by quantification of the chemoluminescent reaction catalyzed by HRP. Our results show, that the activity is not significantly decreased below 10 V, but effects are clearly seen around 14 V and higher. Similar experiments performed with synthetic filamentous actin did not reveal signs of protein aggregation or structural damage of the filaments below 10 V (supp. Fig. 5-6).

Immediately after the applied burst, lysate and surrounding buffer were aspirated into the microcapillary to prevent diffusion of the cellular content.

Subsequent to cell lysis and aspiration, the sub-microliter volumes (200-400 nl) were loaded onto EM grids, negatively stained and inspected by TEM.

TEM images of buffer solution, aspirated from the miniaturized Petri dish in the proximity of a cell after the washing steps, but before a cell lysis event, showed a background of predominantly small particles as expected (Fig. 5-2D); these are most likely residues from the growth medium that were not removed by the buffer washes (see Materials and Methods). TEM images of the sample aspirated from the immediate proximity of an individual adherent BHK cell directly after lysis, reveal cellular content (Fig. 5-2E-G, Fig. 5-4). Membrane patches, filaments and other structures with distinctive shapes can be recognized and correlated to the specific cell using the light microscopy information. Further examples of prominent structures observed in the lysate of single cells are shown in figure 5-4. Although the control experiments documented the presence of some (predominantly small) particles in the bare buffer solution (Fig. 5-2D), distinctive structures similar to those found in the lysate (Fig. 5-2E-G and Fig. 5-4) were not detected.
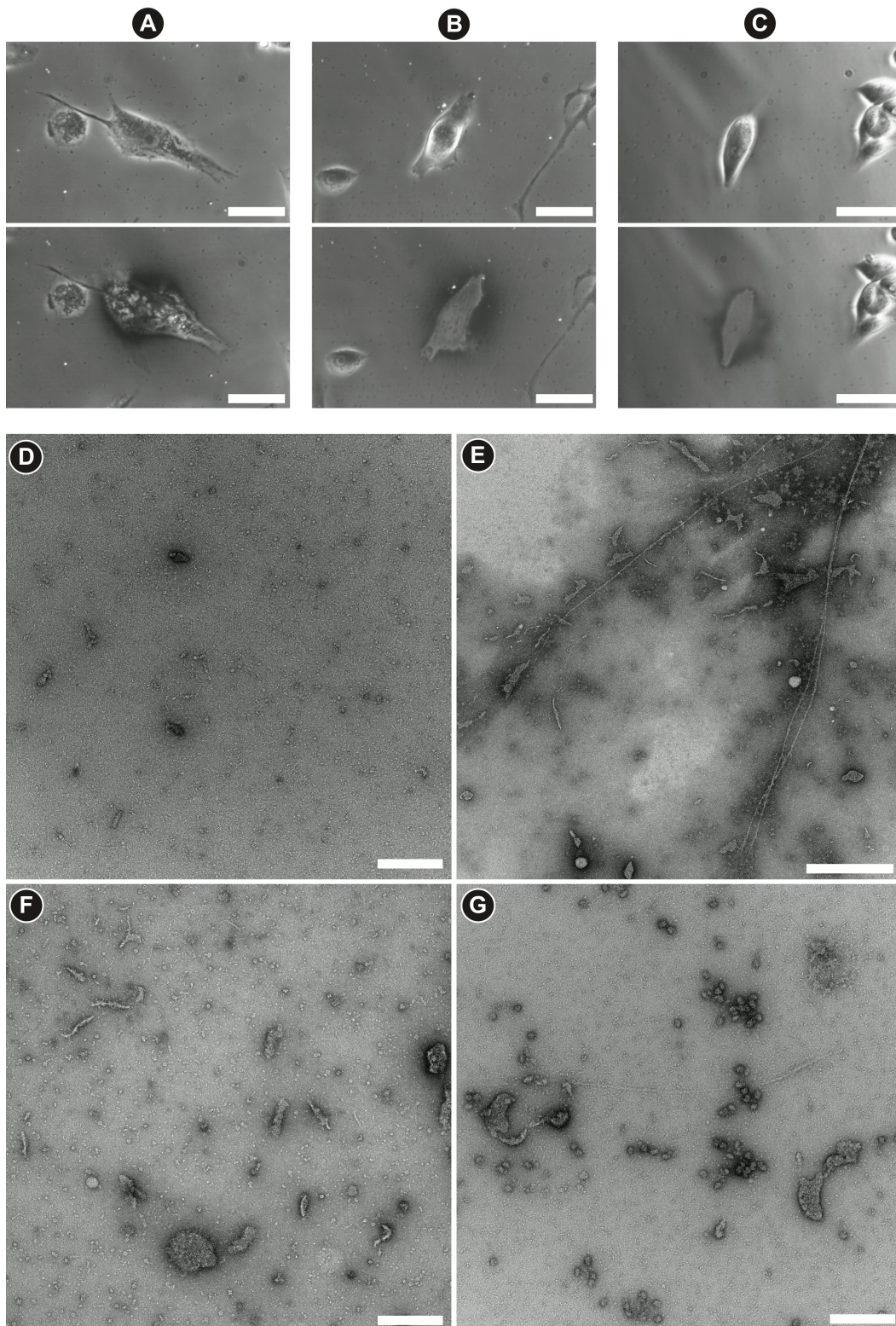
Figure 5-2: *Single-cell lysis and lysate analysis. (A-C) Phase contrast light microscopy images of individual adherent BHK21 cells in PBS (A,B) and HEPES (C) before (top row) and after (bottom row) different procedures. Scale bars: 50 µm. (A) After applying electrical pulses (5 x 50 µs, 10 V DC), the targeted cell is not completely disintegrated but shows necrotic morphology. (B,C) After applying electrical pulses (B: 10 x 50 µs, 6 V DC; C: 5 x 50 µs, 10 V DC) with aspiration, only a ghost imprint of the*

targeted cell remains; the surrounding cells are not affected (bottom row). (D) Overview TEM image of PBS aspirated from the cell culture well after the washing steps but before a cell lysis event. Such control experiments showed predominantly small particles, but distinctive particles and structures were not detected. Negative stain: 2% UA, Scale bar: 200 nm. (E) TEM image of the aspirated lysate of a single cell showing some μm-long filament and membrane patches. Negative stain: 2% AM. Scale bar: 500 nm. (F) TEM image of the aspirated lysate of a single cell showing some membrane structures, helical filaments and particles resembling the shape and dimensions of Hsp60 and the 20s proteasome. Negative stain: 2% UA. Scale bar: 200 nm. (G) TEM image of the aspirated lysate of a single cell showing membrane structures. Negative stain: 2% UA. Scale bar: 200 nm
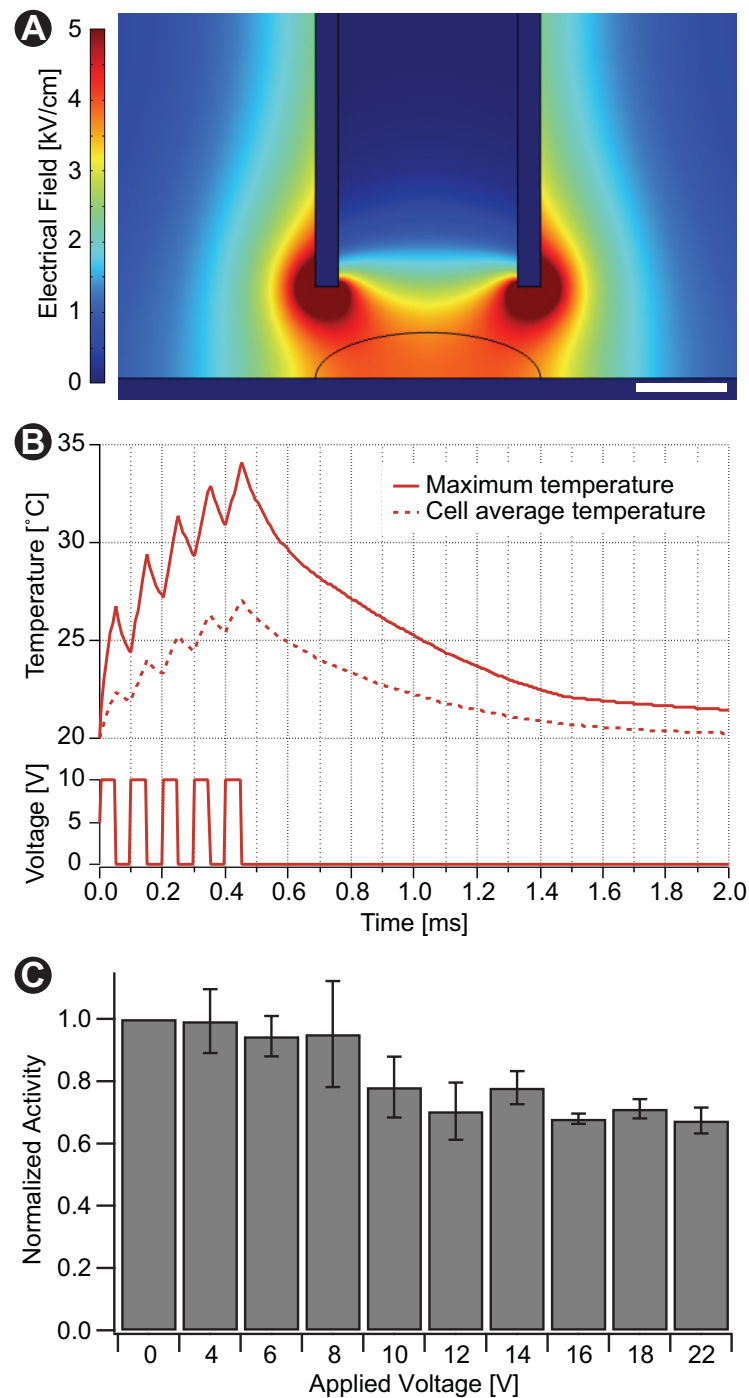
Figure 5-3*: Finite element analysis (FEA) of electroporation characteristics and data on horseradish peroxidase (HRP) stability. (A) FEA simulation to estimate the electric field strength (kV/cm); Scale bar: 20 μm. A potential of 10 V was applied to the microcapillary electrode immersed in PBS buffer; the inter-electrode distance was 20 μm. The profile of a cell (curved black line) placed on the bottom electrode (ITO) was added to the model for illustration. (B) Estimated temperature changes predicted by FEA. The solid line (top panel) shows the variation of the maximum temperature in the solution over time as result of electric pulses (10 V) applied via the gold-coated microcapillary. The dotted line shows the average temperature within the cell region, depicted as curved black line in panel A. (C) Voltage dependence of HRP activity after applying electric pulses. The activity was normalized to that of the control experiments (0 V).*

Figure 5-4: *Examples of distinctive structures observed in negatively stained cell lysates of individual cells. Negative stain: 2% UA. Scale bars 50 nm. (A) Structures that resemble vault organelles, which are large ribonucleoprotein particles found predomi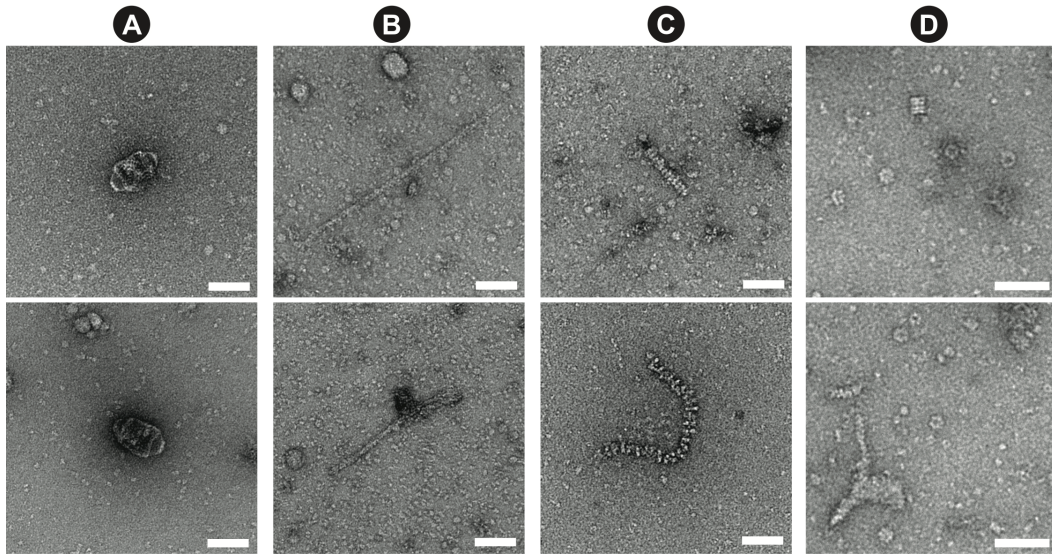nantly in the eukaryotic cytoplasm [25]. (B) Helical structures that have the shape and dimensions of actin filaments [26]. (C) Examples of other less abundant structures observed in the lysate of individual cells. These resemble (top) the CplXAP complex [27] and (bottom) nucleoprotein filaments [28]. (D) More detailed view of the frequently observed ring-like structures shown in figure 5-2F. These have variable dimensions and resemble top views of Hsp60 [29] and the 20s proteasome [30]; the rectangular structure in the top image resembles a side view of one of the latter complexes.*

5.5 Discussion

We present a setup for the controlled lysis of single, adherent eukaryotic cells and a subsequent visual inspection of cellular components by negative-stain TEM. The developed instrument enables (i) live-cell monitoring before and during cell lysis by optical microscopy, (ii) precise selection of individual cells, (iii) fast lysis (<500 ms) without prior disturbance of the cell and (iv) immediate aspiration of the cellular components into a microcapillary for further treatment.

The ITO coating on the glass slide that forms the base of these dishes, features the required electrical and optical properties and serves as ground electrode. In contrast to gold, ITO is suitable for fluorescence microscopy, allows live-cell imaging, and can be combined with various functionalization options to support cell growth if needed [31,32]. The ability to carry out live-cell imaging prior to cell lysis, not only allows studying biological processes, but also enables lysis to be initiated at a defined time-point by means of an optical feedback; for example, a target cell in a specific state can be identified and selected by fluorescence signals of genetically labeled proteins.

Microfluidic chips with fixed electrodes often suffer from bubble formation due to electrolysis. In the flexible-electrode setup described here, sample aspiration and downstream processing were not affected by electrolysis, and there were no signs of bubbles inside the capillary. Furthermore, microfluidic chips with embedded electrodes depend on cells being in suspension and are not well suited to study adherent eukaryotic cells, which must be detached before lysis.

Biological processes involving proteins elapse within time frames of milliseconds to days [33]. This makes the total lysis time an important parameter for cellular dynamics studies. As the method presented here combines fast electrical lysis (≤1 ms) with rapid sample loading (≤400 ms), the described technique offers a temporal resolution that is suitable to study dynamic processes in protein networks of single cells.

The complete detachment and disruption of the cells, observed after sample aspiration (Fig. 5-2B-C and supp. Fig. 5-2B-F), was most likely due to the additional shear forces occurring during the aspiration process. The combination of electrical pulses and mechanical forces, allows applying relatively mild conditions for electrical lysis (low pulse amplitudes and short pulses) in comparison to those reported previously [22,23].

The preservation of the native protein structure and supramolecular assemblies is crucial for the subsequent visual analysis in EM. FEA predicts elevated temperatures on time scales ≤1 ms (Fig. 5-3B and supp. Fig. 5-4) and indicates that thermal protein denaturation is unlikely to occur. All our experimental data corroborate these findings: Quantitative assays using HRP did not show a significant degradation of enzyme activity at the conditions used to lyse individual cells (Fig. 5-3C). Furthermore, experiments with synthetic actin filaments only showed structural effects at voltages exceeding the ones used for lysis (supp. Fig. 5-6).

Negative-stain TEM revealed a variety of cellular components, such as membrane patches, filaments and other particles (Fig. 5-2 and 5-4), and indicates the structural preservation of the observed cellular components. No signs of protein aggregation were observed (compare to supp. Fig. 5-6D). Due to the unique and distinct shape of several particles, assumptions about their identity can be made directly from the raw images, e.g., for the vault organelles [25]. Future template matching algorithms must include scoring algorithms for quantitative analysis [34-36] or complementary, labeling procedures (Giss et al., manuscript in preparation) can be employed. Although the aspects of protein structure and protein complex preservation have to be further consolidated and the recovery of sample constituents has to be improved in the future, the TEM images clearly demonstrate the potential of this method to prepare the lysate of a single cell for a visual

analysis in negative-stain TEM. Furthermore, single cell lysis of adherent eukaryotic cells is also of great interest for other analysis methods, such as mass spectrometry [37] or reverse-phase protein arrays (RPPA) [38]. The application of our lysis method for the detection of actin by RPPA is shown in supplementary figure 5-7.

The "lyse and spread" approach for visual analysis of eukaryotic cells presented here is envisaged to complement classical methods, such as cryo-ET or mass spectroscopy. In comparison to cryo-ET of whole vitrified cells or cellular sections, the here presented approach does not provide information about the 3D arrangement of the proteome. In addition, the excellent preservation capabilities of vitrification have to be replaced by mild and physiological conditions during sample preparation and eventually supported by crosslinking procedures. On the other hand, the "lyse and spread" method, focusing particularly on the cytosolic fraction, has several advantages: (i) Adherent eukaryotic cells can be studied; (ii) the proteins can be prepared by negative staining what provides higher SNR; and (iii) the physical segmentation renders the cell components directly accessible for separation and labeling experiments (Giss et al., in preparation). In contrast to mass spectroscopy, mass determination by STEM is less accurate and the visual analysis by TEM is less high-throughput amenable. However, the single molecule detection limit of the EM allows low-abundance proteins and protein complexes to be studied. Moreover, EM provides additional structural information and facilitates the study of large protein assemblies.

The presented single cell lysis method is only a first step towards the global approach described above as "lyse and spread visual proteomics". Currently, a limiting step is the low transfer efficiency of the cell lysate onto the EM grid, involving several blotting and washing steps. Therefore, the combination with methods exhibiting higher transfer efficiency will be beneficial in order to obtain a more complete access to the proteome. For example, the use of a microfluidic sample-conditioning device, combined with lossless micropatterning of the sample onto an EM grid, could be a suitable solution as shown by Kemmerling et al. [39].

5.6 Conclusion and Outlook

The system presented here allows single-cell lysis to be performed in less than a millisecond and to aspirate the cellular components into a microcapillary within a few hundred milliseconds for further preparation and subsequent analysis. The combination of this setup with an optical system facilitates live imaging and the evaluation of lysis and sample loading. The system is compatible with standard adherent-cell culturing methods and

tools, and can potentially also be applied to biological tissues. Moreover, the system can be easily adapted to different sample carriers, which facilitates the use with additional or alternative analysis techniques such as reverse phase protein arrays (supp. Fig. 5-7).

In combination with a lossless sample deposition onto the EM grids and optional procedures for crosslinking, protein separation and labeling this method for single cell lysis offers the potential for targeted and quantitative visual proteomics studies on eukaryotic single cells.

Acknowledgements

5.7 Supplemental material

5.7.1 Software implementation

The control software was implemented in LabVIEW in an object-oriented way and can be called as a plug-in to the openBEB software framework (www.openBEB.org). All components of the system are addressed in a single user interface, which is shown in supplementary figure 5-1.

The stepper motor can be moved up and down (approach/withdraw) with sub-micrometer precision. In addition, three different values can be assigned for specific positions (e.g., safe, search, or lysis position). Motor speed and acceleration can be changed if needed. The function generator panel is on the right hand side of the motor control panel. The different parameters (e.g., waveform, frequency, amplitude, burst mode, etc.) can be set and saved to an .xml file. The trigger button starts the electric pulse. A live image from the camera with a default frame rate of 30 frames/s is shown next to the function generator panel. Video recording is started and paused by pressing the record button. Scale bars for the two objective lenses of the employed optical microscope (10x and 20x) are displayed at the top and bottom of the live image. The pressure control panel is in the lower region of the interface. On the left, the vacuum and pressure pumps can be switched on and off. The pressure status of the positive and negative pressure buffer is displayed below the two switches. A switch allows the user to quickly select one of the two pressure values (aspirate/dispense). Additional information, such as the system pressure, or whether pressure adjustments are in progress or

completed, are shown to the right (black box). The remaining panel controls the solenoid valve, which is normally closed. The switch allows to open this valve for a defined period of time or continuously.
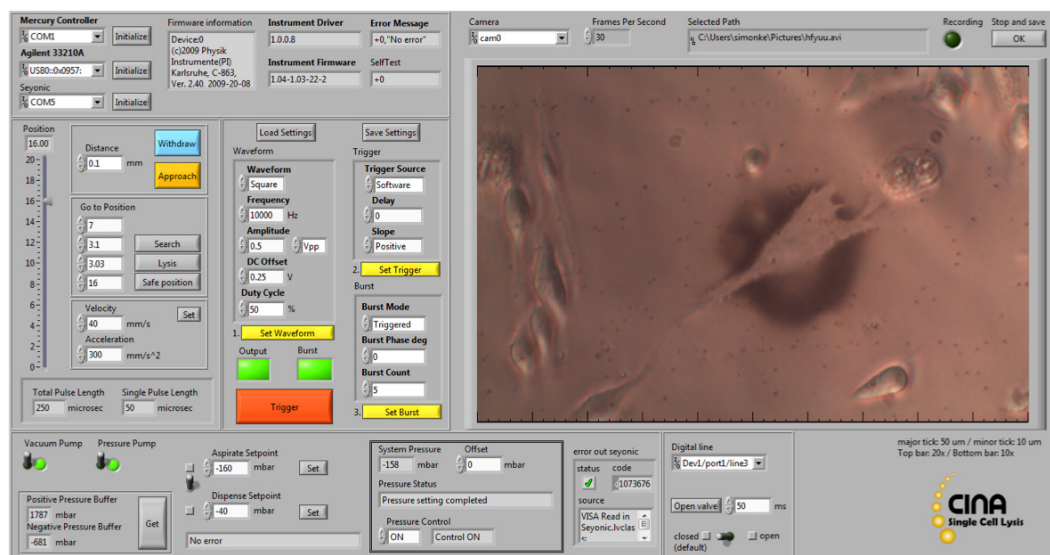
Supplementary Figure 5-1: *Single-cell lysis software user interface. Stepper motor, function generator, pressure, shutter valve, and video recording are controlled from a single user interface.*

5.7.2 Buffers

The ability of the set-up to achieve single-cell lysis was tested in different buffers (supp. Fig. 5-2). In terms of lysis parameters, the conductive buffers PBS and HEPES behaved similarly (supp. Fig. 5-2B-D). However, the electric parameters had to be adjusted to achieve cell lysis in low-conductivity isotonic sucrose buffer. The application of five 100 µs DC square pulses with amplitudes of 40 V to the gold-coated microcapillary was required to achieve lysis. The fields generated were higher than those used in PBS or HEPES buffer, and needed to be applied for a significantly longer time. As a result, some of the cells surrounding the target cell were also affected and showed morphological changes (supp. Fig. 5-2E and 5-2F).
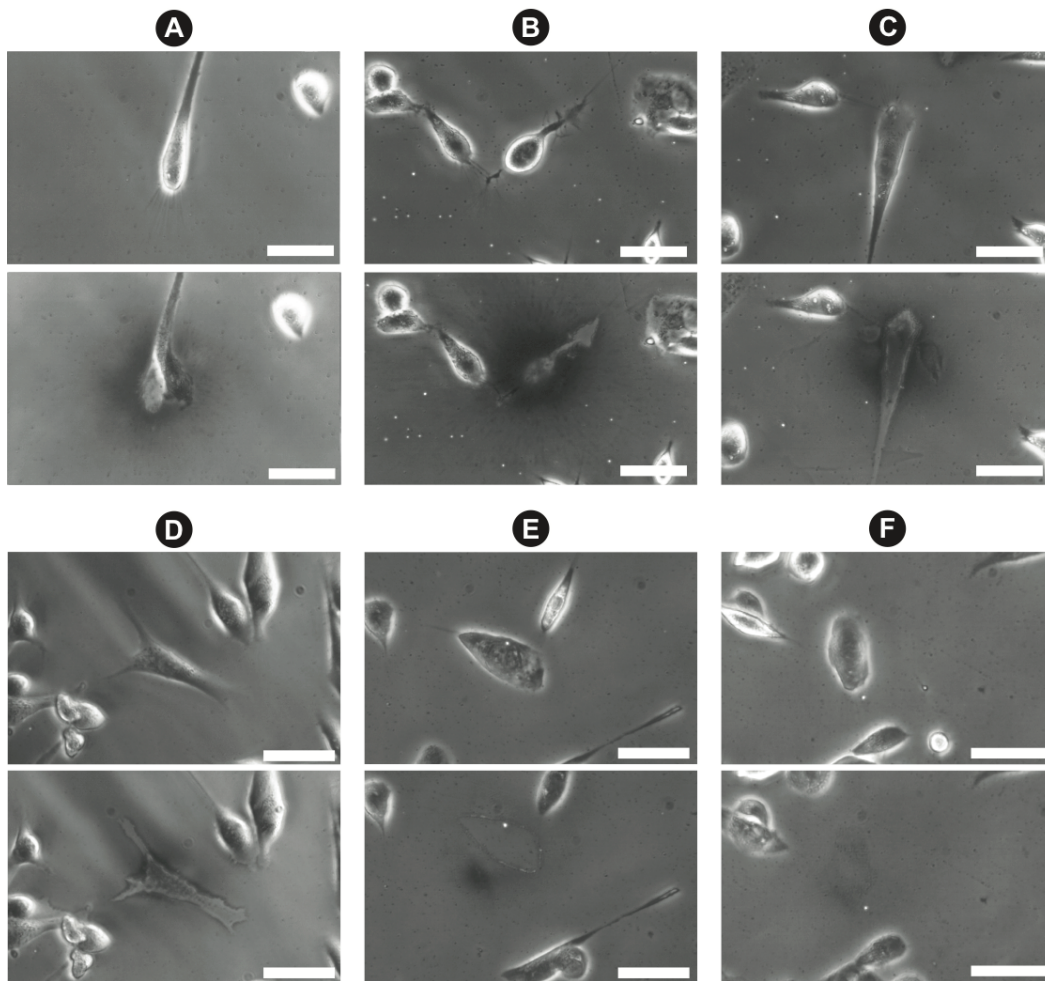
Supplementary Figure 5-2: *Light microscopy images of individual adherent BHK cells in PBS (A-C), HEPES buffer (D) and isotonic sucrose buffer (E, F) before (top rows) and after (bottom rows) lysis. Scale bars: 50 µm. (A) After a burst of electrical pulses has been applied, the targeted cell shows a necrotic morphology. (B-D) After a burst of electrical pulses and subsequent aspiration, only ghost imprints of the targeted cells remain; the surrounding cells are not affected. (E,F) Lysis in low-conductivity isotonic sucrose buffer. Longer electrical pulses with higher amplitudes had to be applied to achieve lysis. This also affected the surrounding cells, which showed a change in morphology.*

5.7.3 Finite element analysis

Finite element analysis (FEA) using an axisymmetric time-dependent model in COMSOL Multiphysics was used to simulate the electrical field and the temperature rise induced by the electrical pulses applied to the microcapillary electrode.

The electric current and heat transfer modules in COMSOL were used for modeling. Parameters of the model included a gold microcapillary tip with 50 µm outer diameter (40 µm inner diameter), immersed in PBS buffer with an electrical conductivity of 1.67 S/m [40]. In the model, the conductive tip was

placed 20 μm above the indium tin oxide (ITO) ground electrode and a potential of 10 V or 20 V was applied to the electrode by means of a square function (5 x 50 μs square pulses). Material properties used in the simulations were either from the COMSOL material library or reported elsewhere [41,42].

The simulations also provide an estimation of the temperature rise in the buffer solution, containing the cells, due to Joule heating [43]. The model implicated the heating caused by the electrical pulses as well as heat dissipation. Heat dissipation, as expected, mainly occurred through the electrodes, which have a high thermal conductivity. Convective heat dissipation was neglected due to the small Rayleigh numbers defined by the micrometer dimensions of the problem [44]. The temperature changes in the fluid are a function of time, applied voltage, and thermal and electrical properties of buffer and electrodes that alter heat generation and sinking. Supplementary figure 5-3 shows the predicted temperature distribution at the end of the fifth 10 V pulse (see also supp. Fig. 5-4). Voltages greater than 10 V were only applied to compensate for electrode aging.
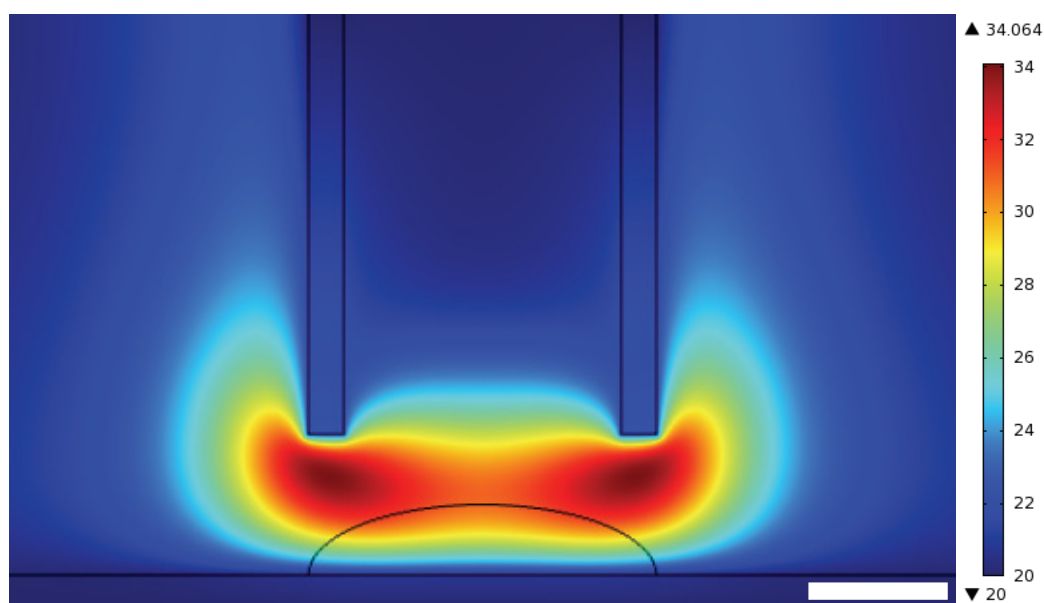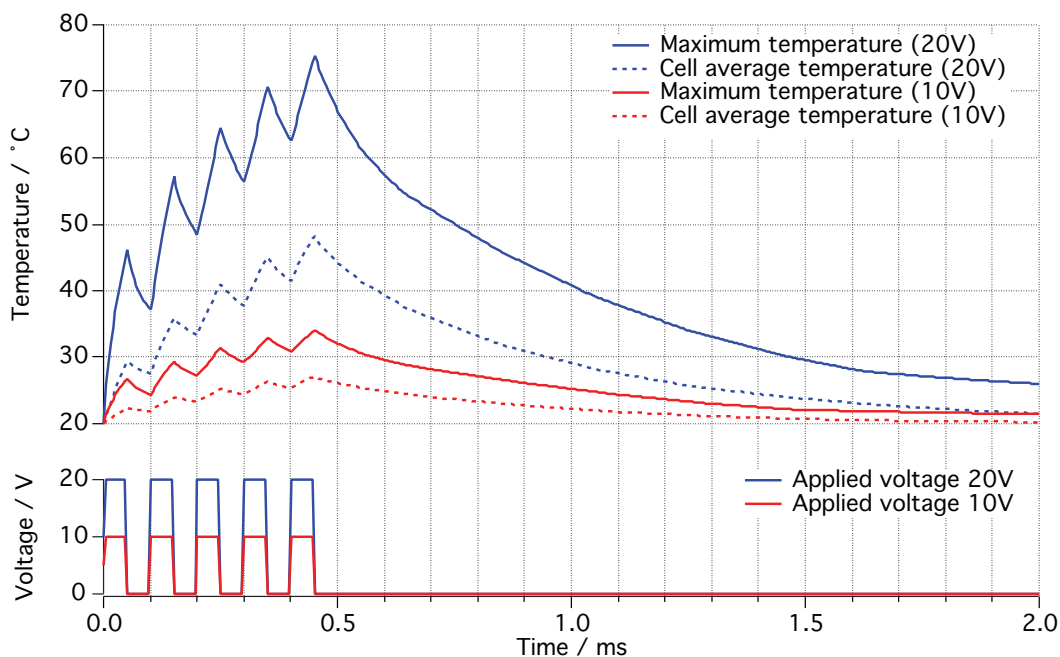

Supplementary Figure 5-3*: Temperature distribution results from simulations in °C; Scale bar: 20 μm. The simulation considered the effect of Joule heating and conductive heat dissipation. The color map indicates the temperature distribution at the end of the fifth 50 μs, 10 V DC square pulse (time point 0.45 ms of the simulation; see supp. Fig. 5-4) when the maximal temperature in the worst-case scenario occurs. The simulations reveal a maximum temperature of 34 °C in close vicinity to the microcapillary electrode tip, where the electric field has its highest strength. The profile of a cell (curved black line) placed on the bottom electrode (ITO) was added to the model in order to estimate the average values within this region.*

Supplementary Figure 5-4: *Temperature changes predicted by FEA. The solid lines (top panel) show the variation of the maximum temperature in the solution over time as result of the electric pulses (bottom panel) applied via the gold-coated microcapillary. Typical experiments for cell lysis were performed with voltages of maximally 10 V. However, to compensate for electrode erosion, voltages up to 20 V were applied in rare cases. The uppermost temperature reached was about 75 °C for amplitudes of 20 V (blue solid line) and about 34 °C for amplitudes of 10 V (red solid line). The dotted lines show the average temperature within the cell region (indicated in supp. Fig. 5-3) over time. The maximum average temperature within the cell region is 48 °C for amplitudes of 20 V (blue dotted line) and about 27 °C for amplitudes of 10 V (red dotted line). (bottom panel) Plot of the electric pulses applied to the microelectrode tip; five DC square pulses with amplitudes of 20 V (blue) and 10 V (red) and a pulse duration of 50 μs.*

As heating can be harmful to cells and proteins, simulations were used for estimating the spatial temperature distribution throughout the model as a result of Joule heating. The simulations using a worst-case scenario (5 x 50 μs DC square pulse with an amplitude of 20 V over a 20 μm gap), predict a maximum temperature of approximately 75 °C in PBS (supp. Fig. 5-4). However, temperatures above 40 °C only occur for ~1 ms, and 20 V amplitudes were only used to compensate for electrode ageing. For amplitudes of 10 V reflecting the standard conditions the simulation predicts a much lower maximum temperature that stays well below 40 °C (supp. Fig. 5-4), which was found to be the onset temperature of thermal protein denaturation in mammalian cells [45]. However, the transition temperatures, Tm, at which half the protein content is denatured, vary from 40-90 °C for different proteins [46]. Moreover, these values are mostly derived on the

basis of equilibrium thermodynamics by differential scanning calorimetry (DSC) and do not reflect the effects of short heat pulses on proteins. In addition to the short peak-temperature durations demonstrated by the model, the estimated average temperatures within the cell region are much lower than the maximum temperatures (supp. Fig. 5-3 and 5-4).

5.7.4   Test proteins

5.7.4.1 Temperature-dependent enzymatic activity of horseradish peroxidase

Horseradish peroxidase (HRP) conjugated goat anti-mouse IgG (8.5 mg/ml, A2554, Sigma, Switzerland) was diluted to 0.85 µg/ml in PBS and heated to 40 °C, 60 °C and 80 °C for 30 min, while the control sample remained on ice. After dilution of the treated samples to 8.5 ng/ml with PBS, the enzymatic activity of HRP was analyzed by enhanced chemiluminescence (ECL) on a dot plot (supp. Fig. 5-5A).

The results shown in supplementary figure 5 illustrate the strong decrease of the enzymatic activity of HRP with temperature. At 40 °C a significant decrease in the enzymatic activity was observed, indicating that the temperature sensitivity of HRP is suitable to further characterize our setup. The complete loss of the enzymatic activity at 80 °C is in good accordance with previous studies showing that the cofactor (heme) of the active site is depleted above 74 °C [24].
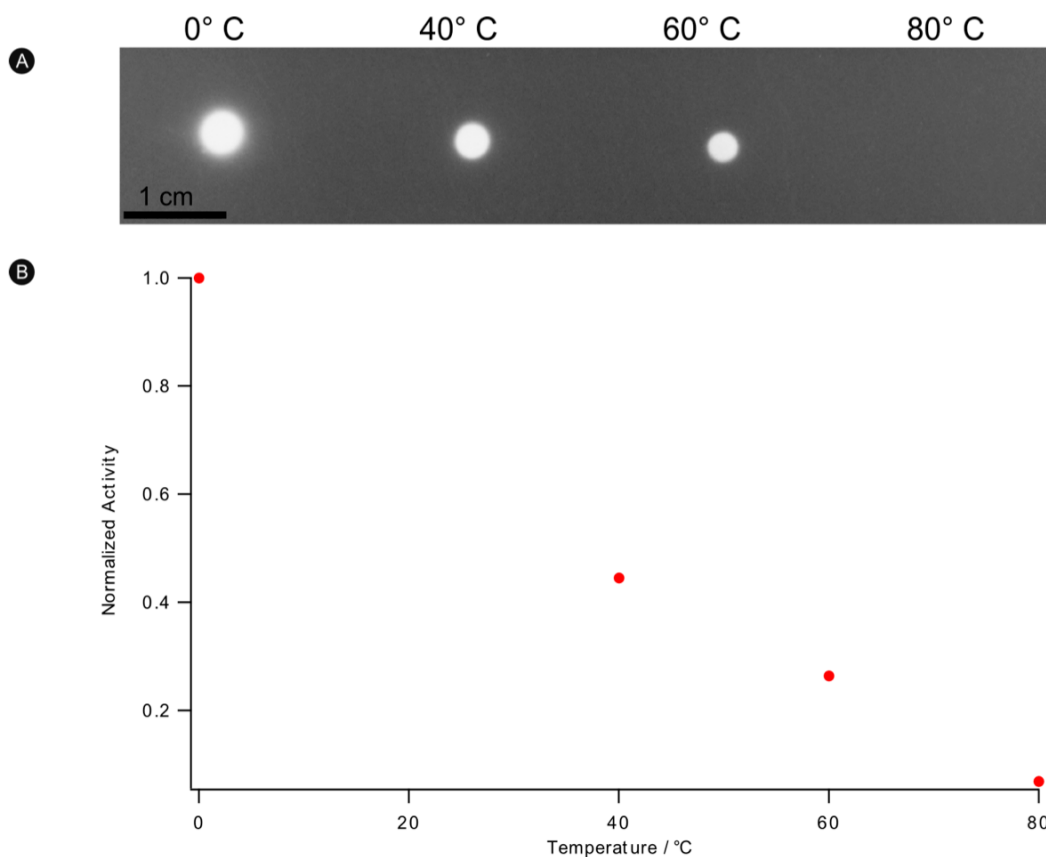
Supplementary Figure 5-5: *Temperature dependence of the enzymatic activity of HRP. (A) The enzymatic activity of HRP in the heated samples was analyzed by ECL on a dot plot. (B) The detected intensities were normalized with respect to the control sample and show a strong decrease with temperature and completely disappear at 80 °C.*

5.7.4.2 Structural preservation of F-actin

Synthetic F-actin was chosen as a test sample to further investigate the effects of electrical pulses on sensitive supramolecular assemblies. 2 µl of 0.1 mg/ml F-actin (polymerized from G-actin; 8101-01, Hypermol, Germany, with polymerization buffer PolyMix; 5000-01, Hypermol, Germany) sample was placed onto an ITO coated glass slide, and the microcapillary electrode was placed in the drop, about 20 µm above the glass slide. Different voltages (6 V, 10 V, 14 V, 20 V, 30 V and 40 V), each with a burst count of 5 and a single pulse length of 50 µs were applied. 1 µl was removed from the treated sample droplet, diluted to 0.01 mg/ml in PolyMix buffer, adsorbed onto an EM grid and negatively stained with 2% uranyl acetate without washing.

The visual inspection of the samples with TEM did not reveal obvious structural differences, due to the treatment, up to 14 V. Compared to the untreated control sample the structural details in the samples exposed to 6 V, 10 V and 14 V were preserved and no signs of protein denaturation were detected (supp. Fig 5-6A and 5-6B). At 20 V the signs of structural damage

such as filament fractionation, were rarely observed (supp. Fig. 5-6C) and became more frequent at 40 V. At 40 V, protein denaturation and aggregation was observed (supp. Fig. 5-6D).
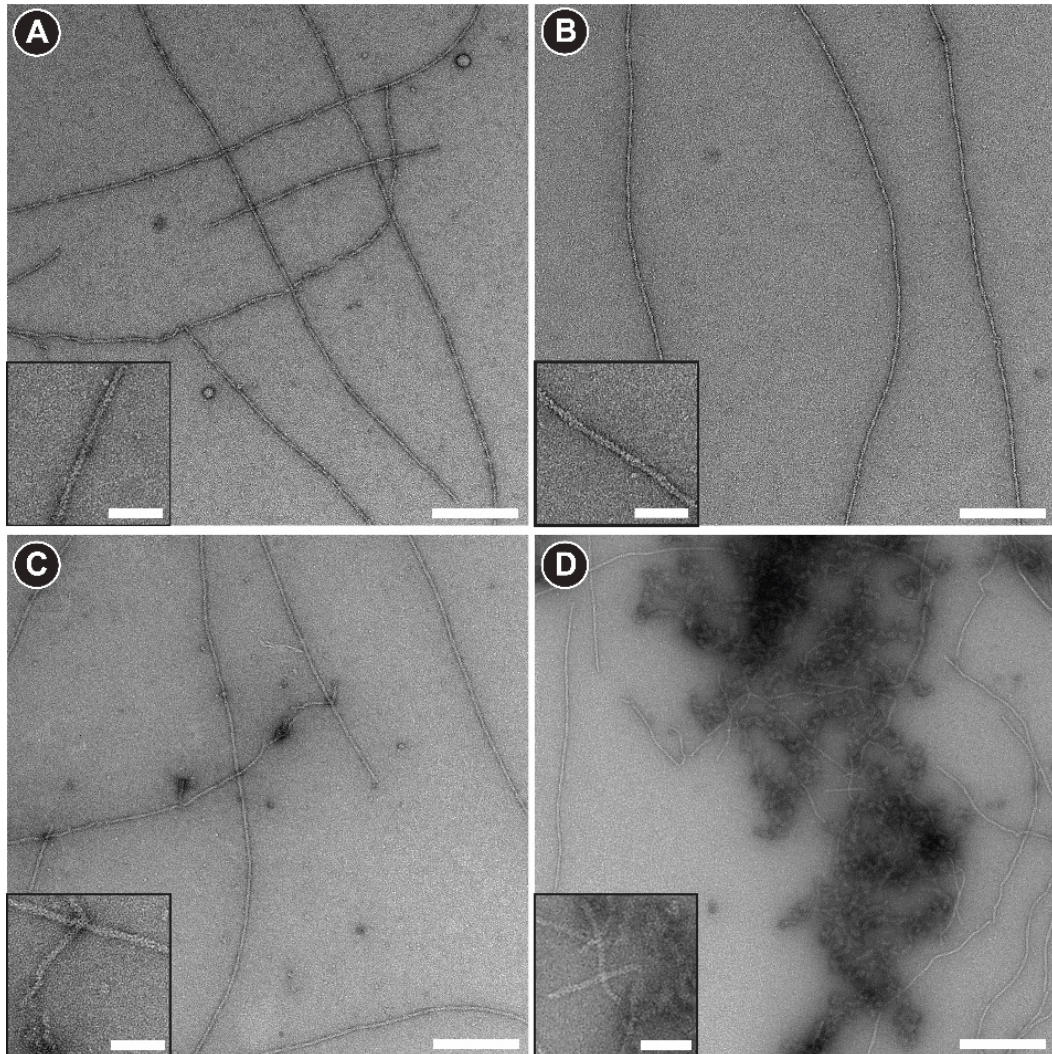
Supplementary Figure 5-6: *Actin filaments exposed to different voltages in the setup. The TEM micrographs illustrate the observed tendency of actin filaments treated with (A) 0 V, (B), 10 V (C) 20 V and (D) 40 V. Scale bars: 200 nm; insets 50 nm.*

5.7.5 Lysis and aspiration movies of fluorescently labeled cells

Human embryonic kidney (HEK293) cells were cultured and prepared similarly to the BHK cells described in the manuscript, except that they were grown in Eagle's minimal essential medium (EMEM) supplemented with 1 % non-essential amino acids, 2 mM glutamine and 10 % fetal bovine serum.

For the fluorescence experiments, cells growing inside a miniaturized Petri dish were gently washed 2x with pre-warmed PBS and 200 μl of 2 μM calcein acetoxymethylester (calcein AM) (Invitrogen, US) in PBS solution was

added to the miniaturized Petri dishes. The cells were incubated for 30 min at 37 °C. Electroporation was performed as described in the manuscript, and the subsequent aspiration was performed with a delay of approximately 1.5 sec (see supplementary movies 1 and 2)[4].

5.7.6 Reverse phase protein array

HEK293 cells were cultured, prepared as described in the previous paragraph. Electroporation and aspiration was performed as described in the manuscript. Inside the miniaturized Petri dishes one culture was growing on a bare ITO surface and a second culture was growing on a collagen coated ITO surface. Collagen coating has been performed as described previously [47].

For the collection of samples with more than one cell, a cluster of cells (up to 23) was lysed and aspirated simultaneously. Subsequent to aspiration the samples were spotted onto a nitrocellulose membrane-coated microscope slide (16-pad FAST slide, Maine Manufacturing, Sanford, Maine, USA).

For a dilution series of batch-lysed cells, HEK293 cells were detached, counted and lysed in batch by sonification. Afterwards the batch lysate was diluted in PBS to give an equivalent of 330, 3300 and 33000 cells and 1 µl was spotted on the nitrocellulose membrane-coated microscopy slides by hand.

The assay procedure followed in principle as described before [38] In brief, the slides were blocked in LiCor Odyssey blocking buffer for 10 min and then incubated with an anti-actin antibody (Millipore, #NG1848416, diluted 1:1000 in 10% LiCor Odyssey blocking buffer (=assay buffer), 24h room temperature) washed three times 5 min in assay buffer. Then the slide was incubated with a fluorescently labeled secondary antibody (LiCor anti-mouse-IRDye800, 1 µg/ml in assay buffer, 1h at room temperature), washed three times 5 min in assay buffer and blown dry. The slide was imaged in a LiCor Odyssey infrared fluorescence scanner in the 800nm channel with intensity 4, quality low, resolution 21 µm. Quantification of spot intensities was done in GenePix Pro 6.0 (Molecular Devices, Sunnyvale, CA, USA) with variable spot diameters. The total spot intensity is reported in supplementary figure 5-7.

---

[4] http://dx.doi.org/10.1016/j.jsb.2013.06.012
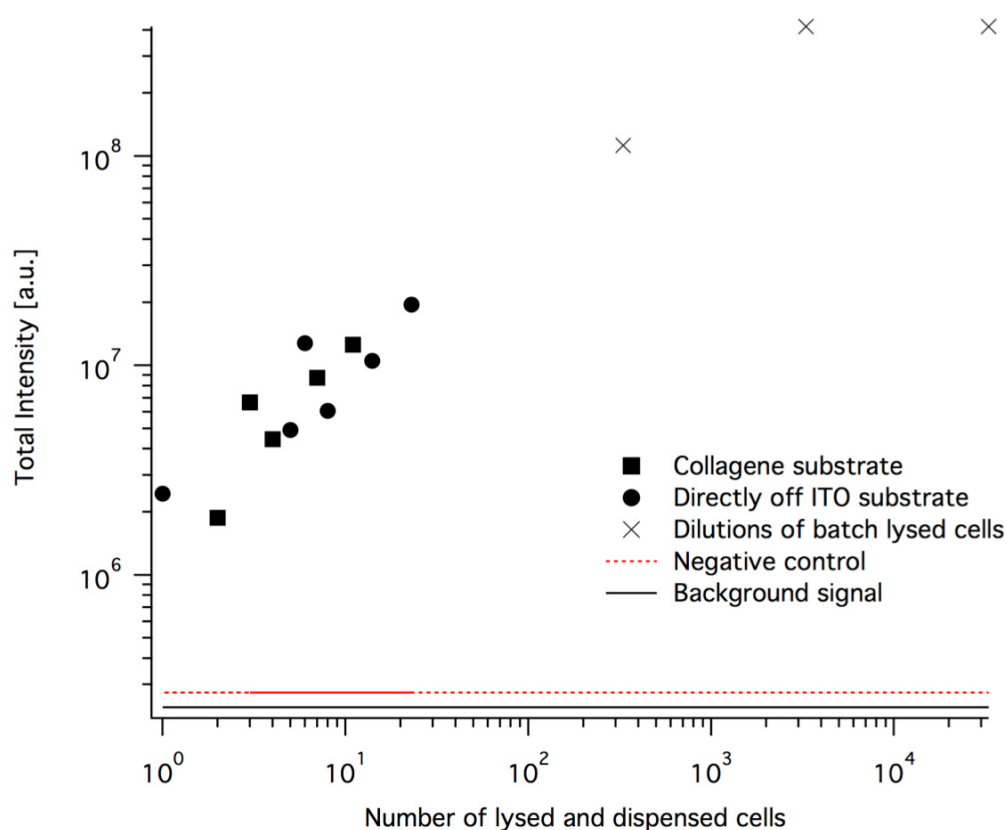
Supplementary Figure 5-7: *Cell lysis and reverse phase protein array. Individual cells were lysed and dispensed as spots on a nitrocellulose membrane-coated microscope slide. After incubation with an anti-actin antibody and a fluorescently labeled secondary antibody the slide was scanned. The total fluorescence intensity was plotted against the number of lysed cells dispensed in each spot.*

5.8 References

[1]   Westerhoff, H. V. **Systems biology left and right.** *Methods Enzymol.* 500, 3-11, (2011).

[2]   Eldar, A. & Elowitz, M. B. **Functional roles for noise in genetic circuits.** *Nature* 467, 167-173, (2010).

[3]   Raj, A. & van Oudenaarden, A. **Nature, nurture, or chance: Stochastic gene expression and its consequences.** *Cell* 135, 216-226, (2008).

[4]   Wang, D. & Bodovitz, S. **Single cell analysis: the new frontier in 'omics'.** *Trends Biotechnol.* 28, 281-290, (2010).

[5]   Zong, C., Lu, S., Chapman, A. R. & Xie, X. S. **Genome-wide detection of single-nucleotide and copy-number variations of a single human cell.** *Science* 338, 1622-1626, (2012).

[6]   Flatz, L., Roychoudhuri, R., Honda, M., Filali-Mouhim, A., Goulet, J.-P. et al. **Single-cell gene-expression profiling reveals qualitatively distinct CD8 T cells elicited by different gene-based vaccines.** *PNAS* 108, 5724-5729, (2011).

[7]   Kalisky, T., Blainey, P. & Quake, S. R. **Genomic analysis at the single-cell level.** *Annu. Rev. Genet.* 45, 431-445, (2011).

[8]   Fiehn, O. **Combining genomics, metabolome analysis, and biochemical modelling to understand metabolic networks.** Comp. *Funct. Genomics.* 2, 155-168, (2001).

[9]   Amantonico, A., Oh, J. Y., Sobek, J., Heinemann, M. & Zenobi, R. **Mass spectrometric method for analyzing metabolites in yeast with single cell sensitivity.** *Angew. Chem. Int. Ed. Engl.* 120, 5462-5465, (2008).

[10]   Picotti, P., Bodenmiller, B., Mueller, L. N., Domon, B. & Aebersold, R. **Full dynamic range proteome analysis of S. cerevisiae by targeted proteomics.** *Cell* 138, 795-806, (2009).

[11]   Henderson, G. P., Gan, L. & Jensen, G. J. **3-D ultrastructure of O. tauri: electron cryotomography of an entire eukaryotic cell.** *PLoS ONE 2*, e749, (2007).

[12]   Medalia, O., Weber, I., Frangakis, A. S., Nicastro, D., Gerisch, G. et al. **Macromolecular architecture in eukaryotic cells visualized by cryoelectron tomography.** *Science* 298, 1209-1213, (2002).

[13]   Nickell, S., Kofler, C., Leis, A. P. & Baumeister, W. **A visual approach to proteomics.** *Nat. Rev. Mol. Cell Biol.* 7, 225-230, (2006).

[14]   Bantscheff, M., Schirle, M., Sweetman, G., Rick, J. & Kuster, B. **Quantitative mass spectrometry in proteomics: a critical review.** *Anal. Bioanal. Chem.* 389, 1017-1031, (2007).

[15]   Diebolder, C. A., Koster, A. J. & Koning, R. I. **Pushing the resolution limits in cryo electron tomography of biological structures.** *J. Microsc.* 248, 1-5, (2012).

[16]   Mader, A., Elad, N. & Medalia, O. **Cryoelectron tomography of eukaryotic cells.** *Methods Enzymol.* 483, 245-265, (2010).

[17]   Engel, A. **Scanning transmission electron microscopy: biological applications** in: Peter Hawkes ed *Advances in Imaging and Electron Physics*, Vol. 159, 357-386, Academic Press, (2009).

[18]   Engel, A. **Assessing biological samples with scanning probes** in: Astrid Gräslund, Rudolf Rigler, & Jerker Widengren eds. *Single*

Molecule Spectroscopy in Chemistry, Physics and Biology, Vol. 96, Ch. 21, 417-431, Springer, (2010).

[19]   Brown, R. B. & Audet, J. **Current techniques for single-cell lysis.** *J. R. Soc. Interface* 5, S131-S138, (2008).

[20]   Movahed, S. & Li, D. **Microfluidics cell electroporation.** *Microfluid. Nanofluid.* 10, 703-734, (2011).

[21]   Fox, M., Esveld, D., Valero, A., Luttge, R., Mastwijk, H. et al. **Electroporation of cells in microfluidic devices: a review.** *Anal. Bioanal. Chem.* 385, 474-485, (2006).

[22]   Han, F., Wang, Y., Sims, C. E., Bachman, M., Chang, R. et al. **Fast electrical lysis of cells for capillary electrophoresis.** *Anal. Chem.* 75, 3688-3696, (2003).

[23]   Nashimoto, Y., Takahashi, Y., Yamakawa, T., Torisawa, Y., Yasukawa, T. et al. **Measurement of gene expression from single adherent cells and spheroids collected using fast electrical lysis.** *Anal. Chem.* 79, 6823-6830, (2007).

[24]   Chattopadhyay, K. & Mazumdar, S. **Structural and conformational stability of horseradish peroxidase: effect of temperature and pH.** *Biochemistry* 39, 263-270, (2000).

[25]   Kedersha, N. L., Miquel, M. C., Bittner, D. & Rome, L. H. Vaults. II. **Ribonucleoprotein structures are highly conserved among higher and lower eukaryotes.** *J. Cell Biol.* 110, 895-901, (1990).

[26]   Aebi, U., Millonig, R., Salvo, H. & Engel, A. **The three dimensional structure of the actin filament revisited.** *Ann. N. Y. Acad. Sci.* 483, 100-119, (1986).

[27]   Ortega, J., Lee, H. S., Maurizi, M. R. & Steven, A. C. **ClpA and ClpX ATPases bind simultaneously to opposite ends of ClpP peptidase to form active hybrid complexes.** *J. Struct. Biol.* 146, 217-226, (2004).

[28]   Sehorn, M. G., Sigurdsson, S., Bussen, W., Unger, V. M. & Sung, P. **Human meiotic recombinase Dmc1 promotes ATP-dependent homologous DNA strand exchange.** *Nature* 429, 433-437, (2004).

[29]   De Carlo, S., Boisset, N. & Hoenger, A. **High-resolution single-particle 3D analysis on GroEL prepared by cryo-negative staining.** *Micron* 39, 934-943, (2008).

[30]   Cascio, P., Call, M., Petre, B. M., Walz, T. & Goldberg, A. L. **Properties of the hybrid form of the 26S proteasome containing both 19S and PA28 complexes.** *EMBO J.* 21, 2636-2645, (2002).

[31]   Luo, W., Westcott, N. P., Pulsipher, A. & Yousaf, M. N. **Renewable and optically transparent electroactive indium tin oxide surfaces for chemoselective ligand immobilization and biospecific cell adhesion.** *Langmuir* 24, 13096-13101, (2008).

[32]   Shah, S. S., Howland, M. C., Chen, L.-J., Silangcruz, J., Verkhoturov, S. V. et al. **Micropatterning of proteins and mammalian cells on indium tin oxide.** *ACS Appl. Mater. Interfaces* 1, 2592-2601, (2009).

[33]   Souchelnytskyi, S. **Bridging proteomics and systems biology: What are the roads to be traveled?** *Proteomics* 5, 4123-4137, (2005).

[34]   Beck, M., Malmström, J. A., Lange, V., Schmidt, A., Deutsch, E. W. et al. **Visual proteomics of the human pathogen Leptospira interrogans.** *Nat. Methods* 6, 817-823, (2009).

[35]   Beck, M., Topf, M., Frazier, Z., Tjong, H., Xu, M. et al. **Exploring the spatial and temporal organization of a cell's proteome.** *J. Struct. Biol.* 173, 483-496, (2011).

[36]   Best, C., Nickell, S. & Baumeister, W. **Localization of protein complexes by pattern recognition.** *Methods Cell Biol.* 79, 615-638, (2007).

[37]   Aebersold, R. & Mann, M. **Mass spectrometry-based proteomics.** *Nature* 422, 198-207, (2003).

[38]   Dernick, G., Obermüller, S., Mangold, C., Magg, C., Matile, H. et al. **Multidimensional profiling of plasma lipoproteins by size exclusion chromatography followed by reverse-phase protein arrays.** *J. Lipid Res.* 52, 2323-2331, (2011).

[39]   Kemmerling, S., Ziegler, J., Schweighauser, G., Arnold, S. A., Giss, D. et al. **Connecting µ-fluidics to electron microscopy.** *J. Struct. Biol.* 177, 128 -134, (2012).

[40]   Gielen, F., Pereira, F., deMello, A. J. & Edel, J. B. **High-resolution local imaging of temperature in dielectrophoretic platforms.** *Anal. Chem.* 82, 7509-7514, (2010).

[41]   Tolk, M., Fenwick, O., Ahmad, S. & Cacialli, F. **The influence of the substrate thermal conductivity on scanning thermochemical lithography.** *J. Appl. Phys.* 111, 1243171-1243178, (2012).

[42]   Yagi, T., Tamano, K., Sato, Y., Taketoshi, N., Baba, T. et al. **Analysis on thermal properties of tin doped indium oxide films by picosecond thermoreflectance measurement.** *J. Vac. Sci. Technol., A* 23, 1180-1186, (2005).

[43]   Erickson, D., Sinton, D. & Li, D. **Joule heating and heat transfer in poly(dimethylsiloxane) microfluidic systems.** *Lab. Chip* 3, 141-149, (2003).

[44]   Guyon, E., Hulin, J.-P., Petit, L. & Mitescu, C. **The mechanism of the Rayleigh - Benard instability, and orders of magnitude** in: *Physical Hydrodynamics*, Ch. 10.2.2, Oxford University Press, (2001).

[45]   Bischof, J. C. & He, X. **Thermal stability of proteins.** *Ann. N. Y. Acad. Sci.* 1066, 12-33, (2005).

[46]   Lepock, J. R. **Cellular effects of hyperthermia: relevance to the minimum dose for thermal damage.** Int. J. Hyperthermia 19, 252-266, (2003).

[47]   Harnett, E. M., Alderman, J. & Wood, T. **The surface energy of various biomaterials coated with adhesion molecules used in cell culture.** *Colloids Surf. B Biointerfaces* 55, 90-97, (2007).

6 General Discussion

6.1 Advantages and disadvantages of the "lyse and spread" approach

The motivation of the "lyse and spread" approach is to provide an alternative and complementary method to investigate the proteome of single eukaryotic cells, which still challenge studies by cryo-ET and MS. Although the goal is to overcome some of the current limitations of these techniques, this new approach also comes with certain drawbacks and challenges, as discussed below.

Compared to visual proteomics of whole vitrified cells by cryo-ET or the investigation of cellular sections, invasive approaches are accompanied by a loss of information about the overall spatial organization of the proteome. The interactome can be studied on the level of protein complexes, but lacks the general cell context. In return, lysis of the cell offers the possibility to investigate the cellular components of large eukaryotic cells with other EM techniques that provide an increased signal-to-noise ratio (e.g., by staining procedures and/or spreading the sample in a thin layer). These preparation procedures normally used in single particle EM, offer the potential to fully exploit the single molecule detection limit of EM, also for complex samples such as cell lysate. The samples are spread in a thin layer, and the possibility of dilution can further decrease the molecular crowding present inside the cell, facilitating the detection of individual proteins and protein complexes. However, standard preparation procedures are always accompanied by a series of washing/blotting steps resulting in the adsorption of less than 1% of the sample constituents on the grid. If the proteomes of single cells are addressed, a thorough sample collection, preparation and deposition is required which ideally does not waste or loose any sample. Admittedly, it is likely that some loss during these steps cannot be avoided, but utilizing methods such as microfluidics or surface passivation can dramatically decrease it. In contrast to the investigation of intact cells, invasive approaches also imply an extra effort in the preparation procedure to preserve the native structure of proteins and the interactions in protein complexes. The excellent preservation properties of vitrification employed for cryo-EM have to be replaced, for example, by mild and physiological conditions during the preparation steps. On the other hand, molecular biology techniques such as crosslinking can be readily applied if additional stabilization of labile structures is required. In addition, other techniques,

that aid the characterization and identification of proteins and macromolecular complexes, can only (e.g., separation) or more easily (e.g., labeling) be applied if the proteins are in solution. Further, the preparation of samples from lysed cells not only allows structural investigation, but also the utilization of STEM for mass measurements. Although mass determination by STEM is less accurate than MS and is not geared to high-throughput, the mass-to-shape correlation obtained is unique and highly beneficial for the analysis of heterogeneous samples. In contrast to MS the total mass of individual biomacromolecules (from 100 kDa to over 100 MDa) can be measured by STEM and directly linked to the observed shape of the particle [1]. Thereby, STEM can make a significant contribution to the identification and characterization of protein complexes especially when used in conjunction with MS batch experiments.

However, the advantages and disadvantages of each individual technique are perhaps not the most important aspect, since the complexity of the proteome has to be tackled by hybrid approaches that combine different analytical techniques and correlate their acquired data. In this respect the "lyse and spread" approach does not aim to be a standalone technique but to complement existing techniques applied in single cell proteomics, by providing complementary information and an additional link between the structure and mass of proteins and macromolecular complexes.

6.2 Established modules of the pipeline

The basis of the microfluidic sample preparation pipeline is the efficient and unbiased deposition of the sample on the sample carriers to allow quantitative conclusions. This is especially true for the preparation of EM grids from complex samples and, consequently, this task was tackled first. Most classical EM grid preparation methods involve various washing and blotting steps, resulting in inefficient and differential adsorption of the sample constituents on the carbon film surface. Thus these procedures waste most of the sample and additionally distort the representation of constituents, which hinders quantitative investigations. A basic setup consisting of a conditioning module (negative staining and/or desalting by microdialysis) and a hand-over module for lossless sample transfer and micro-patterning of EM grids was built to overcome these limitations (see chapter 3 or [2]). In this way a new procedure was established that makes additional preparation steps unnecessary after the sample has been applied to the EM grid. The required sample conditioning steps like staining and/or desalting are implemented prior to the transfer onto the sample carrier. The principle of microdialysis was successfully adapted to condition the flowing sample without dilution. Subsequently, minute volumes of the conditioned

sample can be spread on the EM grids, and all constituents contained in the transferred solution are immobilized on the EM grid when the liquid evaporates. This established semi-automatic procedure is capable of reproducibly yielding negatively stained samples of high quality, even from heterogeneous samples such as batch cell lysate. It can be used with several different negative stains including those (e.g AM and PTA) that are tolerant of phosphate buffers (e.g., PBS) and can be used near physiological pH. Compared to the commonly used stain UA this allows more physiological conditions to be employed. Furthermore, the staining is highly reproducible and the stain distribution is more homogenous than when grids are prepared by hand and the staining characteristics can be finely tuned. In addition, initial tests demonstrate the capability of producing samples that are suitable for mass determination by STEM. The test samples were effectively dialyzed in the conditioning module, yielding grid preparations with a clean background similar to those routinely prepared by hand. Although the samples in these experiments were air-dried (commonly STEM sample preparation includes freeze drying [3]) they clearly show the potential of this preparation procedure to be adapted to the needs of STEM mass measurements with respect to sample quality. As a combination of EM and MS analysis is desired, following experiments were dedicated to the adaption of the hand-over module to MS targets. An adapted deposition procedure was successfully used to spot sample-matrix mixtures onto MALDI plates (see chapter 4 or [4]). The utilization of ionic liquids as matrices not only circumvents the clogging of the micrometer-sized channels, and will most likely allow inline conditioning, but also results in homogenous sample spots for MALDI-MS analysis. In addition this procedure allows high mass samples (up to 1 MDa) to be prepared and analyzed in a MALDI-TOF/TOF mass spectrometer.

In summary, the new negative staining procedure established was shown to be methodologically sound and is ready to be applied to single cell samples. Further, the proof of concept experiments demonstrated the potential of the conditioning and hand-over module combination to also prepare samples suitable for STEM or MS mass measurements.

The next important step in the development of the microfluidic pipeline concerned the collection of single cell samples. The main aim was not only to establish an interface to feed single cell lysate into the micofluidic pipeline, but also to further adapt and optimize previously established procedures. To this end, a system for single-cell lysis and rapid uptake of the cell lysate was developed (see chapter 5 or [5]). This module enables the precise and selective lysis of individual adherent eukaryotic cells growing on a conductive support, *in situ* and under LM observation. Electrical pulses

applied via a freely positionable microcapillary electrode allow single-cell lysis to be achieved in less than a millisecond and aspiration of the cellular components into a microcapillary within a few hundred milliseconds. The combination with LM enables live cell monitoring, thereby facilitating the evaluation of cell lysis and sample aspiration as well as correlation of LM information with subsequently derived data. Initial evaluation of the samples aspirated from the immediate proximity of an individual adherent BHK cell directly after lysis was performed on negatively stained samples prepared by hand. The TEM images revealed a variety of cellular components, such as membrane patches, filaments and other particles with prominent structures. Due to the unique and distinct shape of several particles they could be identified with high certainty directly from the raw images. Nevertheless additional information is required to confirm their identities and to identify others, e.g., from template matching or labeling procedures. Furthermore, this initial TEM analysis indicated that the structure of the observed cellular components was preserved and did not reveal any protein denaturation. Although, this visual impression is supported by FEA simulations, which predict elevated temperatures for only very short time scales during lysis, this has to be further investigated and verified. Besides the application of enzyme activity assays or test samples, the structural preservation of proteins is ideally assessed directly on single cell samples. Combination of the single cell lysis unit with the sample conditioning and hand-over module will allow this and other more profound explorations of the minute sample volumes, including analysis of the sample background resulting from simultaneously aspirated buffer, the stability of protein complexes and the effects of crosslinking.

6.3 References

[1]   Engel, A. **Scanning transmission electron microscopy: Biological applications** in: Advances in Imaging and Electron Physics, Vol. 159, Ch. 9, 357-386, Elsevier Inc., (2009).

[2]   Kemmerling, S., Ziegler, J., Schweighauser, G., Arnold, S. A., Giss, D. *et al.* **Connecting μ-fluidics to electron microscopy.** *J. Struct. Biol.* 177, 128-134, (2012).

[3]   Müller, S., Goldie, K., Burki, R., Haring, R. & Engel, A. **Factors influencing the precision of quantitative scanning transmission electron microscopy**. *Ultramicroscopy* 46, 317-334, (1992).

[4]   Weidmann, S., Kemmerling, S., Mädler, S., Stahlberg, H., Braun, T. *et al.* **Ionic liquids as matrices in microfluidic sample deposition for high-mass matrix-assisted laser desorption/ionization mass spectrometry.** *Eur. J. Mass Spectrom.* 18, 279-286, (2012).

[5]   Kemmerling, S., Arnold, S. A., Bircher, B. A., Sauter, N., Escobedo, C. *et al.* **Single-cell lysis for visual analysis by electron microscopy**. *J. Struct. Biol.* (2013), http://dx.doi.org/10.1016/j.jsb.2013.06.012

7   General Conclusion and Outlook

7.1   Aim and scope of this thesis

The aim of this thesis was to pave the way for a new hybrid approach to the proteomic analysis of single eukaryotic cells. The basic procedures of a novel microfluidic sample preparation workflow have been developed, evaluated and successfully applied to test samples. Individual adherent eukaryotic cells can be targeted, lysed and feed into the pipeline. Live cell and fluorescence imaging allows LM information to be correlated with subsequently derived EM data, and diversifies the experimental possibilities. Additionally, high quality negatively stained EM samples can be prepared from minute sample volumes and complex mixtures. Although future developments are needed to refine some aspects of the developed procedures, and to further increase the versatility of the pipeline, the established modules are already promising tools for single cell analysis and negative stain TEM in general.

7.2   Current and future developments

Current work is dedicated to the fusion of single cell lysis with the sample conditioning and hand-over module. A new setup that accommodates an inverted optical microscope that also allows fluorescence imaging is under construction. The microscope is equipped with a motorized stage that enables long-term cell culture and live cell imaging. This new development will not only expand the capabilities of the pipeline to include fluorescence experiments, but also improve the conditions for the miniaturized cell cultures kept on the microscope stage. In addition, fluorescence experiments will both facilitate the characterization of cell lysis and allow the sample loading efficiency to be assessed. Using fluorescent stains for the cytosol it will be possible to visualize what happens to the cellular content during lysis and aspiration. The main concept of the new setup is to use the same stage as well as the same microcapillary tip to lyse single cells and transfer the conditioned sample to the EM grids (Fig. 7-1). In this case the sample will aspirated into the microcapillary and subsequently into the conditioning module. After a static dialysis procedure the sample will be pushed back into the microcapillary tip and transferred onto the EM grids. This will improve the transfer efficiency and staining quality of the single cell samples. Besides providing the opportunity to further automatize the whole procedure, this will allow the open questions mentioned at the end of the previous chapter to be addressed.

The new setup will be one step further towards the establishment of the whole pipeline, which is expected to advance with the integration of further missing modules in the near future. Proof of concept studies have been performed for the planned crosslinking module and another member of the team has matured a targeted version of the separation and labeling module close to integration [1]. Besides the module-wise extension of the pipeline also other improvements, such as the development of the hand-over module towards the integration of cryo-sample preparation, are also planned.
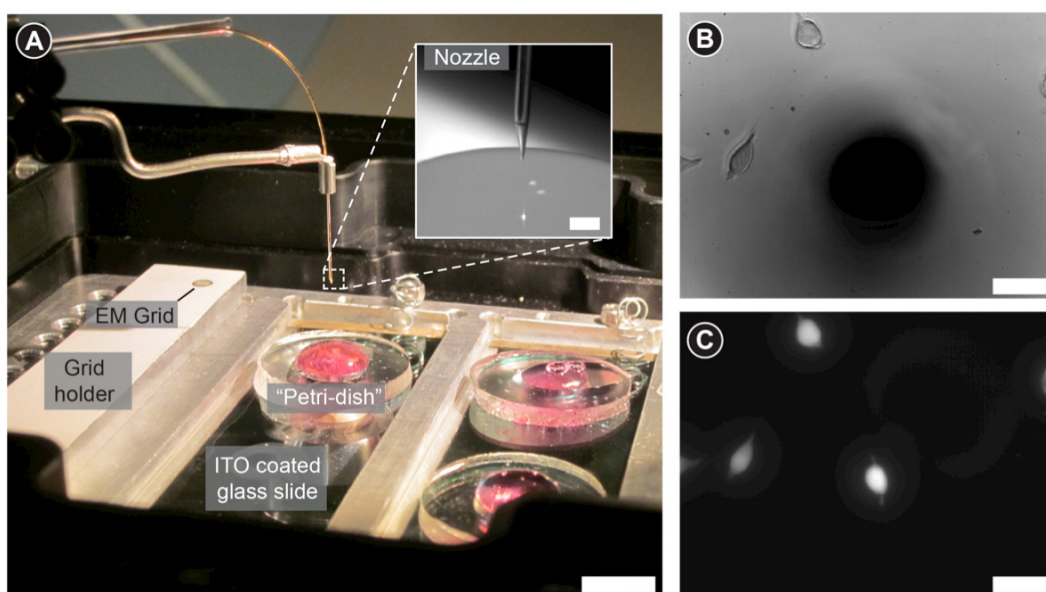

Figure 7-1: *Current status of the new setup. (A) Cell culturing, cell lysis and the hand-over platform are integrated in a motorized stage. Inside the culture stage which enables long-term cell culturing and live cell imaging, ITO coated glass slides and PDMS rings form miniaturized Petri dishes that can be filled with cell culture medium (red) and a grid holder provides a platform for sample transfer to EM grids. The stage moves in the x-y direction and the microcapillary tip can be approached or retracted in the z direction. Scale bar: 12mm. The inset shows the nozzle as seen by the control camera of the set-up. Scale bar: 400µm. (B, C) Optical images taken from below by the light microscope. Scale bars: 100 µm. (B) The phase contrast image shows the microcapillary tip (dark spot) in close proximity to the surface. The cell centered under the tip is not visible. (C) In the flourecence image the cell beneath the microcapillary tip is visible and the lysis and aspiration procedure can be observed directly.*

7.3 Future experiments

With the completion of the new setup described above it will be possible to address biological questions on the single cell level. These experiments will be based on the comparison of individual cells that are known to be in the same or a different state (e.g., comparison of two cancer cells or "normal" cell versus cancer cell) or after applying a certain stimulus (e.g., "normal" cell

versus heat-shocked cell). Such experiments will be of a discovery-driven (without a priory knowledge) or hypothesis-driven (with a priory knowledge) nature. Discovery-driven experiments, based on a global and fully quantitative investigation of the whole proteome still require significant further development. However, hypothesis-driven experiments such as the targeted detection of large protein complexes or protein aggregates are already within the realms of possibility.

For example, the tau inclusion formation and the prion-like spreading of tau aggregation, closely linked to Alzheimer's disease, could be investigated with the "lyse and spread" approach. Tau proteins can missfold and form ordered filaments, which aggregate intracellularly. Several studies indicate that the aggregation can spread from cell to cell [2-5], but the mechanism remains elusive. Initial experiments have already been designed to study this prion-like spreading of tau-inclusions in model cell cultures, and can be extended to primary neurons in the future. During the experiments, live cell imaging will be used to monitor cell morphology and general development. At specific time points or when triggered by events during live cell imaging, specific cells will be picked and prepared for visual analysis by negative stain TEM. For example cells expressing tau will be incubated ("seeded") with various forms of tau and related proteins, e.g., as monomers and their aggregated form, for a specific time period to investigate if tau aggregation was induced in the cell. Moreover, individual cells exhibiting aggregated intracellular tau could later be placed inside a "healthy" culture to study the spatial and temporal spreading of intracellular tau aggregates. Such experiments would allow the transmission of tau-inclusions from cell to cell to be investigated.

7.4 References

[1]   Giss, D., Kemmerling, S., Dandey, V., Stahlberg, H. & Braun, T. **Exploring the Interactome: Microfluidic Isolation of Proteins and Interacting Partners for Quantitative Analysis by Electron Microscopy.** *Manuscript in preparation*, (2013).

[2]   Goedert, M., Clavaguera, F. & Tolnay, M. **The propagation of prion-like protein inclusions in neurodegenerative diseases**. *Trends Neurosci.* 33, 317-325, (2010).

[3]   Frost, B. & Diamond, M. I. **Prion-like mechanisms in neurodegenerative diseases**. *Nat. Rev. Neurosci.* 11, 155-159, (2009).

[4]   Guo, J. L. & Lee, V. M.-Y. **Seeding of normal Tau by pathological Tau conformers drives pathogenesis of Alzheimer-like tangles**. *J. Biol. Chem.* 286, 15317-15331, (2011).

[5]   de Calignon, A., Polydoro, M., Suárez-Calvet, M., William, C., Adamowicz, D. H. *et al.* **Propagation of tau pathology in a model of early Alzheimer's disease**. *Neuron* 73, 685-697, (2012).

8 Acknowledgments

Apart from the efforts of myself, this dissertation would not have been possible without the support of many others. I would like to take this opportunity to thank all the people who have helped me throughout the completion of this thesis.

First of all, I am grateful to Prof. Henning Stahlberg for giving me the opportunity to work in his laboratory and for his support and advice during my PhD.

Further, I would like to thank Prof. Roderick Lim for being my co-referee and Prof. Renato Zenobi for his participation in my PhD committee.

I also would like to acknowledge Prof. Andreas Engel for sharing his vision and providing the basis for this project.

I express my deepest gratitude to Dr. Thomas Braun for being an excellent supervisor and for all his guidance, advice, support, patience and trust in me. Thomas was always there to discuss, to answer my questions and to help with major and minor problems.

Many thanks go to Dr. Shirley Müller for her help with manuscript writing. She always took time to carefully read manuscripts and for fruitful discussions, and provided numerous valuable inputs.

I also would like to express my deep appreciation to all the past and current C-CINA members for always being helpful, sharing their knowledge and expertise and creating a positive environment and a relaxed work atmosphere.

Special thanks go to my colleagues Thomas, Shirley, Phillipe, Gabriel, Jörg, Stefan, Benjamin, Dominic, Nora, Christoph, Michael and my collaborators Carlos and Simon for their participation and support in the project and for many useful discussions and adjuvant comments.

I am deeply thankful to my entire family, and especially to my parents for their love, guidance and encouragement throughout my life and for giving me the opportunity to study.

Last but not least, sincere thanks go to all my friends for all the adventures and the good times we have had and will have together. Very special thanks go to my beloved girlfriend Kristina for offering me her unconditional love and support, having faith in me, enriching my life and giving me so much energy over the last years.

Appendix

List of abbreviations

AF	Apoferritin
AM	Ammonium molybdate
AM$_{6.5}$	Ammonium molybdate at pH 6.5
BHK	Baby Hamster Kidney
BSA	Bovine serum albumin
cDNA	Complementary DNA
CE	Capillary electrophoresis
CLEM	Correlative light and electron microscopy
Cryo-ET	Cryo electron tomography
ddH$_2$O	Double-distilled water
DMEM	Dulbecco`s Modified Eagels Medium
DNA	Deoxyribonucleic acid
DSC	Differential scanning calorimetry
ECL	Enhanced chemiluminescence
EM	Electron microscopy
ESI	Electrospray ionization
FACS	Fluorescence activated cell sorting
FEA	Finite element analysis
FISH	Fluorescence in situ hybridization
FRET	Fluorescence resonance energy transfer
FS	Fused silica
HRP	Horseradish peroxidase
ID	Inner diameter
IDS	Iso-dielectric separation
IMDM	Iscove`s Modified Dulbecco`s Medium
ITO	Indium tin oxide
LC	Liquid chromatography
LCM	Laser capture microdissection

LIF	Laser-induced fluorescence
LM	Light microscopy
MACS	Magnetic activated cell sorting
MALDI	Matrix-assisted laser desorption/ionization
MALDI-TOF	Matrix-assisted laser desorption ionization time of flight
MDA	Multiple displacement amplification
MPL	Mass-per-length
mRNA	Messenger RNA
mRNA-Seq	mRNA sequencing
MS	Mass spectrometry
MS/MS	Tandem MS
NanoV$_{8.0}$	NanoVan® at pH 8.0
NanoW$_{6.8}$	NanoW® at pH 6.8
OD	Outer diameter
OM	Optical microscope
PA	Proton affinity
PCR	Polymerase chain reaction
PDMS	Poly(dimethylsiloxane)
PEEK	Poly(ether-ether-ketone)
PMF	Peptide mass fingerprinting
PTA$_{7.0}$	Phosphotungstic acid at pH 7.0
qPCR	Quantitative PCR
qRT-PCR	Quantitative reverse transcription polymerase chain reaction
RNA	Ribonucleic acid
ROIs	Regions of interest
RPPA	Reverse phase protein array
RT-PCR	Reverse transcription polymerase chain reaction
SA	Sinapinic acid
SCA	Single cell analysis
SD	Standard deviation
Seq	Sequencing
SNR	Signal-to-noise ratio

SRM	Single reaction monitoring
STEM	Scanning transmission electron microscopy
TEM	Transmission electron microscopy
TFA	Trifluoroacetic acid
TMV	Tobacco mosaic virus
UA	Uranyl acetate
UA$_{4.5}$	Uranyl acetate at pH 4.5
UA$_{7.0}$	Uranyl acetate at pH 7.0.
WGA	Whole genome amplification